R. & M. No. 3621

MINISTRY OF TECHNOLOGY

AERONAUTICAL RESEARCH COUNCIL
REPORTS AND MEMORANDA

An Experimental Investigation into the Behaviour of the Turbulent Boundary Layer with Distributed Suction in Regions of Adverse Pressure Gradient

By B. G. J. THOMPSON
Engineering Department, University of Cambridge

An Experimental Investigation into the Behaviour of the Turbulent Boundary Layers with Distributed Suction in Regions of Adverse Pressure Gradient

By B. G. J. Thompson*

Engineering Department, University of Cambridge

MINISTRY OF TECHNOLOGY

Summary.

The developments of seven turbulent boundary layers have been measured on the upper surfaces of three suction aerofoils. Distributed suction was applied, in each case, through a porous plastic suction surface that occupied most of the chord.

Good agreement was obtained between the measured development of R_θ and the predictions of the two-dimensional form of the momentum integral equation when the new skin-friction law taking direct account of the effect of suction was used. The growth of H is predicted very accurately by Head's entrainment approach provided that laminar reversion is absent and that measured H values are used to start the calculations.

The simple assumptions for velocity profile shape are found to be inaccurate when the adverse pressure gradients affect the inner region but, before this problem can be tackled satisfactorily, further investigation is required into profile behaviour in the absence of transpiration.

Spanwise pitot traverses show that the measured layers are closely two-dimensional. The distribution of suction rate along the chord is also known accurately although surface tube traverses indicate that the supporting structure is partly blocking the suction flow.

LIST OF CONTENTS

---

*Now at the National Physical Laboratory, Teddington.
**Replaces A.R.C. 31 144.

_____

1. *Introduction.*

The work described in this Report forms part of an investigation concerned with the use of distributed suction to delay or prevent the separation of the turbulent boundary layer, particularly with the aim of permitting higher lift coefficients on conventional aircraft wings. It was thought that the power required for a given increase in performance would be significantly less than in the existing methods such as flap

blowing, for example, although the choice of system will depend, because of practical considerations, on the particular application. In recent years flight research has been carried out to discover the most efficient way of distributing the available suction flow over wings and flaps in order to achieve the desired performance with the maximum economy. It has been necessary to proceed almost entirely by trial and error as no rational design procedure was available. Consequently, the present investigation was undertaken with two aims in mind,

(a) to derive a method of calculation for the turbulent boundary layer with suction (or injection) from existing calculation methods for layers on smooth impermeable surfaces, and

(b) to measure boundary-layer developments in conditions of combined suction and adverse pressure gradient, in order to provide a test of these simple calculation methods which are necessarily based upon velocity profile assumptions that are only strictly true in zero pressure gradient.

The entrainment equations of Head[3] and more recently of the present author Thompson[13] have been shown to give satisfactory predictions for shape factor development in layers on solid surfaces and in combination with the two-dimensional form of the momentum integral equation, and skin-friction relationships such as those of Thompson[14] or Nash[7] provide suitable procedures for predicting boundary-layer behaviour. In order to take account of transpiration, a new velocity profile family and three-parameter skin-friction law have been derived for layers with small pressure gradients and smooth continuously permeable surfaces (Thompson[15]) and by assuming that the entrainment behaviour is unaffected by suction or injection a method of calculation for these circumstances is obtained.

This calculation procedure was simplified for the present purposes by using the existing solid surface velocity profile relationships (but *not* of course the solid surface skin-friction law) and is only suitable for design purposes if it gives satisfactory predictions in regions of adverse pressure gradient. The only measurements in such conditions available to the present author were those of Wuest[18] which were restricted to only quite small suction rates and pressure gradients†. The new skin-friction law appeared to underestimate (by about 10 per cent) the values needed for agreement with Wuest's momentum growth. However, this disagreement could also have been accounted for by departure from two-dimensional flow and by uncertainties in the distribution of suction rate, and it also seemed probable that the filter paper suction surface was aerodynamically rough.

In view of these uncertainties it was decided to carry out the new series of measurements to provide a more certain test of the calculation methods.

In order to maintain a connection with flight research it was decided to measure boundary layers developing on the upper surface of a simple aerofoil fitted with a suction skin. This basic section was later modified to enable a wide range of conditions to be investigated. Particular attention was paid to the following points in order to overcome some at least of the difficulties associated with the interpretation of Wuest's measurements.

(i) The ideal of a smooth continuously porous suction surface was better approximated by using sheets of porous plastic.

(ii) The actual distribution of suction velocity was to be measured if possible to ± 2 per cent at all points along the chord.

(iii) Tests would be made to see if these was a significant departure from two-dimensional flow and, if so, attempts either to eliminate or to measure this would be made.

---

†Wuest's measurements covered the range

$$0 \leqslant \frac{v_s}{U_1} \leqslant 0.004 \; ; 0 \leqslant \frac{\theta}{U_1} \frac{dU_1}{dx} \leqslant 0.0006 , 1.1 < H < 1.5$$

whereas the new measurements cover

$$0 \leqslant \frac{v_s}{U_1} \leqslant 0.013 \; ; 0 \leqslant \frac{\theta}{U_1} \frac{dU_1}{dx} \leqslant 0.005 \; ; 1.21 \leqslant H \leqslant 2.05.$$

(iv) A much wider range of H, R_θ, $\dfrac{v_0}{U_1}$ and pressure gradient conditions would be covered.

(v) Velocity profiles would be measured in sufficient detail to allow accurate integration for θ and δ^*.

In addition to the primary aim of testing predictions of gross boundary layer behaviour, it was also hoped, in the initial stages of this work, that some insight would be gained from accurate and detailed velocity profiles into the behaviour of the inner region (at least) under the action of adverse pressure gradient and suction. In particular, the simple zero pressure gradient profile description would only be expected to hold over a limited range of pressure gradients, as found for layers on solid surfaces, and some quantitative limit to a suitable pressure gradient parameter was desirable when transpiration is present.

Patel[9] has shown however that at present there is no completely satisfactory description of inner region velocity profiles in regions of strong pressure gradient even in the much simpler conditions of solid surfaces. It was hardly suprising therefore that a more detailed consideration of the suction measurements gave inconclusive results especially as there was insufficient time available to make direct skin-friction measurements and also because the pressure field and wake of the traverse gear interfered with the flow, causing the local pressure gradient at each measuring station to be uncertain. The latter problem does not usually arise when transpiration is absent because the traverse gear can be situated underneath the surface. However, the influence of the traverse gear is shown not to have affected the development of R_θ and H sufficiently to invalidate the new results in their primary role.

Following a description of the experiments and the discussion of the results and boundary-layer calculations, the mean velocity profile data and the smoothed developments of boundary-layer parameters are presented in Tables 1 to 15 inclusive, for the seven layers measured.

2. Experimental Details.

2.1. General Features.

The measurements were made on aerofoils of 4 ft. span mounted vertically, as shown in Fig. 49, in the $5\frac{1}{2}$ ft. × 4 ft. working section of the Cambridge University Engineering Laboratory closed return wind tunnel, of which a general arrangement drawing is given on page 64 of Bradshaw and Pankhurst[1].

A flat suction surface was chosen to simplify construction and setting up of the external traverse gear. Longitudinal wall curvature was avoided also because it might alter the rate of boundary-layer growth and possibly the profile shapes in given conditions of suction and pressure distribution*. Consequently a very simple symmetrical aerofoil was constructed as shown in Fig. 2. This Section resembles that used earlier by Newman[17] for his detailed solid surface boundary-layer measurements.

2.2. Design and Construction of the Basic Suction Aerofoil.

The suction surface was made from sheets of 'Vyon'** porous plastic which has the appearance of a sintered powder. It has several advantages over the materials (such as blotting paper, calendered nylon and electro-deposited wire mesh) used by earlier investigators as it is reasonably rigid, enabling the distance of probes from the surface to be determined accurately, and is smooth on one side. It is both cheaper and available in larger sheets (up to 32 in. × 32 in.) than comparable sintered metal products.

A detailed comparison of such materials is made by McQuaid[5] who showed that the maximum permeability grade of Vyon used here has an effective roughness height (or porosity scale) of 0·001 in. For the present range of Reynolds numbers this means that the suction surface is aerodynamically smooth in small pressure gradients (at least) as deduced by Thompson[15]. The perflec material used by Wuest[18] had 'pores' of 0·016 in. width which may have disturbed the suction flow near the wall thus acting as an effective roughness in raising the skin-friction. This is another reason for being cautious when interpreting Wuest's results.

---

*This has been discussed in connection with the new auxiliary equation by Thompson[13]. A much more detailed investigation including measurements on the walls of a curved channel is described by Patel[9].

**Manufactured by Porous Plastics Ltd., Dagenham Dock, Essex.

For a typical maximum suction rate of $\frac{v_s}{U_1} = 0.015$, at a freestream velocity of 100 ft./sec., preliminary tests showed that Vyon of $\frac{1}{8}$ in. thickness, having a pressure drop of about 12 cms. alcohol at a suction velocity of 1 ft./sec., was suitable for use with the available suction plant. Some typical characteristics for the sheet used in the boundary-layer measurements are shown in Fig. 6. An area of about 8 sq. ft. could be sucked thus dictating the dimensions of the aerofoil in Fig. 2 having a full span (4 ft.) suction surface of $21\frac{1}{2}$ ins. chord.

Samples of Vyon sheet were tested for uniformity of resistance using the apparatus described by McQuaid. Some typical results are shown in Fig. 1 using a Parkinson and Cowan displacement type gasmeter to measure quantity flow to an accuracy of about $\pm 1\%$, in the range 0 to 0·1 cusecs.

Dutton[3] found that, even in a closed return tunnel, dust blockage necessitated frequent recalibration of his suction surface. To avoid this trouble, an inner skin of drilled plywood was used in the present experiments and needed calibration only at the beginning of the investigation because the Vyon filtered out any dust. This double skin structure was influenced by that used earlier by Dutton and by Sarnecki[10]. The construction eventually adopted is shown in Fig. 2 and consisted of a simple wooden rib and spar structure with the 1/16 in. plywood inner skin glued in place. Pine spacers $\frac{1}{2}$ in. deep by $\frac{1}{8}$ in. thick were then glued at $\frac{1}{2}$ in. intervals, using a slotted template to ensure accurate spacing, thereby dividing the surface into 43 cells each with a single row of 1/16 in. diameter holes at $\frac{1}{4}$ in. pitch across the span.
span.

This construction allowed the detailed suction velocity distribution to be determined accurately and, if required later, to be controlled independently of the freestream velocity distribution. The latter refinement is now thought to have been unwarranted for the limited scope of the present measurements where no attempt to set up any 'optimum' suction distribution was made, however the variations of $\pm 10\%$ in suction velocity shown in Fig. 1 for Vyon material should probably not be ignored in general and so the use of narrow cells would be justified if the supporting structure did not affect the suction flow locally. Initially it seemed that the use of $\frac{1}{8}$ in. Vyon and spacers of the same thickness would be satisfactory as the suction flow could redistribute within the Vyon but later results indicate that much thinner strips (0·02 in. metal or plastic, say) should have been used.

Chordwise strips of $\frac{1}{8}$ in. $\times$ $\frac{1}{2}$ in. pine were added at distances of 2 in. and 6 in. either side of the centre line of the aerofoil. These were chamfered as shown in Fig. 2 to minimise any cumulative effects due to blockage along the streamwise direction. This defined the central cells of 4 in. $\times$ $\frac{1}{2}$ in. which were then calibrated as described in the next section.

The Vyon skin was attached to the strips by using 'Holdtite' adhesive. Two coats were painted along the strips and then damped with acetone. The Vyon was also soaked in acetone* and laid smooth side downward on a surface table. The aerofoil was inverted and weighted down onto the Vyon to ensure a good glue joint. This method gave a very flat outer suction surface in spite of small variations in the thickness of the Vyon** and in the height of the pine strips.

A variety of static tappings were added as shown in Fig. 2 to enable the suction rate and surface pressures to be measured.

The outer surfaces of balsa or plywood were covered with tissue and heavily clear doped to minimise leaks.

The completed aerofoil was calibrated and then used in the first series of tests (layers *B*, *D* and *E*).

2.3. *Determination of Suction Velocity as a Function of Pressure Drop across the Inner Perforated Plywood Skin.*

The quantity flow rates, through each 4 in. $\times$ $\frac{1}{2}$ in. cell, corresponding to the range of suction velocity of interest lay between 0·002 cusecs. and 0·02 cusecs. The practical task of measuring these flows to an accuracy of ± 5 per cent or (preferably) better, is one of some difficulty as may be inferred from the reluct-

---

*Now believed to have caused unnecessary blockage by soaking the adhesive into the Vyon.

**The thickness varied between 0·115 in. and 0·126 in. for the central sheet used.

ance of most authors to give details of any procedure for determining the actual variation of transpiration velocity along the developments of their boundary layers. Usually only the overall flow (of the order of cusecs.) through the whole surface is measured.

In the present work the individual cells were calibrated using the duct shown in Fig. 8. This was constructed from thin tinplate, with a rectangular cross section of (nominally) 4 in. $\times \frac{1}{2}$ in. to fit over one cell. The flow rate through the duct was related, by means of the gasmeter, to the pressure drop across a metal gauze fitted as shown in Fig. 8. The calibration curve is given in Fig. 3.

For the calibration of the inner skin, the duct was fitted with a surrounding plenum chamber and the slide valve was adjusted until the pressure difference $(p_2 - p_3)$ across the walls of the duct was nominally zero using a MacMillan micromanometer capable of detecting pressure differences of ± 0.001 cms. alcohol. This ensured that the flow from the duct passed through the suction surface and did not converge or diverge due to chordwise pressure gradients in the Vyon. In practice, a complete balance was not usually achieved but the leakage flow could be found in terms of the pressure difference $(p_2 - p_3)$ using Fig. 4.

Some typical cell characteristics are shown in Fig. 5, and could be repeated to within ± 2 per cent of v_s (at a given pressure drop $(p_i - p_c)$ across the inner skin) even after several weeks had elapsed during which time layers B, D and E had been measured. Reasonable confidence could be placed in this method of finding the distributions of suction velocity, therefore.

The *absolute* values of v_s were of course, at that stage, dependent upon the accuracy of the gasmeter and the dimensions of the duct cross-section*. A check was made by measuring the overall flow rate through the 43 cells using a bottomless box (taped onto the surface as shown in Fig. 7) and streamlined entry of 0.735 ± 0.001 in. bore. The calibrations of the cells were used to find the overall flow rate and these two values are compared in Fig. 9. Results were also obtained using a 1 in. orifice plate but, especially at the lower flow rates, these are less satisfactory**. The gasmeter was also connected to the box and used to check the self-consistency of the cell and duct calibrations at very low suction velocities. The obvious precautions to prevent spanwise flow into or out of the 4 in. wide central strip of cells were taken by sealing the inner skin with Lassotape and the Vyon with sheets of 0.01 in. melinex. The box and all connections were leak tested before use.

Fig. 9 shows that on the average the cell calibrations overestimate the suction velocity by about 5 per cent. The suction distributions presented later are corrected for this and should be subject to systematic errors of less than ± 2 per cent.

2.4. Measurement of Pressure and Distance.

2.4.1. *Manometry*. Pressures were measured on liquid displacement manometers of various types, filled with industrial methylated spirits. In all cases, these manometers were calibrated against a water-filled Betz micromanometer to correct for inaccuracies in scale readings, possible changes in specific gravity of the alcohol due to absorption of water vapour from the atmosphere for example, and for changes in manometer tilt. The air temperature at the down-stream end of the working section was monitored and often rose by 3° to 4° C during a boundary-layer traverse. The tunnel reference pressure was adjusted to maintain a nearly constant value of reference unit Reynolds number for the inner regions of all profiles in a given layer. These mean values are given in the tables where differences of 1 per cent or less are found except for layer D.

2.4.2. *Boundary-layer traverses*. The external traverse gear shown in Fig. 10, was used to avoid the problems of concealing a traverse gear in the aerofoil and of traversing through the suction surface. The foot of the traverse gear was pressed firmly onto the Vyon by spring loading from a streamlined strut

---

*The sharp edge pressed onto the Vyon allowed the area to be known to ± 2 per cent as the width was known to ± 0.01 ins. A flexible seal was rejected as this would create a much greater uncertainty in area.

**See Ower[8].

mounted about 14 ins. from the surface. A one inch micrometer head, turned from outside the tunnel by a flexible drive, was used to position the pitot probes.

The approximate zero for y distance in any traverse was found by zeroing the pitot mouth on the polished face of a gauge block placed on the Vyon. The true zero with the wind on could then be found by traversing towards the wall in steps of 0·001 in. near the approximate position already found. The pitot reading decreases until the wall is touched and then stays constant or rises slowly. y distances were repeatable to $\pm 0\cdot001$ in. or even $\pm 0\cdot0005$ in. using this method and are given to 4 significant figures in the tables.

The pitot pressures were taken relative to a suitable static tapping and yield $\dfrac{u}{U_1}$ values accurate to $\pm 0\cdot005$ for layers B and J and better than $\pm 0\cdot003$ for the other layers*.

Double and triple pitots were used in the thicker layers F to J, as shown in Fig. 10. Except for the lowest pitot used in layer J (which had outside mouth dimensions of 0·01 in. × 0·08 in.) the flattened mouths were nominally 0·007 in. × 0·08 in. as shown in Fig. 11b. To ensure that the tip of the lowest pitot touched the surface first, a downwards pitch angle of about 5° was given as indicated by Fig. 11b. Earlier work by Sarnecki[10] had shown that this results in a negligible error in measured total pressure (*see* Fig. 11a).

The relative positions of the probe mouths, centreline static tappings and traverse gear stem are shown in plan view on Fig. 10. Measurements were not made on the centreline to avoid the possible influence of any cumulative blockage of the suction flow due to the tappings.

The pressure field of the traverse gear was found to modify the centreline pressure distribution at each traverse station and although reduced by using a longer streamlined foot of $\frac{1}{4}$ in. × 1/16 in. steel as shown in Fig. 10 could not be entirely eliminated and was accepted as an imperfection of the system.

2.5. *Data Analysis and Presentation.*

Raw pressure readings, atmospheric pressure and tunnel temperature were stored on punched tape and a digital computer used to evaluate $\dfrac{U_{ref}}{v}, \dfrac{U_1}{v}, \dfrac{u}{U_1}$, and to work out derived quantities such as θ, δ^*, H and R_θ, integrating by means of the trapezium rule those values shown in the tables with the exception of the two measured values closest to the wall which were omitted and a linear interpolation from the origin to the third point was used to find $\dfrac{u}{U_1}$.

The smoothing and differentiation of $\dfrac{U_1}{U_{ref}}$, R_θ etc. was carried out graphically and the values given in the even numbered tables were used as a basis for boundary-layer calculations.

The values in the tables have not been corrected for pitot errors due to displacement or assumed turbulence effects. Displacement effects are small except in layer B as shown in Figs. 23 and 24.

2.6. *Boundary-Layer Calculations.*

The smoothed results in the above tables have been used to carry out momentum calculations on the basis of measured H values and shape factor calculations on the basis of measured $R_\theta(x)$, using Head's or the present author's auxiliary equations. Details are given later.

3. *Boundary-Layer Measurements on the Three Aerofoils.*

3.1. *The Basic Section (Aerofoil I).*

This aerofoil was found to stall because of a separation forming in the corner between the unsucked trailing edge and the ceiling of the working section. Consequently, the stalling incidence was increased by only about one or two degrees by applying the maximum suction available and was rather more dependent upon tunnel speed, being 8° at $U_{ref} \approx 60$ ft./sec. and 12° at $U_{ref} \approx 110$ ft./sec.

---

*The number of significant figures left in the tables is therefore not related to the true accuracy but is a relic of the computer programme subsequently arranged to give this output.

Two incidences were chosen for the first series of measurements:

(i) $\alpha = -6°$, giving the best approximation to zero pressure gradient along the suction surface, and

(ii) $\alpha = +5°$, giving a reasonable adverse pressure gradient over the suction surface without any separated flow or unsteadiness, whether suction was applied or not. The reference velocity was chosen so that the maximum suction flow was equivalent to $\dfrac{v_0}{U_1} \approx -0.01$, together with an acceptable chord Reynolds number of $R_c = 1.22 \times 10^6$.

Transition behaviour was detected by the use of the china clay and paraffin technique on the nose sheeting. The 'short bubble' regions of laminar separation and turbulent reattachment found close to the pressure minima were eliminated and a uniform transition front formed by the use of tripwires of 0.036 in. diameter positioned just in front of the laminar separation position on the 'upper surface' at $\alpha = \pm 5°$, as indicated in Fig. 12. Velocity profiles at $x = -0.1$ ins. and $\alpha = +5°, -6°$ were then checked and found to agree with the Clauser plot (Fig. 22) and the solid surface profile family (Fig. 21). This meant that the layer was fully turbulent before the suction started and exhibited no trace of any disturbance due to the tripwire.

Five different boundary layers were then measured but it was later realised that the layers with nominally zero suction (A at $-6°$, C at $+5°$) were affected by a small but significant transpiration rate which could not be measured accurately. These results are not considered in this Report.

Full details of layers B, D and E are given in Tables 1 to 6 inclusive and Figs. 13 to 17 show the freestream velocity distributions, suction rates and behaviour of their mean velocity profiles. Figs. 23 to 28 show the developments of the parameters H and R_θ, whilst Figs. 29 and 30 show the effects of suction on the inner velocity profiles of layer B; layers D and E are similar in behaviour.

3.2. Discussion.

Figs. 24, 26 and 28 show that the predictions for R_θ development obtained from the two-dimensional form of the momentum integral equation are, as expected, very poor when the relationship for solid surfaces is used but become very satisfactory if the full relationship (Thompson[15]) accounting directly for the effect of suction is employed instead.

This good agreement is meaningful only if these layers are two-dimensional and if blockage to the suction flow (due to the presence of the supporting strips underneath the Vyon surface) is unimportant*. However it is expected that the only departure from two-dimensionality results from the convergence of the external flow due to the growth of the boundary layers on the floor and ceiling of the tunnel working section. This would increase the rate of growth of R_θ in the same sense as the effect of blockage. Therefore, it seemed very reasonable to suppose that neither of these influences was significant in these measurements. The good agreement seen in Figs. 18, 19 and 20 between the measured velocity profiles and the predictions of the new three-parameter family (from which the full skin-friction law is derived) confirmed this supposition. In the region of rising H value found for $x > 8$ ins. in layer B it is thought that the layer is reverting to a laminar state**. The profile family gives poor agreement in this situation, at least when a comparison is made in terms of H and R_θ.

3.3. The Flapped Section (Aerofoil II).

The first series of measurements consisted only of thin layers whose Reynolds numbers were comparatively small and the effects of suction outweighed those of the adverse pressure gradients. Consequently, it was decided to add a nose section to give Aerofoil II as shown in Fig. 12, with the original aerofoil hinged on to form a flap. The nose was set at zero angle of attack and the flap angle (η) increased

---

*This problem has been considered briefly by Head[4] in connection with the behaviour of laminar boundary layers with suction.

**$H \to 2$; $\dfrac{v_s \theta}{v} \to 0.5$ if the reversion continues in wholly zero pressure gradient.

until separation took place at about 19°. The final configuration used an angle of 17° with the endplates of $\frac{1}{8}$ in. aluminium mounted, as shown in Fig. 49, to isolate a slightly unsteady flow in the corner between the unsucked trailing edge and the ceiling. This gave a satisfactorily steady centreline pressure distribution. Tripwires of 0·048 in. diameter were used as shown in Fig. 12 and gave immediate transition.

Two layers were measured with an increased tunnel speed of $U_{ref} = 130$ ft./sec. approximately. Layer F with a low suction rate of $\frac{v_s}{U_1} \approx 0·003$, and layer G at the moderate rate of $\frac{v_s}{U_1} \approx 0·006$. It was necessary to reduce the airspeed to the value used in the previous layers in order to obtain the high suction rate of $\frac{v_s}{U_1} \approx 0·009$ used in layer H. Figs. 31 to 48 show the results of these measurements including additional profiles measured before the pressure minimum over the flap knuckle in layer H. (Figs. 37 and 42). Spanwise traverses were also made as described in the following Sections.

3.4. Spanwise Traverses to Test for Two-Dimensional Flow.

In spite of the encouraging indications, from the earlier results, that three-dimensionality was not a serious problem it was decided to carry out a direct check in the conditions of layer H.

Two cylinders of 16 S.W.G. piano wire were mounted just behind the transition wire, as shown by the arrows in Fig. 49, at distances of 8 in. above and below the centreline of the aerofoil. In the region of intense shear where the thin boundary layers interact with the base of each cylinder, a pair of vortices are formed and trail back along the developing boundary layer, persisting for many hundreds of cylinder diameters downstream. It was assumed that the vortex pairs would follow any convergence or divergence of the mean flow and consequently, by traversing a pitot tube across the span at any station downstream of the cylinders, any such three-dimensionality could be detected by the changes in distance between the centres of each vortex pair.

Fig. 51 shows the results of a traverse, using the apparatus shown in Fig. 50, at $x = 13·25$ ins. Round nosed pitots of 0·04 in. diameter were used, one mounted at a height of 9/16 in. from the Vyon and the second in contact with the surface. The peaks of total pressure in Fig. 51, show that the centres of the two vortex systems have converged only by about 0·35 ins. in a total distance of 45 ins. from the wires.

If it is assumed that the convergence started only at the beginning of the adverse pressure gradient (at $x = -3·2$ ins. from Fig. 32) then the maximum contribution to the momentum balance is given by:

Total angle of convergence $\phi = \dfrac{0·35}{16} \approx 0·22$ radians.

Rate of change of angle with spanwise distance $\dfrac{\partial \phi}{\partial z} = \dfrac{0·022}{16} = 0·0014$ radians/inch.

The momentum integral equation for the assumed wholly radial flow becomes,

$$\frac{dR_\theta}{dx} = \left[\frac{c_f}{2} + \frac{v_0}{U_1} \right] \frac{U_1}{v} - (H+1) \frac{R_\theta}{U_1} \frac{dU_1}{dx} + R_\theta \frac{\partial \phi}{\partial z} \qquad (1)$$

If we assume that the convergence rate is the same for layers F, G and H, the total increase in R_θ at the final station where $x = 20·75$ ins. is respectively,

for layer F, $\Delta R_\theta \approx 400$,
for layer G, $\Delta R_\theta \approx 340$,
and for layer H, $\Delta R_\theta \approx 170$.

These values would affect the level of agreement between calculated and measured $R_\theta(x)$ by an insignificant amount as can be seen from Figs. 44, 46 and 48.

3.5. *Chordwise Surface Tube Traverses to Test for Uniformity of the Suction Flow.*

A wire carriage was made as shown in Fig. 54, to carry a surface pitot and a static tube with its holes positioned directly above the pitot mouth. This assembly was supported on three points, one of these being the pitot mouth itself to ensure contact with the surface at all times. The carriage was traversed along the chord by means of a continuous wire (*A* in the figure) running through a guide tube sunk into the nose sheeting to avoid interference with the boundary layer. This wire was driven by a worm and pulley arrangement operated by a flexible drive from outside the tunnel. The *x*-position of the pitot mouth could be found to ± 0.01 in. approximately, using the scale attached to the floor of the tunnel.

Two sets of surface pitot and local static pressure (assumed not to depend upon height from the wall) readings were taken. The first was across the start of the suction surface as shown in Fig. 52, and the second was in front of station 6 (*see* Fig. 53). Flattened pitots with mouths of 0·006 in. and 0·018 in. overall depth were used in each case. It was found that the pitot mouths tended to scratch the relatively soft surface of the Vyon when traversing towards the leading edge. Consequently the traverses shown were made in the downstream direction. The relatively smooth variation of dynamic pressure near to the leading edge of the Vyon probably results from damage to the surface, but this is not found elsewhere.

The very rapid changes in dynamic pressure even when the larger pitot is used show that the structure of the Vyon itself imposes a pattern on the sublayer flow as its finite pore size causes the suction to take place through an array of small discrete sinks. The reduction in dynamic pressure immediately above the supporting strips indicates a smaller suction rate there and hence a blockage effect.

3.6. *Discussion.*

In practice, suction might well be applied to the upper surfaces of flaps of orthodox aerofoils and so this second series of measurements may be of greater interest than the first.

3.6.1. *Mean velocity profiles.*
The comparison of measured and calculated profiles shown in Figs. 37 and 42, for that part of layer *H* before the suction surface, reveals that the inner regions and overall profiles at $x = -13$ in. and at $x = -10.1$ in. agree with the usual laws for small pressure gradients but at the next station ($x = -5.9$ in.) the favourable pressure gradient in front of the pressure minimum on the flap knuckle has affected the inner profile. The strong adverse pressure gradient that follows the pressure minimum causes the overall profile at *H*1 to depart from the simple two-parameter family although a small logarithmic portion remains in the Clauser plot of Fig. 37. *F*1 and *G*1 behave similarly.

The profiles measured by Stratford[11] in strong adverse pressure gradients showed the same discrepancy (*see* Fig. 29 of Thompson[14]). These were measured on a concave wall whereas the present profiles are affected by flow over a convex surface. It seems therefore, that the direct effects of wall curvature on

profile shape are small in this range of $\dfrac{\delta_1}{R} \leqslant 0.016^*$.

This failure of the profile family to predict correctly the profiles *without* suction means that the complete zero pressure gradient family can hardly be expected to predict the suction profiles until the effects of the strong adverse pressure gradient have died away. Figs. 38, 39 and 40 show this to be true although at the final station profiles *G*7 and *H*7 have almost settled to the shapes given by the simple family. Where the effects of suction and adverse pressure gradient balance each other to some extent as in layer *F*, the profile family for zero transpiration gives better overall predictions for given values of *H* and R_θ, although this is not so for layers *G* and *H* where the suction is proportionately stronger.

3.6.2. *Comparison with predictions of boundary layer development.*
The calculations of $R_\theta(x)$ shown in Figs. 46 and 48 are again very good if the full skin-friction law is used. This is surprising in view of the poor agreement with the profile shapes mentioned above and will be discussed later.

The *H* predictions on the basis of measured $R_\theta(x)$ are again excellent, except close to the flap knuckle (Fig. 47).

---

*Patel[9] has investigated this in greater detail using a curved channel.

3.7. *Measurements on the Cambered Aerofoil III.*

3.7.1. *Layer J.* The effects of the adverse pressure gradient were reduced considerably by moving the pressure minimum further upstream of the suction surface. This was achieved by reducing the 'flap' angle to 12° and adding the fairing shown in Fig. 12. The central circular arc was of radius 30 in. compared with the previous flap knuckle radius of 11 in. on Aerofoil II.

One layer (*J*) was measured using suction rates similar to those of layer *F* and from Fig. 58 the improvement in agreement between the profile family and the measurements can be seen especially in the outer region of *J*1. However, with suction the inner regions do not agree even at *J*7.

The agreement with the two-dimensional momentum balance is better than that found previously in layer *F* as comparison of Figs. 44 and 60 shows.

The prediction for *H* is again very satisfactory when measured $R_\theta(x)$ is used (*see* Fig. 59).

3.7.2. *Yawmeter comb measurements.* The comb of three-tube yawmeters used originally by Patel[9] was employed to check the convergence or divergence of this layer. Readings were taken at three chordwise positions (x = 3·75, 11·75 and 19·75 in.). In each case the comb was mounted at heights of 7 in. above and below the centreline of the aerofoil with a dummy 'image' comb and pressure tubing positioned to ensure symmetry of the flow about the centreline.

The flow angles calculated from the individual yawmeters (using Patel's original calibration curves) were rather scattered but the convergence at a given height *y* from the wall could be found by taking the difference in readings (of the given probe) obtained at the two spanwise stations associated with a given *x*-position.

The contribution to the momentum balance was found to be even smaller than that indicated for layer *F* by the results of Section 3.4, and has been ignored completely in the calculations presented in this Report. The disagreement between calculated $R_\theta(x)$ and the measured development shown in Fig. 60 is much larger than the measured crossflow term.

4. *Discussion.*

4.1. *Interference due to the Traverse Gear.*

At each traverse position the presence of the traverse gear stem (and its wake) alters the pressure distribution and hence the boundary-layer development for some distance upstream, from that occurring without any traverse arrangement in place. The uncertainty in $\dfrac{U_1}{U_{ref}}$ can be observed from Figs. 13, 31, 32 and 55 and is only about $\pm\frac{1}{2}$ per cent about the mean curves used to perform boundary-layer calculations. The effect upon $\dfrac{d\,U_1/U_{ref}}{dx}$ is much larger however, although layers *F*, *G* and *H* are rather better than the remainder owing to the use of a longer 'foot' on the traverse gear.

In layer *J* the centreline static pressure distributions have been measured with the traverse gear in the normal position for profile *J*2 (that is the stem at x = 3·5 in.; z = −1 in.) and also with the stem on the centreline (at x = 3·5 in.; z = 0 in.) giving the distributions of $\dfrac{U_1}{U_{ref}}$ (x) shown in Fig. 61.

Curve *A* thus corresponds to the static pressure distribution in the plane of the boundary layer when *J*2 was measured, whilst curve *B* corresponds to the smoothed mean curve through the static pressures taken as usual in a plane offset one inch from the plane in which the velocity profiles were measured.

Hence by comparing the predicted *H* and R_θ developments obtained from Head's method using curves *A* and *B* in turn, some idea of the local effect of the traverse gear on boundary-layer development can be obtained. As seen from Fig. 61 the effect on *H* values is less than 0·5 per cent at the relevant traverse station *J*2 (x = 2·25 ins.). The corresponding effect on R_θ is less than 0·1 per cent and is not plotted here.

Consequently, although the inner region will be affected by the local pressure field with the traverse gear in position, the values of *H* and R_θ are likely to be affected less by this than by other sources of experimental error. In particular, the mean curves of $\dfrac{U_1}{U_{ref}}$, *H* and R_θ are quite accurate enough to serve

as a test for simple integral calculation procedures of the present type.

4.2. Non-Uniformity of Suction.

The irregularities in the histograms of $\dfrac{v_0}{U_1}$ are small and consistent from layer to layer thus giving confidence in the chosen mean curves. The maximum departures are of the order of ± 5 per cent at $\dfrac{v_0}{U_1} \approx -0.004$, falling to ± 3 per cent at -0.01, and occur principally at $x = 15.5$ to 16.5 in. and $x = 17.5$ to 18 in.—see especially Figs. 14 and 33. Elsewhere, if the underlying structure had a negligible effect upon the local suction flow, the suction distributions would be smooth enough to satisfy the requirements of the boundary-layer approximation that $\dfrac{\partial v_0}{\partial x}$ should be small (except very near to the ends of the suction surface).

However, the present structure has been shown by the surface tube traverses, to reduce the suction rate immediately above the supporting strips that divide the cells, in spite of the transverse flow that is possible within the Vyon.

By assuming that the velocity profile is given everywhere close to the wall by the asymptotic zero pressure gradient viscous sublayer expression,

$$\frac{u}{U_1} = \frac{U_\tau^2}{v_0 U_1}\left[1 - \exp\left(\frac{v_0\, y}{v}\right) \right] \tag{2}$$

the dynamic pressure traverses at $y = 0.009$ in. and 0.003 in. shown in Fig. 53 were used to determine the approximate variation of $\dfrac{v_0}{U_1}$ and c_f. It was found that, above the strips, the suction rates fell by about 20 per cent of the mean values (from the histogram) and were roughly 20 per cent above the mean value at the centre of each cell. Throughout the present investigation velocity profiles have been measured at x-positions corresponding to the centres of cells and so their sublayer profiles are unlikely to fit the predicted profiles.

Fig. 30 indicates that in layer B the effect of the blockage has become negligible for distances greater than 0.02 ins. from the surface. Similar results are found for layers D, E, G and H but owing to the effects of the pressure gradient on the inner regions of layers F and J no definite conclusions can be made.

It is not possible to say how this blockage affects the overall boundary-layer development until further measurements have been made on a surface where the blockage is negligible. McQuaid[5] has reported a very careful series of injection measurements on a surface made from Vyon of the same grade as used here. However, he supported his Vyon sheets on a diagonal grid of 1 mm. plywood thereby reducing the area blocked by the supports from the present 25 per cent to about 4 per cent. There appears to be no blockage effect in McQuaid's results. However, he did not attempt any surface tube traverses of the type used here and it would be of considerable interest to try this in order to see if such a structure produced an effect distinguishable from that due to the finite pore size of the Vyon.

The rapid variations of surface tube readings with distance along the surface means that isolated readings of small Preston tubes, for example, are unlikely to yield trustworthy values for local skin friction. It appears that the minimum spanwise dimension for surface tubes or wires must be about 0.25 ins. in order to integrate out the influence of individual pores.

The good agreement generally obtained for $R_\theta(x)$ (and hence $c_f(x)$) when the new skin-friction law is used may result from the fact that it was made to give agreement with the momentum developments of zero pressure gradient layers measured by Sarnecki[10] on a suction surface similar in many respects to the present one*.

---

*$\tfrac{1}{8}$ in. strips at $\tfrac{5}{8}$ in. intervals supporting a perforated brass sheet covered with calendared nylon having 100 threads to the inch.

4.3. *Momentum Development and Skin Friction.*

The level of agreement for $R_\theta(x)$ and hence for the skin-friction law is rather surprising in layers F, G, H and J in view of the (not unexpected) failure of the profile family from which this law has been derived. The effect of adverse pressure gradient is to reduce the value of c_f associated with given values of H, R_θ and $\dfrac{v_0}{U_1}$ (*see* Patel[9] for discussion of velocity profiles without suction or injection) and so a law derived from zero pressure gradient assumptions would be expected to *overestimate c_f* values and hence the growth of $R_\theta(x)$. The present agreement must be due to either,

(a) the momentum growth being affected by the second order terms that have not been measured in this investigation or

(b) the blockage to the suction flow has increased the effective skin friction, as in the laminar layer considered by Head[4].

(a) is probably significant only in layer F and may account for the more rapid growth of R_θ in the measured layer (*see* Fig. 44), (b) seems to be most likely in the other layers.

4.4. *Calculation of Shape-Factor Development.*

Figs. 23, 25, 27, 43, 45, 47 and 59 show the predictions of Head's auxiliary equation

$$\frac{d\,R_\theta H_1}{dx} = \left[\, F(H_1) + \frac{v_0}{U_1}\, \right] \frac{U_1}{v} \tag{3}$$

The solid surface relationships for $F(H_1)$ and $H(H_1)$ have been extrapolated to small values of H in agreement with the turbulent asymptotic suction layer measured by Dutton[2] where

$$F = \frac{v_s}{U_1} = 0\cdot0044 \text{ and } H_1 \approx 23, \tag{4}$$

and this accounts for the surprisingly good agreement obtained in layers B and E, where $H(H_1)$ is approximated by the analytic expression shown in Fig. 62, and $F(H_1)$ by

$$F = 0\cdot0299\,(H_1 - 3\cdot0)^{-0\cdot6169} \tag{5}$$

The new equation proposed by the present author[13] is also used for layers D and E as shown in Figs. 25 and 27.

In these H calculations the measured $R_\theta(x)$ has been used although full calculations would give very similar results except for layer F.

The agreement with the measured $H(x)$ values is quite comparable with results obtained for layers on solid surfaces and is good except in regions of falling H as in layers D and E. (Figs. 25 and 27).

Head's shape-factor relationship is shown (in Fig. 62) to be a reasonable mean curve through the present data but in any given layer systematic departures occur and lead to errors as shown in Figs. 63 and 65 where the use of smoothed $H(H_1)$ curves through the measured values for the appropriate layer have been used in making additional calculations. The disagreement remaining in the latter calculations is due entirely to inadequate entrainment assumptions.

The flux calculations shown in Figs. 64 and 66 confirm that the simple F curve underestimates entrainment when H is decreasing and slightly overestimates entrainment when H is increasing.

The new equation proposed by the present author includes a term accounting to some extent for the influence of rate-of-change of shape factor on entrainment.

4.5. *Velocity Profiles in Conditions of Combined Suction and Adverse Pressure Gradient.*

From the results of the previous Section it is apparent that a completely satisfactory calculation method requires a profile family capable of describing the effects of strong pressure gradient on profile

shape (as well as on the associated skin-friction law). This has been shown by Patel[9] to be very difficult for layers *without* transpiration as even the description of the inner profile needs knowledge of the local flow accelerations as well as of the pressure gradient ($d\,c_f/dx$ as well as dp/dx, say). No satisfactory proposal for the outer region in non-equilibrium layers is at present available although a modified form of one of the available profile models (Thompson[14], Stevenson[12], for example) may be satisfactory once the inner region is described.

Further work should be carried out on smooth solid walls before attempting to tackle suction or injection in detail, as direct measurements of skin friction and shear stress are required.

Attempts to find the range of pressure gradient over which the zero pressure gradient inner region is satisfactory when suction is present, were unsuccessful on the basis of the present measurements as the parameter for which limiting values are required is (from McQuaid[6]).

$$\Delta_i = \frac{\nu}{(U_\tau^2 + v_0\,\bar{u})^{3/2}}\,\frac{1}{\rho}\,\frac{dp}{dx}, \tag{6}$$

where $\bar{u}$ is the mean velocity in the turbulent inner region, and neither U_τ, nor $\dfrac{dp}{dx}$ are known accurately from the present measurements.

5. *Conclusions and Suggestions for Further Work.*

The measured layers with suction appear to be suitable for testing calculation methods because:

(i) The smoothed suction distribution is known accurately.

(ii) The flow is closely two-dimensional.

The presence of the traverse gear modifies the pressure distribution and boundary-layer development slightly. This means that,

(iii) the measured inner profiles are not appropriate to the smoothed distributions of static pressure and so the present measurements are not suitable for determining new profile relationships which take account of the effects of adverse pressure gradient as well as of suction. However,

(iv) the values of H and R_θ are little affected by this disturbance and the present data are therefore suitable for calculations involving such variables not strongly dependent upon the exact shape of the inner profile.

The calculations of boundary-layer development show that, for *this* suction surface,

(v) momentum thickness development is accurately predicted by means of the simple two-dimensional form of the momentum integral equation provided the new skin friction law, taking account of the effects of suction, is used. Agreement is poor if solid surface assumptions are used instead.

(vi) The development of H is predicted to the same order of accuracy as in layers with zero transpiration if Head's auxiliary equation and solid surface assumptions for shape factor and entrainment behaviour are used, provided that measured H values are used to start the calculations.

The velocity profile comparisons show, however, that

(vii) the simple zero pressure gradient profile model upon which the skin friction law is based is unsatisfactory in strong adverse pressure gradients, near a flap knuckle for example, unless the suction is also large.

The surface tube traverses show that,

(viii) careful investigation is needed into the effects, on the sub-layer profiles and on skin friction, of blockage to the suction flow due to the supporting structure beneath the suction surface. The results of the previous investigations of Dutton and of Sarnecki may also be in doubt because of this.

(ix) The use of surface tube traverses appears to provide a satisfactory test for such blockage.

(x) Surface tubes and other devices for measuring local skin friction are unlikely to be satisfactory unless their lateral dimensions are much greater than the average pore size of the suction surface.

(xi) The combined effects of blockage and adverse pressure gradients in the present experiments probably accounts for the unexpected success of the simple skin friction law.

14

The present work provides a useful guide to the gross features of boundary layer behaviour in practical conditions on aerofoils and flaps. The suction surface should however be reconstructed along the lines of the more recent work of McQuaid[5] and surface tube traverses used to check blockage. This should be negligible and consequently the present uncertainty regarding the effects of blockage on the momentum development (and effective c_f) can be resolved by repeating layer J, for example. An improved traverse gear and measurements of static pressure variation normal to the surface and of normal Reynolds stresses are also required to obtain a completely reliable momentum balance.

It is not known at present how sensitive design predictions will be to the exact form of the assumptions made, in the calculation procedure, for the skin-friction or shape-factor relationships. Consequently, it is preferable to use the present oversimplified calculation method to investigate this before attempting more detailed experiments (in which direct c_f measurements might be made, for example).

Using one of the modern numerical techniques such as dynamic programming, it would be possible to find the best way of (say) applying suction on a given aerofoil to achieve a desired high lift coefficient. This calculation could then be repeated with suitable variations from the present c_f law. For example, these values could be increased or decreased by 20 per cent everywhere, or a linear variation of c_f with Δ_i at given values of H, R_θ and $\dfrac{v_0}{U_1}$ could be assumed. Changes might also be tried in the $H(H_1)$ relationships.

If these exploratory computations showed that the predicted optima were relatively insensitive to such alterations then the use of the present over-simplified assumptions would be justified for predicting design trends. Final quantitative values of suction rate would then be accepted only after a limited number of measurements had been made in conditions near to the predicted optima.

The skin-friction law will be strongly affected by the exact nature of the suction surface but as in the case of roughness the effect can only be determined by direct measurements on the type of surface envisaged in the final application. The present surface is not ideal for fundamental work as blockage may be significant but it represents a reasonably rigid type of construction that might be similar to that adopted in practice.

6. *Acknowledgements.*

LIST OF SYMBOLS

c	Aerofoil chord length
c_f	Local skin-friction coefficient
D	Outside depth of pitot mouth
$F(H_1)$	Head's entrainment function
H, H_1	Velocity profile shape factors
p	Local static pressure, assumed independent of y
p_2	Static pressure below gauze in calibration duct
p_3	Static pressure inside duct plenum chamber
p_c	Static pressure registered by tappings inside aerofoil plenum chamber
p_i	Static pressure in cells between the two skins of the suction surface
p_o	Local total pressure within the boundary layer
R	Local radius of longitudinal curvature of the surface
R_c, R_θ	Reynolds numbers, $R_c = \dfrac{U_{\text{ref}} c}{v}$; $R_\theta = \dfrac{U_1 \theta}{v}$
u	Local x-component of velocity inside boundary layer
U_1	Local free-stream velocity
U_{ref}	Velocity obtained from tunnel reference pressure difference
U_τ	Local friction velocity $\left[= U_1 \sqrt{\dfrac{c_f}{2}} \right]$
v_0	Local transpiration velocity (positive for injection)
v_s	Local suction velocity ($= -v_0$)
x	Distance downstream of start of suction
y	Distance normal to surface
z	Distance above centreline of aerofoil as mounted in the tunnel
α	Angle of incidence of aerofoil
δ_1	Local boundary-layer thickness
δ^*	Displacement thickness
Δ_i	Inner region pressure gradient parameter defined in Section 4.5
η	Angle of flap deflection
θ	Momentum loss thickness
v	Kinematic viscosity
ρ	Air density
ϕ	Local convergence angle of flow

16

REFERENCES

No.	Author(s)	Title, etc.
1	P. B. Bradshaw and R. C. Pankhurst	The design of low speed wind tunnels. *J. Progress in Aero. Sci.*, Vol. 5, pp 1–69, Pergamon Press (1964).
2	R. A. Dutton	The effects of distributed suction on the development of turbulent boundary layers. A.R.C. R. & M. 3155 (1958).
3	M. R. Head	Entrainment in the turbulent boundary layer. A.R.C. R. & M. 3152 (1958).
4	M. R. Head	Approximate calculations of the laminar boundary layer with suction, with particular reference to the suction requirements for boundary-layer stability on aerofoils of different thickness/chord ratios. A.R.C. R. & M. 3124 (1957).
5	J. McQuaid	Experiments on incompressible turbulent boundary layers with distributed injection. A.R.C. R. & M. 3549 (1967).
6	J. McQuaid	The calculation of turbulent boundary layers with injection. A.R.C. R. & M. 3542 (1967).
7	J. F. Nash	A note on skin-friction laws for the incompressible turbulent boundary layer. A.R.C. C.P. 862 (1964).
8	E. Ower	*The measurement of airflow.* pp 138–141, Chapman and Hall (1949).
9	V. C. Patel	Ph.D. Dissertation, Cambridge University (1965).
10	A. J. Sarnecki	Ph.D. Dissertation, Cambridge University (1959).
11	B. S. Stratford	An experimental flow with zero skin friction throughout its region of pressure rise. *J. Fluid Mech.*, Vol. 5, pp 17–35 (1959).
12	T. N. Stevenson	The mean flow in the outer region of turbulent boundary layers. *AGARDograph 97*, pp 281–314 (1965).
13	B. G. J. Thompson	The calculation of shape-factor development in incompressible turbulent boundary layers with or without transpiration. *AGARDograph 97*, pp 159–190 (1965).
14	B. G. J. Thompson	A new two-parameter family of mean velocity profiles for incompressible turbulent boundary layers on smooth walls. A.R.C. R. & M. 3463 (1965).

15 B. G. J. Thompson ..   ..   A three-parameter family of mean velocity profiles for incompressible turbulent boundary layers with distributed suction and small pressure gradients.
A.R.C. R. & M. 3622 (1969).

16 W. Pechau   ..   ..   ..   Calculation of the turbulent boundary layer with continuously distributed suction.
AGARD. Rept. 259 (1960).

17 B. G. Newman..   ..   ..   Some contributions to the study of the turbulent boundary layer.
Australian Dept. of Supply. Report No. A.C.A. 53 (1951).

18 W. Wuest   ..   ..   ..   Experimental investigation on boundary-layer suction by a series of slits and holes.
AGARD. Report 258 (1960).

TABLE 1

Layer 'B'

PROFILE

	B 1	B 2	B 3	B 4	B 5	B 6	B 7
X INCHES FROM START OF SUCTION	-0.10	2.25	4.75	8.75	12.75	16.75	20.75
REFERENCE REYNOLDS NUMBER PER INCH U_{REF}/ν	38780	38510	38650	38640	38740	38690	38820
FREE STREAM VELOCITY U_1 FT/SEC	81.53	77.87	75.55	77.53	75.61	74.40	72.26
REYNOLDS NUMBER PER INCH U_1/ν	41811	39548	38754	38754	37905	37439	36299
SUCTION VELOCITY RATIO V_0/U_1	0.0000	-0.0092	-0.0104	-0.0109	-0.0103	-0.0112	-0.0122
MOMENTUM THICKNESS (THETA) INCHES	0.0218	0.0201	0.0167	0.0122	0.0086	0.0069	0.0054
DISPLACEMENT THICKNESS (DELTA-STAR) INCHES	0.0354	0.0271	0.0212	0.0152	0.0113	0.0091	0.0079
SHAPE FACTOR H	1.626	1.352	1.270	1.238	1.309	1.312	1.466
R-THETA	910	794	648	475	328	259	196

Y INCHES	U/U1	Y INCHES	U/U1	Y INCHES	U/U1	Y INCHES	U/U1	Y INCHES	U/U1	Y INCHES	U/U1	Y INCHES	U/U1
0.3000	1.0000	0.2990	1.0000	0.3340	1.0000	0.4410	1.0000	0.4060	1.0000	0.4510	1.0000	0.4420	1.0000
0.2500	1.0000	0.2490	1.0000	0.2840	1.0000	0.3910	0.9996	0.3560	1.0000	0.3510	0.9995	0.3920	1.0000
0.2000	0.9992	0.2240	0.9979	0.2590	0.9991	0.3410	0.9979	0.3060	0.9991	0.3010	0.9981	0.3420	1.0000
0.1750	0.9970	0.1990	0.9966	0.2340	0.9987	0.2910	0.9970	0.2560	0.9964	0.2760	0.9981	0.2920	0.9985
0.1500	0.9859	0.1740	0.9886	0.2090	0.9943	0.2410	0.9944	0.2310	0.9951	0.2510	0.9958	0.2420	0.9971
0.1250	0.9514	0.1490	0.9664	0.1840	0.9844	0.2160	0.9901	0.2060	0.9924	0.2260	0.9944	0.2170	0.9961
0.1000	0.8866	0.1240	0.9293	0.1590	0.9668	0.1910	0.9841	0.1810	0.9874	0.2010	0.9916	0.1920	0.9951
0.0800	0.8200	0.0990	0.8832	0.1340	0.9442	0.1660	0.9750	0.1560	0.9801	0.1760	0.9870	0.1670	0.9921
0.0600	0.7484	0.0790	0.8460	0.1090	0.9162	0.1410	0.9640	0.1310	0.9719	0.1510	0.9827	0.1420	0.9882
0.0500	0.7083	0.0590	0.8081	0.0840	0.8919	0.1160	0.9475	0.1060	0.9631	0.1260	0.9780	0.1170	0.9847
0.0400	0.6709	0.0490	0.7913	0.0590	0.8673	0.0910	0.9375	0.0810	0.9570	0.1010	0.9733	0.0920	0.9802
0.0300	0.6319	0.0390	0.7780	0.0490	0.8586	0.0660	0.9261	0.0660	0.9504	0.0760	0.9676	0.0670	0.9762
0.0250	0.6093	0.0290	0.7650	0.0390	0.8519	0.0510	0.9201	0.0560	0.9490	0.0610	0.9642	0.0520	0.9747
0.0200	0.5838	0.0240	0.7556	0.0340	0.8477	0.0410	0.9164	0.0460	0.9486	0.0510	0.9628	0.0420	0.9737
0.0150	0.5455	0.0190	0.7479	0.0290	0.8441	0.0360	0.9150	0.0360	0.9457	0.0410	0.9623	0.0370	0.9732
0.0100	0.4717	0.0170	0.7422	0.0240	0.8394	0.0310	0.9136	0.0310	0.9452	0.0360	0.9609	0.0320	0.9732
0.0080	0.4189	0.0150	0.7366	0.0190	0.8336	0.0260	0.9108	0.0260	0.9438	0.0310	0.9609	0.0270	0.9717
0.0060	0.3433	0.0130	0.7309	0.0170	0.8299	0.0210	0.9089	0.0240	0.9433	0.0260	0.9594	0.0220	0.9701
0.0050	0.3034	0.0110	0.7147	0.0150	0.8256	0.0190	0.9061	0.0220	0.9419	0.0210	0.9589	0.0180	0.9666
0.0040	0.2704	0.0090	0.6879	0.0130	0.8203	0.0170	0.9028	0.0200	0.9410	0.0190	0.9570	0.0170	0.9646
		0.0070	0.6400	0.0110	0.8094	0.0150	0.9009	0.0180	0.9400	0.0170	0.9556	0.0160	0.9620
		0.0050	0.5628	0.0090	0.7929	0.0130	0.8980	0.0160	0.9381	0.0150	0.9536	0.0140	0.9538
		0.0040	0.5228	0.0070	0.7542	0.0110	0.8866	0.0140	0.9352	0.0130	0.9478	0.0120	0.9383
				0.0060	0.7145	0.0090	0.8656	0.0120	0.9271	0.0110	0.9350	0.0100	0.9096
				0.0050	0.6519	0.0070	0.8154	0.0100	0.9085	0.0090	0.9120	0.0080	0.8436
				0.0040	0.6005	0.0060	0.7697	0.0090	0.8886	0.0070	0.8593	0.0070	0.7859
						0.0050	0.7211	0.0080	0.8568	0.0050	0.7726	0.0060	0.7316
						0.0040	0.6677	0.0070	0.8096	0.0040	0.7141	0.0050	0.6634
								0.0060	0.7445			0.0040	0.6005
								0.0050	0.6745				

19

TABLE 2

Layer 'B'

Smoothed Data Used in Boundary-Layer Calculations

MEAN VALUE OF REFERENCE REYNOLDS NUMBER PER INCH 38650

X INCHES	U1/UREF	V0/U1	H	R-THETA	DU1/UREF/DX
-0.10	1.080	0.00000	1.626	910	-0.0300
0.75	1.059	-0.00860	1.470	896	-0.0225
1.75	1.039	-0.00870	1.383	829	-0.0166
2.25	1.032	-0.00920	1.352	794	-0.0138
2.75	1.025	-0.00980	1.333	760	-0.0128
3.75	1.015	-0.01030	1.300	702	-0.0090
4.75	1.007	-0.01040	1.270	648	-0.0072
5.75	1.000	-0.01060	1.245	601	-0.0056
6.75	0.995	-0.01080	1.232	557	-0.0044
7.75	0.991	-0.01090	1.226	515	-0.0034
8.75	0.988	-0.01090	1.238	475	-0.0026
9.75	0.986	-0.01090	1.268	433	-0.0021
10.75	0.984	-0.01090	1.290	395	-0.0018
11.75	0.982	-0.01060	1.304	359	-0.0018
12.75	0.980	-0.01030	1.310	328	-0.0020
13.75	0.978	-0.01020	1.310	300	-0.0024
14.75	0.974	-0.01050	1.305	282	-0.0030
15.75	0.971	-0.01110	1.302	269	-0.0037
16.75	0.966	-0.01120	1.310	259	-0.0046
17.75	0.961	-0.01080	1.335	249	-0.0057
18.75	0.955	-0.01090	1.370	239	-0.0078
19.75	0.945	-0.01140	1.414	222	-0.0120
20.75	0.931	-0.01220	1.466	196	-0.0170
21.75	0.911	0.00000	1.520	156	-0.0220

TABLE 3

Layer 'D'

PROFILE

D 1	D 2	D 3	D 4	D 5	D 6	D 7

X INCHES FROM START OF SUCTION

-0.10	2.25	4.75	8.75	12.75	16.75	20.75

REFERENCE REYNOLDS NUMBER PER INCH   UREF/$\sqrt{}$

38230	38400	38880	38490	38540	38370	38150

FREE STREAM VELOCITY U1 FT/SEC

112.90	101.43	94.39	89.17	85.19	80.54	74.19

REYNOLDS NUMBER PER INCH   U1/$\sqrt{}$

57496	52107	48668	45458	43162	41019	38150

SUCTION VELOCITY RATIO VO/U1

0.0000	-0.0046	-0.0056	-0.0064	-0.0065	-0.0072	-0.0082

MOMENTUM THICKNESS (THETA)   INCHES

0.0421	0.0614	0.0707	0.0778	0.0843	0.0922	0.1092

DISPLACEMENT THICKNESS (DELTA-STAR) INCHES

0.0799	0.1065	0.1116	0.1098	0.1125	0.1187	0.1399

SHAPE FACTOR H

1.900	1.735	1.578	1.411	1.334	1.288	1.281

R-THETA

2418	3200	3442	3536	3639	3781	4165

Y INCHES	U/U1	Y INCHES	U/U1	Y INCHES	U/U1	Y INCHES	U/U1	Y INCHES	U/U1	Y INCHES	U/U1	Y INCHES	U/U1
0.4470	1.0000	1.2940	1.0000	0.6860	1.0000	0.6930	1.0000	0.8900	1.0000	0.8880	1.0000	1.6870	1.0000
0.3470	1.0000	0.9940	1.0000	0.5860	1.0000	0.5930	0.9963	0.7900	1.0000	0.8440	0.9972	1.1810	0.9980
0.2970	0.9994	0.8440	0.9986	0.4860	0.9980	0.5430	0.9879	0.6900	0.9944	0.7880	0.9898	1.0870	0.9967
0.2720	0.9963	0.6580	0.9979	0.4360	0.9889	0.4930	0.9723	0.5900	0.9738	0.6880	0.9726	0.9870	0.9933
0.2470	0.9844	0.5580	0.9979	0.3860	0.9617	0.4430	0.9458	0.5400	0.9555	0.5880	0.9414	0.8870	0.9853
0.2220	0.9539	0.4580	0.9972	0.3360	0.9130	0.3930	0.9088	0.4900	0.9313	0.5380	0.9202	0.8510	0.9765
0.1970	0.9055	0.4080	0.9965	0.2860	0.8458	0.3430	0.8671	0.4400	0.9038	0.4880	0.8979	0.8380	0.9785
0.1720	0.8439	0.3580	0.9893	0.2350	0.7743	0.2930	0.8239	0.3900	0.8753	0.4380	0.8808	0.7510	0.9551
0.1470	0.7730	0.3080	0.9521	0.1860	0.7042	0.2430	0.7794	0.3400	0.8429	0.3880	0.8561	0.6510	0.9283
0.1220	0.6981	0.2580	0.8742	0.1610	0.6710	0.1930	0.7380	0.2900	0.8123	0.3380	0.8328	0.5510	0.8903
0.0970	0.6175	0.2080	0.7759	0.1360	0.6367	0.1430	0.6960	0.2400	0.7825	0.2880	0.8046	0.4510	0.8529
0.0870	0.5841	0.1580	0.6728	0.1110	0.6045	0.1180	0.6771	0.1900	0.7515	0.2380	0.7819	0.3510	0.8179
0.0770	0.5512	0.1330	0.6208	0.0960	0.5867	0.0930	0.6591	0.1400	0.7254	0.1880	0.7658	0.3010	0.7949
0.0670	0.5202	0.1080	0.5703	0.0860	0.5754	0.0830	0.6528	0.1150	0.7128	0.1380	0.7487	0.2510	0.7780
0.0570	0.4878	0.0980	0.5488	0.0760	0.5640	0.0730	0.6449	0.0900	0.7020	0.1130	0.7389	0.2010	0.7624
0.0470	0.4556	0.0880	0.5317	0.0660	0.5545	0.0630	0.6392	0.0800	0.6977	0.0880	0.7281	0.1510	0.7439
0.0370	0.4243	0.0780	0.5135	0.0560	0.5434	0.0530	0.6333	0.0700	0.6941	0.0780	0.7258	0.1260	0.7376
0.0270	0.3920	0.0680	0.4981	0.0460	0.5335	0.0430	0.6275	0.0600	0.6897	0.0680	0.7219	0.1010	0.7331
0.0170	0.3543	0.0580	0.4822	0.0360	0.5250	0.0330	0.6208	0.0500	0.6853	0.0580	0.7196	0.0760	0.7249
0.0120	0.3203	0.0480	0.4665	0.0260	0.5164	0.0280	0.6171	0.0400	0.6808	0.0480	0.7141	0.0510	0.7175
0.0070	0.2464	0.0380	0.4534	0.0210	0.5093	0.0230	0.6110	0.0300	0.6733	0.0380	0.7101	0.0410	0.7138
0.0050	0.1869	0.0280	0.4383	0.0160	0.4971	0.0180	0.6034	0.0250	0.6711	0.0280	0.7021	0.0310	0.7082
0.0040	0.1587	0.0180	0.4210	0.0110	0.4770	0.0130	0.5887	0.0200	0.6627	0.0230	0.6941	0.0210	0.6978
		0.0130	0.4039	0.0060	0.4049	0.0110	0.5783	0.0150	0.6512	0.0180	0.6867	0.0160	0.6804
		0.0080	0.3671	0.0040	0.3555	0.0090	0.5571	0.0100	0.6094	0.0130	0.6701	0.0110	0.6423
		0.0050	0.3061			0.0070	0.5121	0.0080	0.5735	0.0100	0.6444	0.0090	0.6039
		0.0040	0.2820			0.0060	0.4746	0.0060	0.4969	0.0080	0.6075	0.0070	0.5325
						0.0050	0.4317	0.0050	0.4521	0.0060	0.5387	0.0060	0.4800
						0.0040	0.3889	0.0040	0.4195	0.0040	0.4536	0.0050	0.4146
												0.0040	0.3688

TABLE 4

Layer 'D'

Smoothed Data Used in Boundary-Layer Calculations

MEAN VALUE OF REFERENCE REYNOLDS NUMBER PER INCH   38400

X INCHES	U1/UREF	VO/U1	H	R-THETA	DU1/UREF/DX
-0.10	1.504	0.00000	1.880	2415	-0.0800
0.75	1.439	-0.00370	1.822	2770	-0.0645
1.75	1.380	-0.00420	1.757	3090	-0.0520
2.25	1.357	-0.00462	1.725	3195	-0.0460
2.75	1.334	-0.00492	1.693	3271	-0.0410
3.75	1.298	-0.00536	1.631	3369	-0.0328
4.75	1.268	-0.00562	1.575	3435	-0.0276
5.75	1.242	-0.00585	1.522	3477	-0.0242
6.75	1.220	-0.00603	1.475	3507	-0.0215
7.75	1.200	-0.00622	1.435	3530	-0.0193
8.75	1.181	-0.00636	1.405	3550	-0.0180
9.75	1.165	-0.00645	1.382	3567	-0.0160
10.75	1.150	-0.00646	1.360	3585	-0.0150
11.75	1.135	-0.00645	1.343	3605	-0.0141
12.75	1.120	-0.00645	1.328	3627	-0.0133
13.75	1.108	-0.00647	1.312	3653	-0.0130
14.75	1.095	-0.00668	1.300	3684	-0.0130
15.75	1.082	-0.00698	1.292	3722	-0.0133
16.75	1.069	-0.00716	1.285	3778	-0.0138
17.75	1.054	-0.00710	1.280	3842	-0.0146
18.75	1.038	-0.00718	1.278	3933	-0.0160
19.75	1.022	-0.00753	1.278	4040	-0.0192
20.75	1.000	-0.00817	1.278	4160	-0.0253
21.75	0.970	0.00000	1.278	4265	-0.0347

TABLE 5

Layer 'E'

PROFILE	E 1	E 2	E 3	E 4	E 5	E 6	E 7
X INCHES FROM START OF SUCTION	-0.10	2.25	4.75	8.75	12.75	16.75	20.75
REFERENCE REYNOLDS NUMBER PER INCH U_{REF}/γ	38480	38280	38240	38460	38560	38500	38280
FREE STREAM VELOCITY U_1 FT/SEC	114.43	99.35	95.16	89.20	84.05	80.35	73.75
REYNOLDS NUMBER PER INCH U_1/γ	58103	52102	48562	45532	43266	41113	37977
SUCTION VELOCITY RATIO V_O/U_1	0.0000	-0.0065	-0.0082	-0.0092	-0.0090	-0.0102	-0.0116
MOMENTUM THICKNESS (THETA) INCHES	0.0417	0.0566	0.0627	0.0628	0.0644	0.0665	0.0788
DISPLACEMENT THICKNESS (DELTA-STAR) INCHES	0.0781	0.0957	0.0949	0.0839	0.0817	0.0816	0.0952
SHAPE FACTOR H	1.873	1.691	1.514	1.336	1.270	1.227	1.208
R-THETA	2423	2948	3044	2860	2784	2734	2994

Y INCHES	U/U1	Y INCHES	U/U1	Y INCHES	U/U1	Y INCHES	U/U1	Y INCHES	U/U1	Y INCHES	U/U1	Y INCHES	U/U1
0.4475	1.0000	0.8620	1.0000	0.6860	1.0000	0.6930	1.0000	0.8900	1.0000	0.8880	1.0000	1.3870	1.0000
0.3475	1.0000	0.5620	1.0000	0.5860	1.0000	0.5930	0.9991	0.7900	1.0000	0.8440	1.0000	1.1870	1.0000
0.2975	0.9997	0.4620	0.9989	0.4860	1.0000	0.5430	0.9963	0.6900	0.9990	0.7880	0.9977	1.0870	0.9851
0.2725	0.9966	0.4120	0.9985	0.4360	0.9964	0.4930	0.9893	0.5900	0.9912	0.6880	0.9921	0.9870	0.9865
0.2475	0.9854	0.3620	0.9963	0.3860	0.9808	0.4430	0.9733	0.5400	0.9808	0.5880	0.9754	0.8770	0.9966
0.2225	0.9574	0.3120	0.9740	0.3360	0.9452	0.3930	0.9488	0.4900	0.9670	0.5380	0.9614	0.8510	0.9872
0.1975	0.9108	0.2620	0.9094	0.2860	0.8879	0.3430	0.9146	0.4400	0.9461	0.4880	0.9460	0.7510	0.9844
0.1725	0.8508	0.2120	0.8151	0.2360	0.8203	0.2930	0.8754	0.3900	0.9218	0.4380	0.9273	0.6510	0.9679
0.1475	0.7812	0.1620	0.7115	0.1860	0.7498	0.2430	0.8349	0.3400	0.8958	0.3880	0.9070	0.5510	0.9412
0.1215	0.7041	0.1370	0.6619	0.1610	0.7151	0.1930	0.7952	0.2900	0.8666	0.3380	0.8862	0.4510	0.9100
0.0975	0.6272	0.1120	0.6094	0.1360	0.6810	0.1430	0.7547	0.2400	0.8395	0.2880	0.8649	0.3510	0.8709
0.0875	0.5942	0.1020	0.5886	0.1110	0.6494	0.1180	0.7367	0.1900	0.8108	0.2380	0.8458	0.3010	0.8591
0.0775	0.5633	0.0920	0.5703	0.0960	0.6305	0.0930	0.7196	0.1400	0.7850	0.1870	0.8255	0.2510	0.8441
0.0675	0.5301	0.0820	0.5520	0.0860	0.6195	0.0830	0.7131	0.1150	0.7738	0.1380	0.8075	0.2010	0.8273
0.0575	0.4991	0.0720	0.5352	0.0760	0.6070	0.0730	0.7060	0.0900	0.7637	0.1130	0.7976	0.1510	0.8117
0.0475	0.4679	0.0620	0.5178	0.0660	0.5983	0.0630	0.7027	0.0800	0.7597	0.0880	0.7912	0.1260	0.8059
0.0375	0.4377	0.0520	0.5034	0.0560	0.5888	0.0530	0.6967	0.0700	0.7570	0.0780	0.7912	0.1010	0.8009
0.0275	0.4058	0.0420	0.4901	0.0460	0.5798	0.0430	0.6927	0.0600	0.7515	0.0680	0.7898	0.0740	0.7941
0.0175	0.3683	0.0320	0.4765	0.0360	0.5714	0.0330	0.6881	0.0500	0.7494	0.0580	0.7869	0.0510	0.7924
0.0125	0.3374	0.0220	0.4640	0.0260	0.5621	0.0230	0.6813	0.0400	0.7467	0.0480	0.7848	0.0410	0.7882
0.0075	0.2712	0.0170	0.4553	0.0210	0.5563	0.0180	0.6766	0.0300	0.7432	0.0380	0.7812	0.0310	0.7882
0.0055	0.2162	0.0120	0.4389	0.0160	0.5483	0.0150	0.6704	0.0250	0.7419	0.0280	0.7783	0.0210	0.7813
0.0045	0.1871	0.0090	0.4166	0.0140	0.5431	0.0130	0.6662	0.0200	0.7363	0.0230	0.7754	0.0160	0.7736
		0.0070	0.3884	0.0110	0.5326	0.0100	0.6543	0.0150	0.7293	0.0180	0.7695	0.0110	0.7471
		0.0050	0.3369	0.0080	0.5101	0.0080	0.6306	0.0100	0.6968	0.0130	0.7592	0.0090	0.7187
				0.0060	0.4723	0.0070	0.6098	0.0080	0.6620	0.0100	0.7442	0.0070	0.6551
						0.0060	0.5731	0.0060	0.5773	0.0080	0.7218	0.0060	0.6072
						0.0050	0.5198	0.0050	0.5328	0.0060	0.6682	0.0050	0.5393

23

TABLE 6

Layer 'E'

Smoothed Data Used in Boundary-Layer Calculations

MEAN VALUE OF REFERENCE REYNOLDS NUMBER PER INCH   38400

X INCHES	U1/UREF	VO/U1	H	R-THETA	DU1/UREF/DX
-0.10	1.510	0.00000	1.880	2405	-0.0795
0.75	1.448	-0.00442	1.806	2658	-0.0670
1.75	1.388	-0.00479	1.722	2868	-0.0540
2.25	1.361	-0.00654	1.680	2945	-0.0480
2.75	1.340	-0.00746	1.642	3006	-0.0420
3.75	1.302	-0.00800	1.570	3060	-0.0342
4.75	1.270	-0.00819	1.505	3045	-0.0285
5.75	1.244	-0.00844	1.450	3009	-0.0246
6.75	1.221	-0.00860	1.404	2970	-0.0216
7.75	1.202	-0.00890	1.366	2932	-0.0192
8.75	1.184	-0.00921	1.335	2894	-0.0180
9.75	1.166	-0.00926	1.311	2858	-0.0162
10.75	1.150	-0.00930	1.290	2829	-0.0152
11.75	1.136	-0.00915	1.275	2803	-0.0142
12.75	1.122	-0.00900	1.262	2780	-0.0134
13.75	1.109	-0.00902	1.250	2758	-0.0130
14.75	1.096	-0.00940	1.240	2743	-0.0132
15.75	1.082	-0.00998	1.231	2733	-0.0137
16.75	1.068	-0.01021	1.225	2735	-0.0146
17.75	1.052	-0.01008	1.220	2755	-0.0160
18.75	1.036	-0.01014	1.214	2800	-0.0185
19.75	1.016	-0.01063	1.208	2875	-0.0220
20.75	0.992	-0.01159	1.203	2990	-0.0262
21.75	0.964	0.00000	1.200	3150	-0.0310

TABLE 7

Layer 'F'

PROFILE	F 1	F 2	F 3	F 4	F 5	F 6	F 7
X INCHES FROM START OF SUCTION	-0.10	2.25	4.75	8.75	12.75	16.75	20.75
REFERENCE REYNOLDS NUMBER PER INCH UREF/√	64180	64680	64260	64190	64420	64400	64490
FREE STREAM VELOCITY U1 FT/SEC	182.84	170.50	163.41	150.99	144.37	137.32	128.33
REYNOLDS NUMBER PER INCH U1/√	92873	86873	82012	76964	72317	68426	64664
SUCTION VELOCITY RATIO VO/U1	0.0000	-0.0018	-0.0024	-0.0032	-0.0031	-0.0037	-0.0042
MOMENTUM THICKNESS (THETA) INCHES	0.0787	0.1020	0.1243	0.1543	0.1866	0.2298	0.2903
DISPLACEMENT THICKNESS (DELTA-STAR) INCHES	0.1222	0.1696	0.2118	0.2662	0.3306	0.4284	0.5958
SHAPE FACTOR H	1.552	1.662	1.704	1.725	1.772	1.864	2.052
R-THETA	7313	8863	10192	11875	13491	15725	18775

F1 Y INCHES	U/U1	F2 Y INCHES	U/U1	F3 Y INCHES	U/U1	F4 Y INCHES	U/U1	F5 Y INCHES	U/U1	F6 Y INCHES	U/U1	F7 Y INCHES	U/U1
0.9030	1.0000	0.9150	1.0000	1.0050	1.0000	1.2570	1.0000	1.3550	1.0000	1.5560	1.0000	1.9115	1.0000
0.8030	1.0000	0.8650	1.0000	0.9800	1.0000	1.1570	1.0000	1.3050	1.0000	1.5060	1.0000	1.8115	1.0000
0.7030	0.9976	0.8150	0.9978	0.9550	0.9992	1.0570	0.9975	1.2550	0.9990	1.4560	0.9988	1.7615	0.9952
0.6530	0.9932	0.7650	0.9939	0.9050	0.9966	1.0320	0.9967	1.2050	0.9976	1.4060	0.9977	1.7265	0.9969
0.6030	0.9852	0.7150	0.9856	0.9010	0.9940	0.9820	0.9929	1.1550	0.9941	1.3560	0.9946	1.7085	0.9947
0.5530	0.9720	0.6650	0.9749	0.8740	0.9947	0.9570	0.9894	1.1050	0.9895	1.3060	0.9897	1.6615	0.9925
0.5030	0.9549	0.6150	0.9581	0.8560	0.9931	0.9320	0.9870	1.0550	0.9819	1.2560	0.9823	1.5615	0.9789
0.4530	0.9331	0.5650	0.9381	0.8510	0.9892	0.9030	0.9777	0.9800	0.9632	1.1560	0.9553	1.4615	0.9611
0.4030	0.9112	0.5150	0.9175	0.8010	0.9821	0.8630	0.9716	0.9550	0.9552	1.0560	0.9125	1.3615	0.9188
0.3530	0.8866	0.4650	0.8933	0.7510	0.9720	0.8570	0.9693	0.9300	0.9462	0.9810	0.8744	1.2615	0.8748
0.3030	0.8608	0.4150	0.8668	0.7010	0.9565	0.8520	0.9653	0.9050	0.9347	0.9560	0.8595	1.1615	0.8213
0.2530	0.8280	0.3650	0.8375	0.6510	0.9368	0.8030	0.9480	0.9010	0.9278	0.9310	0.8452	1.0115	0.7413
0.2030	0.7890	0.3150	0.7998	0.6010	0.9157	0.7530	0.9286	0.8850	0.9245	0.9060	0.8289	0.9115	0.6872
0.1530	0.7232	0.2650	0.7471	0.5510	0.8911	0.7030	0.9047	0.8600	0.9133	0.9020	0.8228	0.9065	0.6801
0.1280	0.6752	0.2150	0.6803	0.5010	0.8638	0.6530	0.8761	0.8510	0.9064	0.8960	0.8233	0.8765	0.6635
0.1030	0.6204	0.1650	0.6003	0.4510	0.8300	0.6030	0.8443	0.8010	0.8799	0.8660	0.8074	0.8585	0.6538
0.0780	0.5556	0.1400	0.5592	0.4010	0.7904	0.5480	0.8046	0.7510	0.8514	0.8520	0.7947	0.8565	0.6522
0.0680	0.5297	0.1150	0.5197	0.3510	0.7427	0.5030	0.7695	0.7010	0.8194	0.8020	0.7688	0.8065	0.6247
0.0580	0.5030	0.0900	0.4808	0.3010	0.6890	0.4530	0.7283	0.6500	0.7802	0.7520	0.7371	0.7565	0.5970
0.0480	0.4752	0.0790	0.4665	0.2510	0.6283	0.4030	0.6845	0.6010	0.7465	0.7020	0.7036	0.7065	0.5676
0.0380	0.4461	0.0690	0.4509	0.2010	0.5697	0.3530	0.6398	0.5510	0.7073	0.6520	0.6703	0.6565	0.5428
0.0280	0.4203	0.0590	0.4373	0.1510	0.5139	0.3030	0.5961	0.5010	0.6725	0.6020	0.6415	0.6065	0.5196
0.0180	0.3878	0.0490	0.4213	0.1260	0.4852	0.2530	0.5542	0.4510	0.6369	0.5520	0.6062	0.5565	0.4896
0.0130	0.3687	0.0390	0.4033	0.1010	0.4576	0.2030	0.5105	0.4010	0.6012	0.5020	0.5776	0.5065	0.4662
0.0080	0.3396	0.0290	0.3871	0.0760	0.4320	0.1780	0.4927	0.3510	0.5636	0.4520	0.5467	0.4565	0.4416
0.0060	0.3169	0.0240	0.3775	0.0510	0.4092	0.1530	0.4741	0.3010	0.5312	0.4020	0.5211	0.4065	0.4192
0.0050	0.2991	0.0190	0.3648	0.0410	0.3994	0.1280	0.4576	0.2510	0.5009	0.3520	0.4938	0.3565	0.3988
		0.0170	0.3584	0.0310	0.3881	0.1030	0.4411	0.2010	0.4708	0.3020	0.4669	0.3065	0.3773
		0.0160	0.3546	0.0200	0.3739	0.0780	0.4285	0.1510	0.4430	0.2520	0.4423	0.2555	0.3558
		0.0150	0.3497	0.0160	0.3640	0.0530	0.4147	0.1260	0.4315	0.2020	0.4190	0.2065	0.3406
		0.0140	0.3461	0.0110	0.3448	0.0430	0.4109	0.1010	0.4197	0.1520	0.4002	0.1565	0.3262
		0.0130	0.3397	0.0090	0.3279	0.0330	0.4035	0.0760	0.4100	0.1270	0.3880	0.1315	0.3138
		0.0120	0.3338	0.0070	0.2985	0.0230	0.3957	0.0510	0.3984	0.1020	0.3774	0.1065	0.3089
		0.0110	0.3260			0.0180	0.3892	0.0410	0.3931	0.0770	0.3713	0.0815	0.3032
		0.0100	0.3172			0.0130	0.3807	0.0310	0.3864	0.0520	0.3580	0.0565	0.2958
		0.0090	0.3053			0.0110	0.3748	0.0210	0.3773	0.0420	0.3548	0.0465	0.2906
		0.0080	0.2895			0.0090	0.3668	0.0160	0.3680	0.0320	0.3482	0.0365	0.2876
		0.0070	0.2711			0.0070	0.3515	0.0140	0.3652	0.0220	0.3398	0.0265	0.2830
		0.0060	0.2532			0.0060	0.3415	0.0120	0.3565	0.0170	0.3318	0.0215	0.2743
								0.0100	0.3491	0.0140	0.3235	0.0165	0.2629
						0.0080	0.3343	0.0120	0.3175	0.0135	0.2535		
						0.0060	0.3067	0.0100	0.3045	0.0115	0.2429		
						0.0050	0.2837	0.0080	0.2929	0.0095	0.2318		
								0.0060	0.2653	0.0075	0.2047		
										0.0065	0.1903		
										0.0055	0.1744		

25

TABLE 8

Layer 'F'

Smoothed Data Used in Boundary-Layer Calculations

MEAN VALUE OF REFERENCE REYNOLDS NUMBER PER INCH 6437(

X INCHES	U1/UREF	VO/U1	H	R-THETA	DU1/UREF/1
-0.10	1.446	0.00000	1.550	7310	-0.0587
0.75	1.403	-0.00112	1.600	7940	-0.0447
1.75	1.366	-0.00160	1.640	8570	-0.0347
2.25	1.350	-0.00179	1.655	8862	-0.0320
2.75	1.334	-0.00196	1.666	9150	-0.0302
3.75	1.306	-0.00224	1.683	9690	-0.0268
4.75	1.280	-0.00240	1.698	10200	-0.0244
5.75	1.257	-0.00255	1.702	10645	-0.0225
6.75	1.235	-0.00279	1.708	11070	-0.0209
7.75	1.215	-0.00309	1.716	11470	-0.0206
8.75	1.196	-0.00318	1.721	11870	-0.0183
9.75	1.179	-0.00321	1.733	12270	-0.0175
10.75	1.161	-0.00321	1.745	12650	-0.0166
11.75	1.145	-0.00318	1.758	13050	-0.0160
12.75	1.129	-0.00312	1.770	13490	-0.0160
13.75	1.113	-0.00312	1.790	14020	-0.0155
14.75	1.098	-0.00333	1.812	14580	-0.0146
15.75	1.084	-0.00367	1.838	15190	-0.0148
16.75	1.068	-0.00375	1.870	15830	-0.0160
17.75	1.052	-0.00352	1.910	16500	-0.0166
18.75	1.035	-0.00357	1.950	17210	-0.0170
19.75	1.017	-0.00384	1.998	17970	-0.0160
20.75	1.002	-0.00425	2.050	18770	-0.0130
21.75	0.991	0.00000	2.102	19760	-0.0090

26

TABLE 9

Layer 'G'

PROFILE	G1	G2	G3	G4	G5	G6	G7
X INCHES FROM START OF SUCTION	-0.10	2.25	4.75	8.75	12.75	16.75	20.75
REFERENCE REYNOLDS NUMBER PER INCH U_{REF}/ν	64370	64400	64090	63950	64300	64340	64100
FREE STREAM VELOCITY U_1 FT/SEC	188.10	174.16	164.28	152.82	145.49	133.14	127.58
REYNOLDS NUMBER PER INCH U_1/ν	94101	88097	82397	77203	72665	68388	63450
SUCTION VELOCITY RATIO V_O/U_1	0.0000	-0.0035	-0.0044	-0.0054	-0.0052	-0.0060	-0.0068
MOMENTUM THICKNESS (THETA) INCHES	0.0789	0.1015	0.1179	0.1402	0.1630	0.1941	0.2392
DISPLACEMENT THICKNESS (DELTA-STAR) INCHES	0.1214	0.1637	0.1908	0.2238	0.2613	0.3191	0.4174
SHAPE FACTOR H	1.539	1.613	1.618	1.596	1.603	1.644	1.745
R-THETA	7420	8942	9716	10823	11845	13275	15180

G1 Y INCHES	U/U1	G2 Y INCHES	U/U1	G3 Y INCHES	U/U1	G4 Y INCHES	U/U1	G5 Y INCHES	U/U1	G6 Y INCHES	U/U1	G7 Y INCHES	U/U1
0.9010	1.0000	0.9840	1.0000	1.0160	1.0000	1.2070	1.0000	1.3550	1.0000	1.5045	1.0000	1.6080	1.0000
0.8010	1.0000	0.9590	1.0000	0.9910	1.0000	1.1570	1.0000	1.3050	1.0000	1.4045	1.0000	1.5580	1.0000
0.7010	0.9960	0.9050	0.9974	0.9660	0.9995	1.1070	0.9991	1.1550	0.9997	1.3045	0.9994	1.5080	0.9996
0.6510	0.9927	0.9040	0.9983	0.9410	0.9980	1.0570	0.9981	1.1050	0.9976	1.1545	0.9901	1.4080	0.9939
0.6010	0.9817	0.8690	0.9976	0.9260	0.9980	1.0070	0.9964	1.0550	0.9933	1.1045	0.9817	1.3580	0.9872
0.5510	0.9698	0.8550	0.9957	0.9150	0.9974	0.9570	0.9940	0.9800	0.9846	1.0045	0.9563	1.2580	0.9663
0.5010	0.9525	0.8050	0.9925	0.9120	0.9962	0.9320	0.9918	0.9300	0.9750	0.9545	0.9359	1.2080	0.9526
0.4510	0.9319	0.7550	0.9888	0.9060	0.9972	0.9070	0.9898	0.9010	0.9628	0.9045	0.9132	1.1580	0.9353
0.4010	0.9098	0.7050	0.9813	0.8960	0.9966	0.9030	0.9871	0.8950	0.9660	0.9005	0.9070	1.1080	0.9157
0.3510	0.8867	0.6550	0.9700	0.8860	0.9958	0.8770	0.9854	0.8680	0.9576	0.8565	0.8918	1.0580	0.8904
0.3010	0.8595	0.6050	0.9553	0.8810	0.9972	0.8720	0.9837	0.8510	0.9482	0.8505	0.8841	1.0080	0.8673
0.2510	0.8275	0.5550	0.9359	0.8750	0.9969	0.8600	0.9824	0.8010	0.9289	0.8005	0.8572	0.9830	0.8540
0.2010	0.7899	0.5050	0.9137	0.8620	0.9944	0.8530	0.9788	0.7510	0.9046	0.7505	0.8298	0.9330	0.8320
0.1510	0.7256	0.4550	0.8910	0.8120	0.9883	0.8030	0.9655	0.7010	0.8770	0.7005	0.8011	0.9030	0.8094
0.1260	0.6774	0.4050	0.8649	0.7620	0.9805	0.7530	0.9495	0.6510	0.8484	0.6505	0.7740	0.8600	0.7929
0.1010	0.6203	0.3550	0.8359	0.7120	0.9670	0.7030	0.9313	0.6010	0.8173	0.6005	0.7418	0.8530	0.7870
0.0720	0.5491	0.3050	0.7999	0.6620	0.9522	0.6530	0.9097	0.5510	0.7852	0.5505	0.7096	0.8030	0.7595
0.0490	0.4861	0.2550	0.7495	0.6120	0.9314	0.6030	0.8825	0.5010	0.7515	0.5005	0.6812	0.7530	0.7319
0.0410	0.4619	0.2050	0.6840	0.5620	0.9103	0.5530	0.8546	0.4510	0.7174	0.4505	0.6528	0.7030	0.7060
0.0310	0.4337	0.1550	0.6071	0.5120	0.8847	0.5030	0.8198	0.4010	0.6814	0.4005	0.6212	0.6530	0.6812
0.0220	0.4059	0.1300	0.5655	0.4620	0.8584	0.4520	0.7798	0.3510	0.6462	0.3505	0.5947	0.6020	0.6510
0.0170	0.3914	0.1050	0.5266	0.4120	0.8246	0.4030	0.7390	0.3010	0.6152	0.3005	0.5669	0.5530	0.6276
0.0120	0.3702	0.0800	0.4865	0.3620	0.7839	0.3530	0.6993	0.2510	0.5832	0.2505	0.5400	0.5030	0.5965
0.0070	0.3303	0.0700	0.4686	0.3120	0.7354	0.3030	0.6591	0.2010	0.5517	0.2005	0.5175	0.4530	0.5735
0.0050	0.2977	0.0600	0.4550	0.2620	0.6794	0.2530	0.6163	0.1510	0.5260	0.1505	0.4977	0.4030	0.5468
		0.0500	0.4410	0.2120	0.6217	0.2030	0.5748	0.1260	0.5121	0.1255	0.4849	0.3530	0.5217
		0.0400	0.4273	0.1620	0.5662	0.1530	0.5411	0.1000	0.5002	0.1005	0.4774	0.3030	0.5024
		0.0300	0.4123	0.1370	0.5385	0.1280	0.5184	0.0760	0.4898	0.0755	0.4698	0.2530	0.4811
		0.0200	0.3932	0.1120	0.5111	0.1030	0.5036	0.0510	0.4810	0.0505	0.4593	0.2030	0.4616
		0.0150	0.3772	0.0870	0.4867	0.0780	0.4890	0.0410	0.4774	0.0405	0.4563	0.1530	0.4428
		0.0120	0.3618	0.0720	0.4716	0.0530	0.4772	0.0310	0.4731	0.0305	0.4532	0.1280	0.4352
		0.0100	0.3443	0.0610	0.4624	0.0430	0.4739	0.0210	0.4672	0.0205	0.4455	0.1030	0.4284
		0.0080	0.3140	0.0520	0.4548	0.0330	0.4687	0.0140	0.4621	0.0155	0.4392	0.0780	0.4221
		0.0070	0.2969	0.0420	0.4458	0.0230	0.4644	0.0140	0.4587	0.0125	0.4341	0.0530	0.4130
		0.0060	0.2839	0.0320	0.4370	0.0180	0.4644	0.0120	0.4527	0.0105	0.4275	0.0430	0.4130
				0.0270	0.4346	0.0160	0.4590	0.0100	0.4462	0.0083	0.4175	0.0330	0.4087
				0.0210	0.4271	0.0140	0.4567	0.0080	0.4341	0.0065	0.4048	0.0280	0.4032
				0.0200	0.4261	0.0120	0.4536	0.0060	0.4089	0.0045	0.3737	0.0230	0.3987
				0.0180	0.4233	0.0100	0.4485	0.0050	0.3874			0.0180	0.3919
				0.0160	0.4192	0.0080	0.4409					0.0130	0.3762
				0.0140	0.4137	0.0060	0.4230					0.0110	0.3604
				0.0130	0.4114	0.0050	0.4081					0.0090	0.3333
				0.0120	0.4058							0.0070	0.2887
				0.0110	0.4008							0.0050	0.2271
				0.0100	0.3958								
				0.0090	0.3872								
				0.0080	0.3717								
				0.0070	0.3528								
				0.0060	0.3436								

TABLE 10

Layer 'G'

Smoothed Data Used in Boundary-Layer Calculations

MEAN VALUE OF REFERENCE REYNOLDS NUMBER PER INCH   64220

X INCHES	U1/UREF	VO/U1	H	R-THETA	DU1/UREF/DX
-0.10	1.464	0.00000	1.527	7560	-0.0542
0.75	1.422	-0.00243	1.566	8160	-0.0442
1.75	1.383	-0.00315	1.598	8710	-0.0377
2.25	1.365	-0.00345	1.607	8930	-0.0351
2.75	1.348	-0.00374	1.615	9110	-0.0327
3.75	1.318	-0.00413	1.620	9430	-0.0287
4.75	1.291	-0.00435	1.615	9730	-0.0251
5.75	1.268	-0.00453	1.604	10020	-0.0226
6.75	1.246	-0.00478	1.599	10300	-0.0215
7.75	1.225	-0.00518	1.595	10570	-0.0200
8.75	1.206	-0.00536	1.592	10830	-0.0186
9.75	1.188	-0.00535	1.591	11090	-0.0181
10.75	1.170	-0.00532	1.593	11350	-0.0174
11.75	1.152	-0.00524	1.595	11610	-0.0167
12.75	1.136	-0.00516	1.601	11870	-0.0162
13.75	1.120	-0.00513	1.607	12140	-0.0164
14.75	1.103	-0.00531	1.617	12460	-0.0165
15.75	1.086	-0.00603	1.630	12840	-0.0165
16.75	1.070	-0.00601	1.644	13250	-0.0163
17.75	1.054	-0.00557	1.663	13680	-0.0165
18.75	1.038	-0.00573	1.687	14120	-0.0175
19.75	1.019	-0.00613	1.713	14610	-0.0188
20.75	0.999	-0.00681	1.743	15170	-0.0196
21.75	0.981	0.00000	1.777	15860	-0.0202

TABLE 11

Layer 'H'

PROFILE						
H 1	H 2	H 3	H 4	H 5	H 6	H 7

X INCHES FROM START OF SUCTION

-0.13	2.25	4.75	8.75	12.75	16.75	20.75

REFERENCE REYNOLDS NUMBER PER INCH UREF/ν

37980	38010	38230	38155	37990	37960	37960

FREE STREAM VELOCITY U1 FT/SEC

108.25	101.96	96.27	89.69	83.18	77.94	71.96

REYNOLDS NUMBER PER INCH U1/ν

56031	52254	49271	45904	42979	40147	37070

SUCTION VELOCITY RATIO VO/U1

0.0000	-0.0062	-0.0078	-0.0094	-0.0092	-0.0103	-0.0111

MOMENTUM THICKNESS (THETA) INCHES

0.0785	0.0981	0.1096	0.1226	0.1325	0.1484	0.1762

DISPLACEMENT THICKNESS (DELTA-STAR) INCHES

0.1227	0.1566	0.1718	0.1856	0.1962	0.2189	0.2676

SHAPE FACTOR H

1.562	1.597	1.568	1.514	1.481	1.475	1.519

R-THETA

4400	5126	5399	5629	5694	5958	6531

Y INCHES	U/U1	Y INCHES	U/U1	Y INCHES	U/U1	Y INCHES	U/U1	Y INCHES	U/U1	Y INCHES	U/U1	Y INCHES	U/U1
0.9020	1.0000	0.9010	1.0000	1.0010	1.0000	1.1600	1.0000	1.2080	1.0000	1.2580	1.0000	1.3625	1.0000
0.8020	1.0000	0.8510	1.0000	0.9010	1.0000	1.1100	1.0000	1.1580	1.0000	1.1580	1.0000	1.2625	1.0000
0.7020	0.9987	0.8010	0.9986	0.8510	0.9988	1.0600	0.9996	1.1080	0.9995	1.1080	0.9994	1.1625	0.9944
0.6520	0.9952	0.7500	0.9948	0.8010	0.9957	1.0100	0.9991	1.0580	0.9995	1.0580	0.9988	1.1125	0.9888
0.6020	0.9878	0.7010	0.9889	0.7510	0.9894	0.9600	0.9991	1.0080	0.9984	1.0080	0.9941	1.0625	0.9804
0.5520	0.9741	0.6510	0.9776	0.7010	0.9796	0.9100	0.9978	0.9580	0.9964	0.9580	0.9881	1.0125	0.9711
0.5020	0.9566	0.6010	0.9630	0.6510	0.9648	0.9020	0.9978	0.9080	0.9927	0.9080	0.9803	0.9625	0.9545
0.4520	0.9359	0.5510	0.9426	0.6010	0.9452	0.8600	0.9946	0.9010	0.9943	0.9010	0.9760	0.9125	0.9384
0.4020	0.9120	0.5010	0.9218	0.5510	0.9236	0.8520	0.9942	0.8580	0.9869	0.8580	0.9669	0.9045	0.9332
0.3520	0.8850	0.4510	0.8959	0.5010	0.9001	0.8020	0.9874	0.8510	0.9859	0.8450	0.9626	0.8625	0.9159
0.3020	0.8571	0.4010	0.8685	0.4510	0.8689	0.7520	0.9760	0.8010	0.9743	0.8010	0.9434	0.8545	0.9152
0.2520	0.8241	0.3510	0.8351	0.4010	0.8352	0.7020	0.9621	0.7510	0.9592	0.7510	0.9231	0.8045	0.8914
0.2020	0.7831	0.3010	0.7978	0.3510	0.7946	0.6520	0.9428	0.7010	0.9412	0.7010	0.9003	0.7545	0.8677
0.1520	0.7153	0.2510	0.7453	0.3010	0.7446	0.6020	0.9173	0.6510	0.9161	0.6510	0.8737	0.7045	0.8392
0.1270	0.6670	0.2010	0.6798	0.2510	0.6921	0.5520	0.8935	0.6010	0.8891	0.6010	0.8454	0.6545	0.8166
0.1020	0.6128	0.1510	0.6060	0.2010	0.6352	0.5020	0.8588	0.5510	0.8552	0.5510	0.8177	0.6045	0.7889
0.0870	0.5763	0.1010	0.5331	0.1760	0.6090	0.4520	0.8253	0.5010	0.8274	0.5010	0.7874	0.5545	0.7639
0.0770	0.5525	0.0760	0.4988	0.1510	0.5842	0.4020	0.7892	0.4510	0.7948	0.4490	0.7599	0.5045	0.7389
0.0670	0.5268	0.0510	0.4688	0.1260	0.5570	0.3520	0.7466	0.4010	0.7608	0.4010	0.7305	0.4545	0.7122
0.0570	0.4989	0.0410	0.4561	0.1010	0.5342	0.3020	0.7072	0.3490	0.7274	0.3510	0.7008	0.4045	0.6833
0.0470	0.4740	0.0300	0.4438	0.0910	0.5246	0.2520	0.6674	0.3010	0.6923	0.3010	0.6749	0.3545	0.6585
0.0370	0.4466	0.0210	0.4303	0.0810	0.5164	0.2020	0.6315	0.2510	0.6617	0.2510	0.6481	0.3045	0.6338
0.0270	0.4186	0.0160	0.4156	0.0710	0.5096	0.1760	0.6092	0.2010	0.6328	0.2010	0.6230	0.2545	0.6149
0.0170	0.3862	0.0110	0.3898	0.0610	0.5011	0.1520	0.5935	0.1760	0.6196	0.1760	0.6124	0.2045	0.5919
0.0120	0.3607	0.0060	0.3051	0.0510	0.4964	0.1270	0.5767	0.1510	0.6043	0.1510	0.6007	0.1795	0.5764
0.0090	0.3358			0.0410	0.4901	0.1020	0.5593	0.1260	0.5930	0.1260	0.5898	0.1545	0.5704
0.0070	0.3089			0.0310	0.4821	0.0920	0.5553	0.1010	0.5780	0.1010	0.5807	0.1295	0.5581
0.0060	0.2915			0.0210	0.4765	0.0820	0.5529	0.0910	0.5762	0.0760	0.5745	0.1045	0.5543
0.0050	0.2667			0.0160	0.4699	0.0720	0.5463	0.0810	0.5717	0.0660	0.5704	0.0945	0.5531
				0.0140	0.4657	0.0620	0.5414	0.0710	0.5680	0.0560	0.5694	0.0845	0.5518
				0.0120	0.4590	0.0520	0.5381	0.0610	0.5671	0.0460	0.5652	0.0745	0.5493
				0.0100	0.4530	0.0420	0.5339	0.0510	0.5625	0.0360	0.5631	0.0645	0.5455
				0.0080	0.4364	0.0320	0.5331	0.0410	0.5588	0.0260	0.5578	0.0545	0.5429
				0.0060	0.4011	0.0220	0.5297	0.0310	0.5588	0.0160	0.5471	0.0445	0.5378
						0.0170	0.5255	0.0210	0.5523	0.0110	0.5317	0.0395	0.5365
						0.0150	0.5220	0.0170	0.5485	0.0090	0.5182	0.0345	0.5365
						0.0130	0.5195	0.0130	0.5428	0.0070	0.4864	0.0295	0.5326
						0.0110	0.5125	0.0110	0.5312	0.0050	0.4212	0.0265	0.5300
						0.0080	0.4856	0.0090	0.5174			0.0235	0.5274
						0.0060	0.4401	0.0070	0.4810			0.0205	0.5234
						0.0050	0.4139	0.0050	0.4249			0.0175	0.5140
												0.0145	0.5031
												0.0115	0.4673
												0.0085	0.3931
												0.0075	0.3561
												0.0065	0.3147
												0.0055	0.2821

TABLE 12

Layer 'H'

Smoothed Data Used in Boundary-Layer Calculations

MEAN VALUE OF REFERENCE REYNOLDS NUMBER PER INCH   38051

X INCHES	U1/UREF	VO/U1	H	R-THETA	DU1/UREF/DX
-0.10	1.476	0.00000	1.563	4430	-0.0542
0.75	1.434	-0.00394	1.585	4750	-0.0442
1.75	1.394	-0.00560	1.595	5010	-0.0354
2.25	1.377	-0.00621	1.596	5110	-0.0326
2.75	1.363	-0.00675	1.594	5190	-0.0302
3.75	1.335	-0.00743	1.583	5310	-0.0271
4.75	1.308	-0.00789	1.567	5400	-0.0248
5.75	1.285	-0.00825	1.553	5480	-0.0233
6.75	1.262	-0.00869	1.539	5540	-0.0223
7.75	1.240	-0.00914	1.527	5580	-0.0214
8.75	1.219	-0.00945	1.515	5610	-0.0205
9.75	1.199	-0.00947	1.504	5630	-0.0200
10.75	1.179	-0.00943	1.494	5645	-0.0191
11.75	1.160	-0.00932	1.486	5655	-0.0177
12.75	1.142	-0.00921	1.480	5670	-0.0163
13.75	1.127	-0.00907	1.476	5710	-0.0164
14.75	1.109	-0.00936	1.475	5770	-0.0173
15.75	1.091	-0.01008	1.475	5850	-0.0180
16.75	1.073	-0.01026	1.475	5950	-0.0185
17.75	1.055	-0.00955	1.480	6070	-0.0197
18.75	1.035	-0.00957	1.488	6200	-0.0208
19.75	1.013	-0.00990	1.501	6350	-0.0208
20.75	0.993	-0.01110	1.518	6530	-0.0200
21.75	0.974	0.00000	1.545	6770	-0.0184

TABLE 13 *Layer "H"* (BEFORE PRESSURE MINIMUM.)

PROFILES.   PROFILES CONTINUED.

	H_{2u}	H_{4u}	H_{5Bu}
X INCHES FROM START OF SUCTION			
	-13.12	-10.15	-5.90
REFERENCE REYNOLDS NUMBER PER INCH UREF/ν			
	37804	37883	38110
FREE STREAM VELOCITY U1 FT/SEC			
	106.58	106.44	114.41
REYNOLDS NUMBER PER INCH U1/ν			
	54665	54591	59396
SUCTION VELOCITY RATIO VO/U1			
	0.0000	0.0000	0.0000
MOMENTUM THICKNESS (THETA) INCHES			
	0.0575	0.0618	0.0529
DISPLACEMENT THICKNESS (DELTA-STAR) INCHES			
	0.0810	0.0863	0.0700
SHAPE FACTOR H			
	1.408	1.397	1.324
R-THETA			
	3145	3374	3142

	H_{2u}		H_{4u}		H_{5Bu}	
	Y INCHES	U/U1	Y INCHES	U/U1	Y INCHES	U/U1
	0.8080	1.0000	0.9040	1.0000	0.6960	1.0000
	0.6080	1.0000	0.8040	0.9995	0.5960	1.0000
	0.5580	1.0000	0.7040	0.9995	0.5460	0.9973
	0.5080	0.9973	0.6540	0.9991	0.4940	0.9914
	0.4580	0.9891	0.6040	0.9982	0.4460	0.9800
	0.4080	0.9726	0.5540	0.9968	0.3960	0.9613
	0.3480	0.9416	0.5040	0.9909	0.3460	0.9376
	0.3080	0.9160	0.4540	0.9777	0.2960	0.9129
	0.2580	0.8784	0.4040	0.9572	0.2460	0.8826
	0.2080	0.8348	0.3540	0.9294	0.1960	0.8527
	0.1580	0.7866	0.3040	0.8984	0.1460	0.8165
	0.1080	0.7333	0.2540	0.8604	0.0960	0.7751
	0.0830	0.7020	0.2040	0.8196	0.0710	0.7492
	0.0580	0.6665	0.1540	0.7761	0.0610	0.7382
	0.0470	0.6487	0.1290	0.7519	0.0510	0.7234
	0.0360	0.6262	0.1040	0.7244	0.0410	0.7060
	0.0280	0.6065	0.0790	0.6946	0.0310	0.6848
	0.0230	0.5907	0.0540	0.6593	0.0210	0.6559
	0.0180	0.5713	0.0440	0.6405	0.0160	0.6306
	0.0130	0.5381	0.0340	0.6191	0.0110	0.5880
	0.0110	0.5194	0.0290	0.6073	0.0080	0.5305
	0.0090	0.4845	0.0240	0.5915	0.0050	0.4044
	0.0080	0.4646	0.0190	0.5721		
	0.0070	0.4346	0.0140	0.5438		
	0.0060	0.3978	0.0120	0.5270		
	0.0050	0.3611	0.0100	0.5016		
			0.0080	0.4633		
			0.0060	0.3961		
			0.0050	0.3489		

31

TABLE 14

Layer 'J'

PROFILE

	J1	J2	J3	J4	J5	J6	J7
X INCHES FROM START OF SUCTION	-0.10	2.25	4.75	8.75	12.75	16.75	20.75
REFERENCE REYNOLDS NUMBER PER INCH UREF/ν	63790	63300	63340	63420	63340	63340	63340
FREE STREAM VELOCITY U1 FT/SEC	168.53	162.36	155.56	147.70	143.20	137.24	130.25
REYNOLDS NUMBER PER INCH U1/ν	83491	80382	77991	74289	71173	67809	64356
SUCTION VELOCITY RATIO VO/U1	0.0000	-0.0023	-0.0030	-0.0036	-0.0036	-0.0040	-0.0044
MOMENTUM THICKNESS (THETA) INCHES	0.1429	0.1610	0.1779	0.2064	0.2394	0.2823	0.3425
DISPLACEMENT THICKNESS (DELTA-STAR) INCHES	0.2526	0.2902	0.3163	0.3635	0.4262	0.5116	0.6709
SHAPE FACTOR H	1.768	1.803	1.779	1.761	1.780	1.812	1.959
R-THETA	11932	12939	13871	15333	17040	19142	22043

Y INCHES	U/U1	Y INCHES	U/U1	Y INCHES	U/U1	Y INCHES	U/U1	Y INCHES	U/U1	Y INCHES	U/U1	Y INCHES	U/U1
1.5360	1.0000	1.4135	1.0000	1.3700	1.0000	1.6630	1.0000	1.6140	1.0000	1.9425	1.0000	2.4110	1.0000
1.3860	1.0000	1.3635	1.0000	1.3200	1.0000	1.6130	1.0000	1.5640	1.0000	1.8875	1.0000	2.3110	1.0000
1.2860	0.9997	1.3135	1.0000	1.2200	0.9972	1.5630	1.0000	1.5140	1.0000	1.8375	1.0000	2.2110	1.0000
1.1860	0.9987	1.2635	1.0000	1.1200	0.9935	1.5130	1.0000	1.4140	0.9942	1.7875	1.0000	2.1110	0.9983
1.0860	0.9982	1.2135	0.9994	1.0450	0.9792	1.4630	0.9990	1.3140	0.9817	1.7645	0.9996	2.0110	0.9954
1.0360	0.9966	1.1635	0.9980	0.9950	0.9748	1.4130	0.9980	1.2140	0.9548	1.7525	0.9992	1.9110	0.9880
0.9860	0.9931	1.0885	0.9963	0.9440	0.9609	1.3130	0.9970	1.1140	0.9196	1.7325	0.9988	1.8610	0.9838
0.9360	0.9886	1.0385	0.9923	0.9130	0.9474	1.2130	0.9895	1.0390	0.8850	1.7225	0.9977	1.8110	0.9748
0.9010	0.9841	0.9885	0.9860	0.8900	0.9415	1.1130	0.9715	0.9890	0.8580	1.7155	0.9969	1.7610	0.9661
0.8840	0.9801	0.9385	0.9776	0.8690	0.9330	1.0380	0.9475	0.9390	0.8323	1.6645	0.9957	1.7120	0.9555
0.8740	0.9771	0.9065	0.9662	0.8130	0.9107	0.9880	0.9295	0.9050	0.8120	1.5645	0.9855	1.6630	0.9413
0.8240	0.9665	0.8835	0.9642	0.7630	0.8837	0.9380	0.9055	0.8630	0.7889	1.4645	0.9683	1.5630	0.9083
0.7730	0.9537	0.8735	0.9603	0.7130	0.8519	0.9040	0.8897	0.8550	0.7834	1.3645	0.9395	1.4630	0.8693
0.7240	0.9361	0.8615	0.9571	0.6630	0.8192	0.8650	0.8674	0.8050	0.7561	1.2645	0.8976	1.3630	0.8283
0.6730	0.9171	0.8565	0.9550	0.6130	0.7848	0.8540	0.8642	0.7550	0.7283	1.1645	0.8565	1.2630	0.7842
0.6240	0.8924	0.8165	0.9385	0.5630	0.7451	0.8040	0.8340	0.7050	0.7004	1.0645	0.8075	1.1630	0.7384
0.5730	0.8590	0.7565	0.9171	0.5130	0.7088	0.7540	0.8042	0.6550	0.6729	1.0145	0.7832	1.0630	0.6908
0.5240	0.8249	0.7065	0.8914	0.4630	0.6692	0.7040	0.7729	0.6050	0.6442	0.9645	0.7599	1.0130	0.6711
0.4730	0.7851	0.6565	0.8619	0.4130	0.6300	0.6540	0.7407	0.5550	0.6166	0.9145	0.7330	0.9630	0.6472
0.4240	0.7398	0.6065	0.8291	0.3630	0.5913	0.6040	0.7075	0.5050	0.5888	0.9055	0.7282	0.9130	0.6267
0.3740	0.6928	0.5565	0.7884	0.3130	0.5515	0.5540	0.6752	0.4550	0.5629	0.8945	0.7215	0.9040	0.6194
0.3240	0.6436	0.5065	0.7500	0.2630	0.5153	0.5040	0.6429	0.4050	0.5374	0.8555	0.7051	0.8730	0.6092
0.2740	0.5894	0.4565	0.7056	0.2130	0.4802	0.4540	0.6094	0.3550	0.5167	0.8055	0.6840	0.8640	0.6028
0.2240	0.5419	0.4065	0.6620	0.1880	0.4646	0.4040	0.5787	0.3050	0.4906	0.7555	0.6549	0.8540	0.6003
0.1990	0.5155	0.3565	0.6190	0.1630	0.4484	0.3540	0.5474	0.2550	0.4685	0.7055	0.6334	0.8040	0.5797
0.1740	0.4926	0.3065	0.5723	0.1390	0.4345	0.3040	0.5188	0.2050	0.4487	0.6555	0.6086	0.7540	0.5568
0.1490	0.4690	0.2565	0.5312	0.1130	0.4216	0.2540	0.4907	0.1800	0.4381	0.6055	0.5854	0.7040	0.5350
0.1240	0.4472	0.2315	0.5077	0.0870	0.4069	0.2040	0.4667	0.1550	0.4297	0.5555	0.5619	0.6540	0.5165
0.0990	0.4230	0.2065	0.4847	0.0630	0.3946	0.1790	0.4534	0.1300	0.4204	0.5055	0.5407	0.6040	0.4942
0.0740	0.4039	0.1815	0.4651	0.0530	0.3691	0.1540	0.4413	0.1050	0.4130	0.4555	0.5178	0.5540	0.4754
0.0490	0.3756	0.1565	0.4456	0.0430	0.3827	0.1290	0.4305	0.0800	0.4033	0.4035	0.4955	0.5040	0.4578
0.0390	0.3627	0.1315	0.4259	0.0330	0.3746	0.1040	0.4217	0.0550	0.3943	0.3555	0.4787	0.4540	0.4390
0.0340	0.3547	0.1065	0.4082	0.0280	0.3705	0.0790	0.4112	0.0450	0.3915	0.3055	0.4587	0.4040	0.4214
0.0300	0.3479	0.0815	0.3908	0.0230	0.3655	0.0540	0.4020	0.0350	0.3874	0.2555	0.4418	0.3540	0.4019
0.0250	0.3380	0.0565	0.3728	0.0180	0.3579	0.0440	0.3969	0.0250	0.3794	0.2055	0.4247	0.3040	0.3899
0.0200	0.3269	0.0465	0.3638	0.0160	0.3513	0.0340	0.3926	0.0200	0.3748	0.1805	0.4173	0.2540	0.3746
0.0150	0.3125	0.0365	0.3557	0.0140	0.3475	0.0240	0.3857	0.0150	0.3650	0.1555	0.4107	0.2040	0.3586
0.0120	0.2969	0.0265	0.3453	0.0120	0.3376	0.0140	0.3696	0.0100	0.3425	0.1305	0.4021	0.1790	0.3519
0.0100	0.2833	0.0215	0.3370	0.0100	0.3237	0.0110	0.3612	0.0080	0.3243	0.1055	0.3947	0.1540	0.3457
0.0080	0.2594	0.0165	0.3242	0.0080	0.2970	0.0090	0.3479	0.0060	0.2891	0.0805	0.3892	0.1290	0.3394
0.0060	0.2250	0.0135	0.3140	0.0060	0.2535	0.0070	0.3268			0.0555	0.3770	0.1040	0.3329
0.0050	0.2052	0.0105	0.2941	0.0050	0.2311					0.0455	0.3744	0.0790	0.3250
		0.0085	0.2685							0.0355	0.3697	0.0540	0.3169
		0.0075	0.2517							0.0255	0.3601	0.0440	0.3142
		0.0065	0.2282							0.0205	0.3530	0.0340	0.3086
		0.0055	0.2053							0.0155	0.3446	0.0230	0.2986
		0.0045	0.1892							0.0105	0.3242	0.0190	0.2913
										0.0085	0.3100	0.0140	0.2721
										0.0065	0.2858	0.0090	0.2363
												0.0070	0.2080

TABLE 15

Layer 'J'

Smoothed Data Used in Boundary-Layer Calculations

MEAN VALUE OF REFERENCE REYNOLDS NUMBER PER INCH 63414

X INCHES	U1/UREF	VO/U1	H	R-THETA	DU1/UREF/DX
-0.10	1.313	0.00000	1.768	11930	-0.0330
0.75	1.291	-0.00136	1.796	12320	-0.0161
1.75	1.279	-0.00205	1.806	12740	-0.0115
2.25	1.274	-0.00233	1.804	12940	-0.0115
2.75	1.268	-0.00256	1.799	13130	-0.0120
3.75	1.255	-0.00285	1.788	13500	-0.0131
4.75	1.242	-0.00300	1.778	13860	-0.0145
5.75	1.227	-0.00313	1.769	14220	-0.0154
6.75	1.211	-0.00330	1.764	14590	-0.0157
7.75	1.196	-0.00358	1.761	14970	-0.0155
8.75	1.180	-0.00364	1.761	15350	-0.0151
9.75	1.165	-0.00363	1.762	15750	-0.0142
10.75	1.152	-0.00368	1.766	16170	-0.0133
11.75	1.138	-0.00372	1.771	16610	-0.0127
12.75	1.126	-0.00364	1.778	17080	-0.0124
13.75	1.113	-0.00360	1.785	17560	-0.0124
14.75	1.101	-0.00370	1.793	18060	-0.0126
15.75	1.088	-0.00400	1.802	18610	-0.0131
16.75	1.075	-0.00402	1.812	19190	-0.0139
17.75	1.060	-0.00370	1.828	19820	-0.0146
18.75	1.045	-0.00377	1.853	20530	-0.0152
19.75	1.030	-0.00402	1.895	21280	-0.0155
20.75	1.014	-0.00439	1.960	22050	-0.0154
21.75	0.999	0.00000	2.040	22850	-0.0148

Sample of Vyon sheet used as the suction
surface in the new experiments

$$\frac{\text{Local } V_o}{\text{Mean } V_o}$$
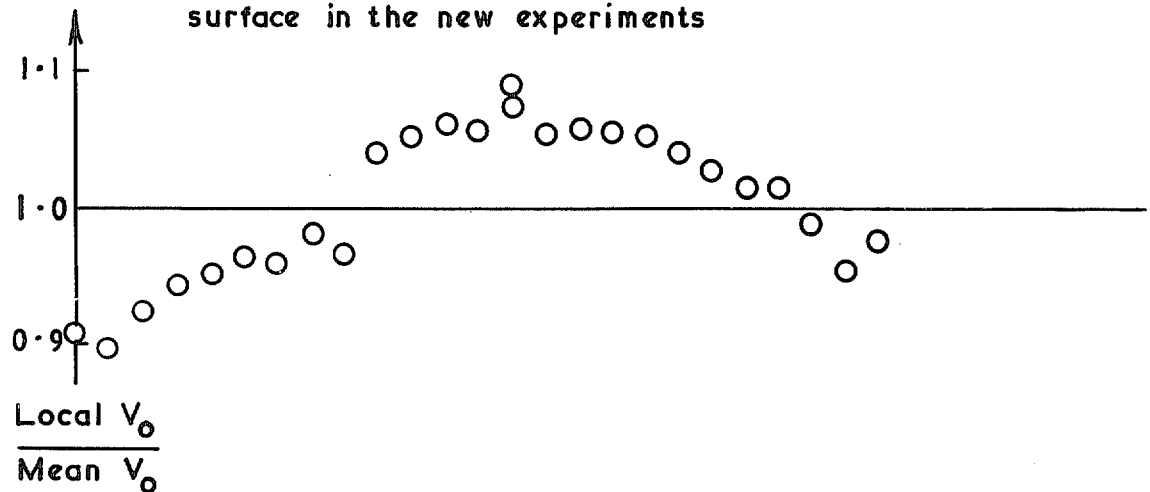
Typical results for two further sheets:~

Distance along sheet (inches)
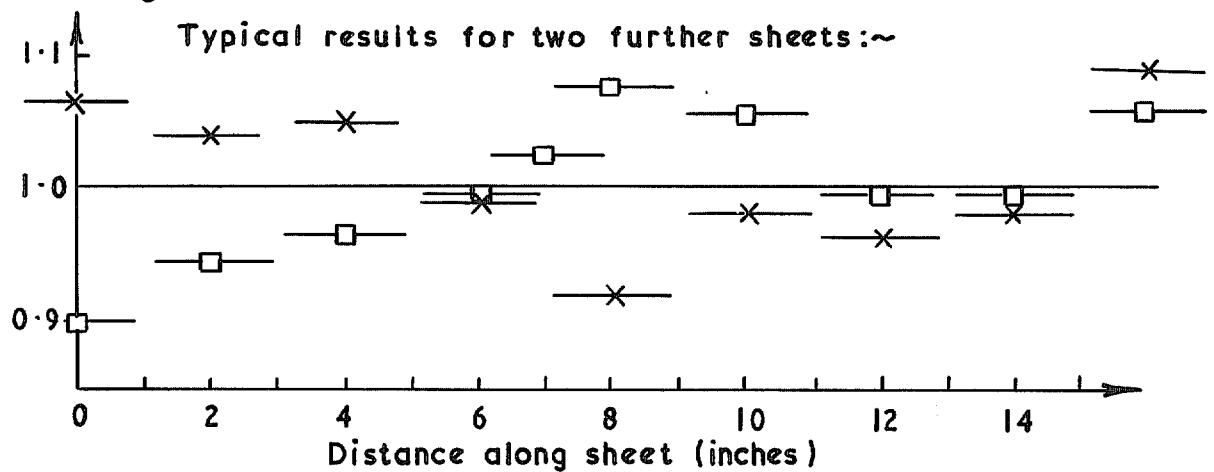
○ V_o from flow rate through area 1·54 dia.
at pressure drop of 25 cm alcohol

×}
□} V_o from measurements of McQuaid (Ref. 5)
(averages over dia, of 1·75")

FIG. 1.   Variation of suction velocity across three samples of $\frac{1}{8}''$ Vyon sheet.

CHORD 32"

SUCTION SURFACE 21½" CHORD.

* 43 INTERAL PRESSURE (Pᵢ) TAPPINGS
ONE PER CELL FROM ⅛" O.D. BRASS
TUBE; ENDS SEALED WITH SOLDER;
0·025" HOLE DRILLED IN SIDE.

1/16" PLYWOOD INNER SKIN DRILLED
WITH ONE ROW PER CELL OF
1/16" HOLES AT ¼" CENTRES.

⅛" VYON SINTERED POLYTHENE
SHEET SUCTION SURFACE.

THREE LAMINATIONS
OF 1/16" BALSA.

L.E. STATIC TAPPINGS
FROM BRASS TUBING
SLEEVED WITH HYPO.
TUBE 0·025" BORE.

⅛" × ½" PINE SPACERS.

BALSA TRAILING
EDGE COVERED
WITH ⅛" PLYWOOD.

NOSE
RADIUS
3 ¼"

PLENUM CHAMBER
PRESSURE (Pᴄ)
TAPPING GLUED
TO RIB

(A)

(A)

(A)

(A)

(A)

(A)

ALL
STRINGERS AND SPARS
FROM SPRUCE.

DETACHABLE ⅛" PLYWOOD
UNDERSURFACE HELD ON BY
WOODSCREW (A) AND TAPE
OVER ALL JOINTS.

3/16" PLYWOOD RIBS FRETTED OUT
AS SHOWN.

SCALE
0 1 2 3 4 5 6
INCHES

VYON SURFACE

℄ z = 0

DOPED TISSUE COVERED
LEADING EDGE SHEETING

* STATIC TAPPINGS 1/16" O.D. 0·03"
BORE BRASS TUBING GLUED
TO ALTERNATE SPACERS. FILED
FLUSH WITH VYON SURFACE.

z = +2"

z = 0
℄
x

z = -2"

z = z

AREA OF
ONE CELL ½ × 4"

* INTERNAL TAPPINGS IN
EACH CELL TO MONITOR
PRESSURE DROP (Pᵢ - Pᴄ)
ACROSS INNER DRILLED
PLY SKIN.

½" × ⅛"
PINE SPACERS
DOPED TO REDUCE
LEAKAGE BETWEEN CELLS.

A SINGLE SPANWISE ROW OF 1/16"
HOLES ARE DRILLED AT ¼"
SPACING IN EACH CELL.

FIG. 2.   Construction of basic suction aerofoil.
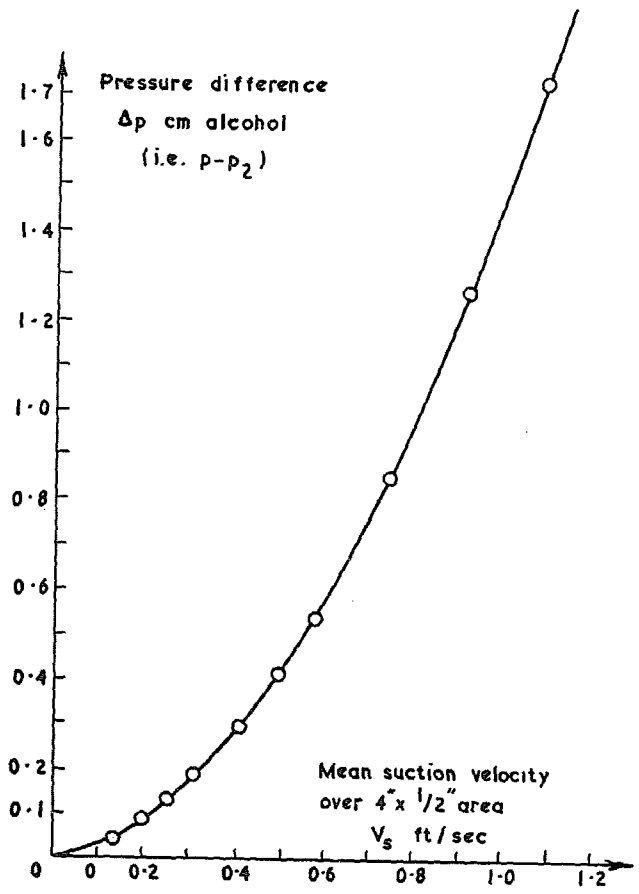
FIG. 3.   Meter calibration.
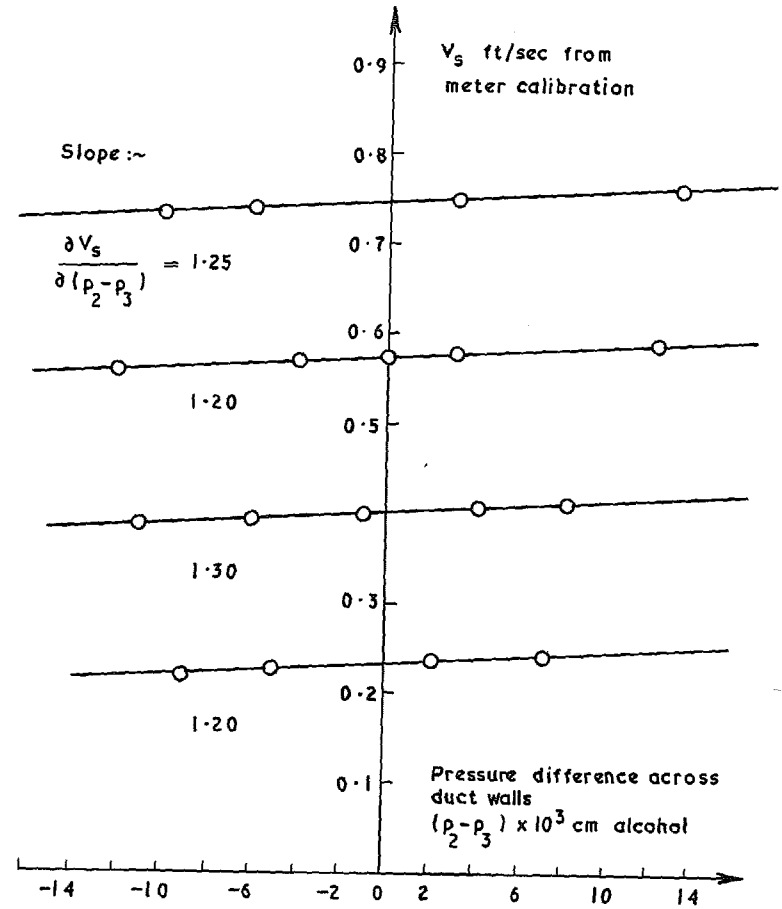
FIG. 4.   Leakage flowrate due to out-of-balance
pressure across meter duct walls.

36

37

FIG. 5. Typical cell characteristics.

Pressure drop across drilled plywood inner skin

$P_i - P_c$ cm alcohol

Distance of cells from leading edge of suction surface

● 1·5 — 2·0 inches
● 3·0 — 3·5
◇ 9·0 — 9·5
△ 14·0 — 14·5
✕ 15·0 — 15·5
+ 14·5 — 15·0
○ 15·5 — 16·0
□ 18·5 — 19·0

V_s^2 ft^2/sec^2
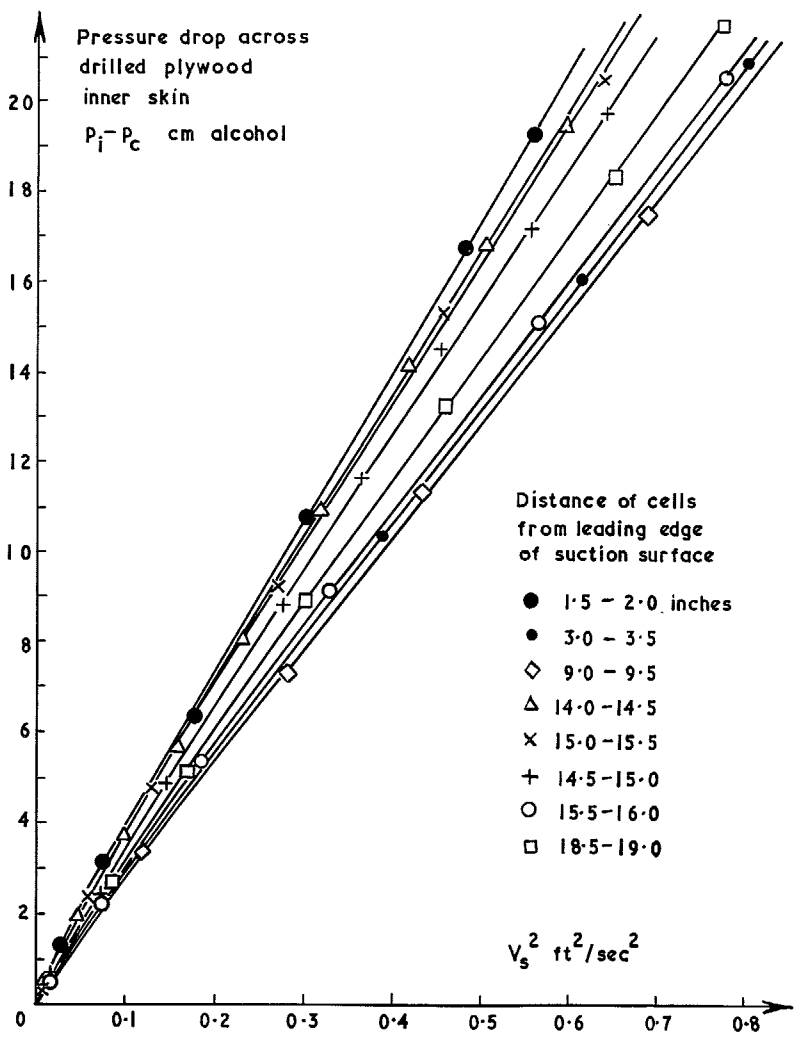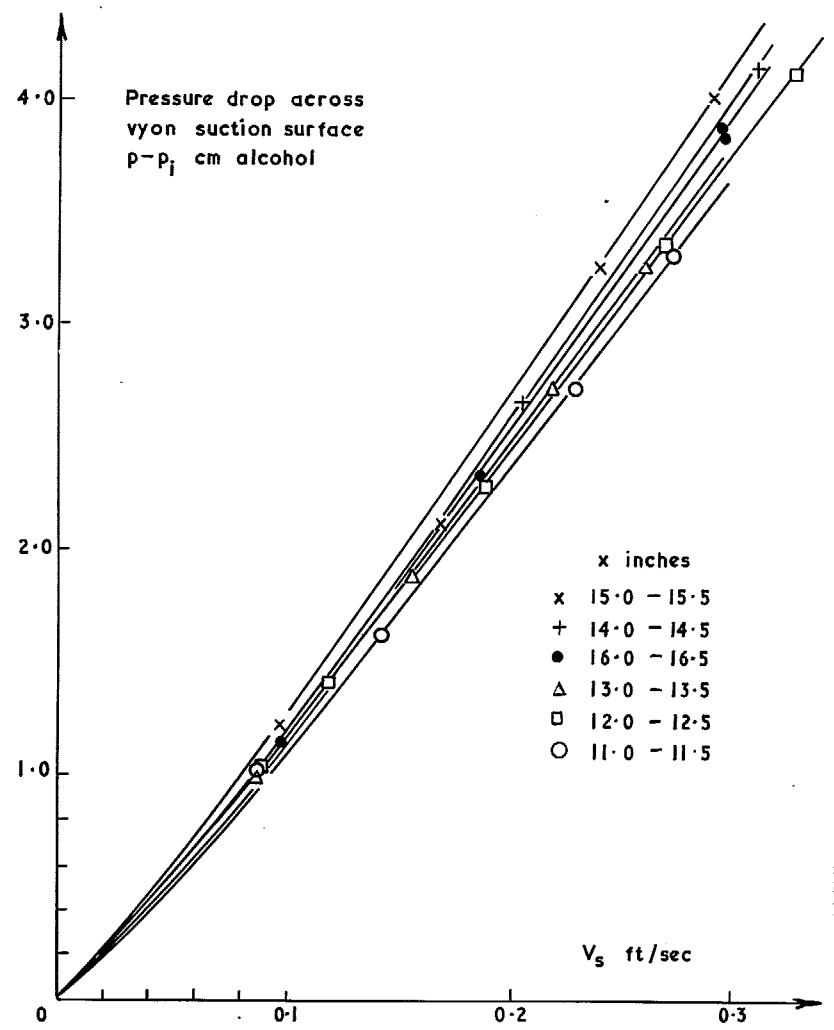
FIG. 6. Typical suction surface characteristics.

Pressure drop across vyon suction surface

$p - p_i$ cm alcohol

x inches

✕ 15·0 — 15·5
+ 14·0 — 14·5
● 16·0 — 16·5
△ 13·0 — 13·5
□ 12·0 — 12·5
○ 11·0 — 11·5

V_s ft/sec
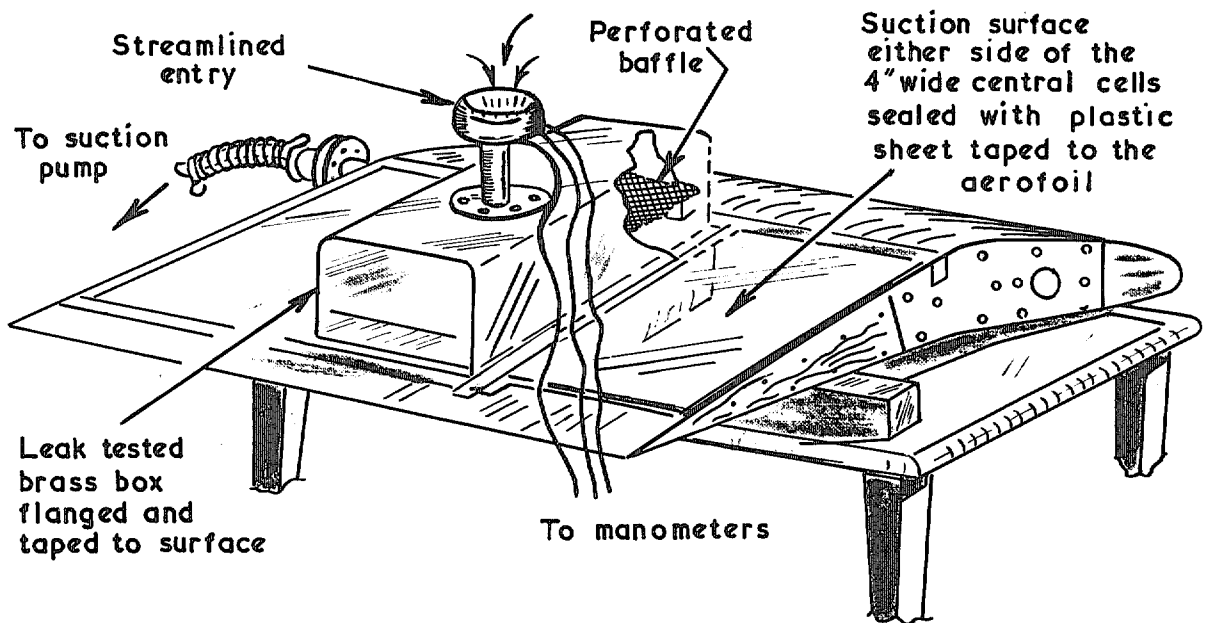
FIG. 7.   Measurement of total flow through central cells.
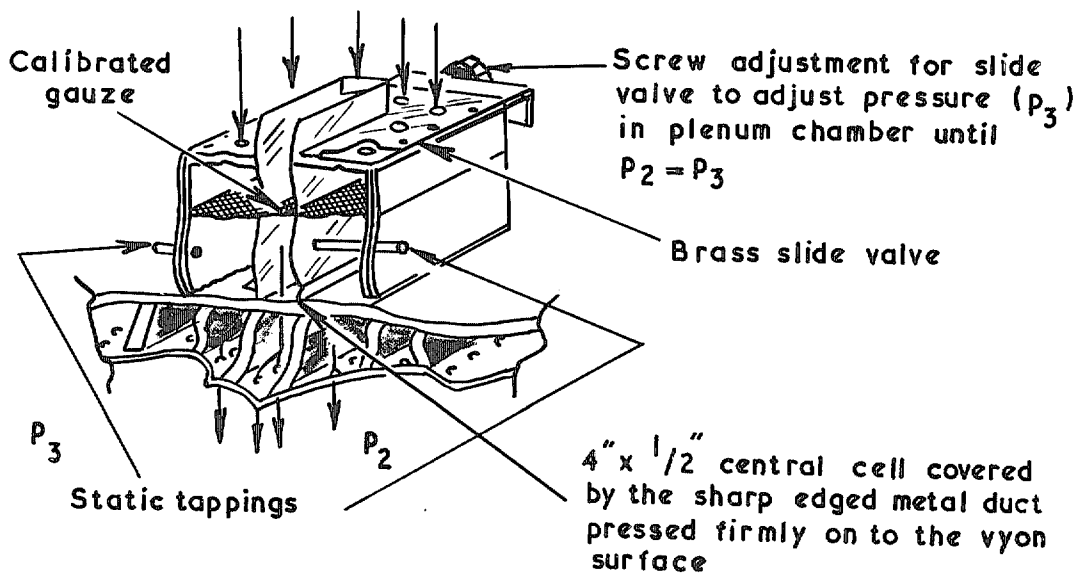
FIG. 8.   Sketch of cell calibration meter.

38

$V_{s_2} = V_s$ / ft / sec from the mean of the cell calibrations

For the boundary layer calculations, value of V_0 from cell calibrations were reduced by 5% in agreement with this mean line

$V_{s_2} = 1.05\ V_{s_1}$

$V_{s_1} = V_{s_2}$

$V_{s_1} = V_s$ ft/sec from meters

O 1" orifice and box

△ Box and $\frac{5}{8}$" streamlined entry (discharge coeff. = 0.99 assumed)

□ Gasmeter and box

39
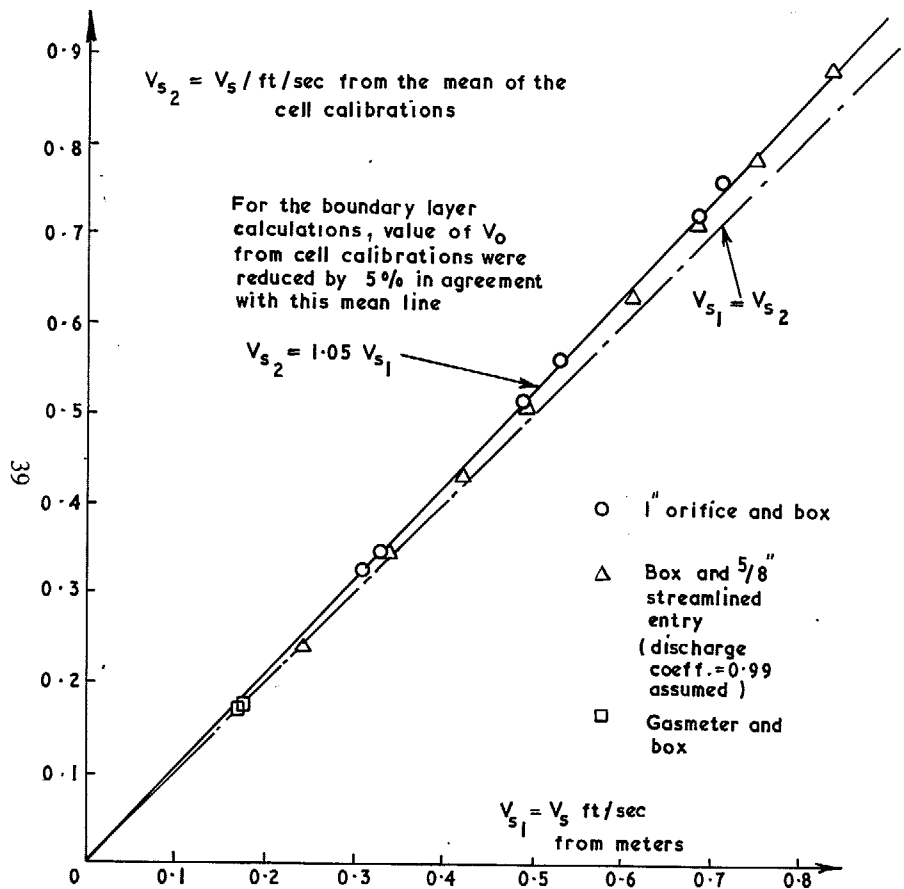
FIG. 9. Comparison of suction flow rates from cell calibrations and standard meters.

$\frac{1}{4}$" O.D STEEL TUBE STEM

SLIDING ROD CARRYING PROBE HOLDER & DRIVEN BY 1" MIC. HEAD.

PROBE HOLDER.

$\frac{1}{4}$" x $\frac{1}{16}$" STREAMLINED SECTION STEEL "FOOT" SPRUNG ON TO THE SUCTION SURFACE

SIDE VIEW OF END OF TRAVERSE GEAR SHOWING THE TRIPLE PITOT USED FOR LAYER "J" (SCALE: FULL SIZE)

STATIC TAPPINGS

$\mathⅬ\ Z = 0$

MOUTHS OF PROBES

u, U

$Z = -1"$

POSITION OF STEM FOR AEROFOIL Ⅲ (LAYER "J")

PLAN VIEW

$Z = -3"$

POSITION FOR (LAYERS "A" TO "H" INCLUSIVE)

NOTE :~ A SHORTER "FOOT" $1\frac{1}{4}$" INSTEAD OF 4" WAS USED FOR THE LAYERS "A" TO "E"

FIG. 10. Details of traverse arrangement.
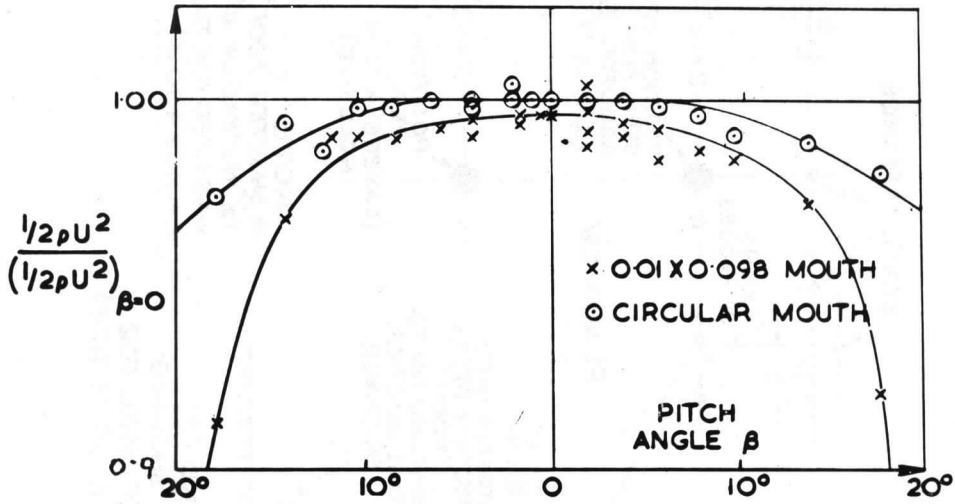
FIG. 11a. The effect of pitch angle on pitot readings (reproduced from Sarnecki[10]).
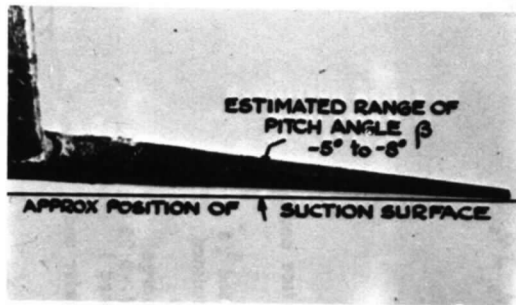
SIDE VIEW OF TYPICAL LOWER PITOT
0·007" X 0·078" MOUTH SHOWN BELOW) TOUCHING THE
"SURFACE" WITH ABOUT −5° PITCH ANGLE
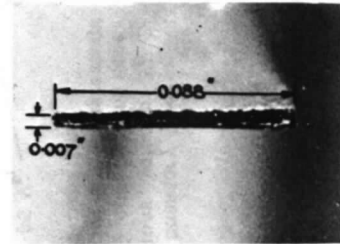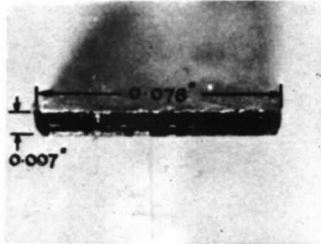
CLOSE UP VIEWS OF THE MOUTHS OF THE
TWO PITOT TUBES USED FOR MEASURING LAYERS
"D" TO "H" (LOWER PITOT ON R.H.S.)

FIG. 11b. Details of mouths of flattened pitots.

Tripwires
0·036" dia.

₵

U_∞

Suction surface

Angle of attack
$\alpha = +5^0$ for D, E; $\alpha = -6^0$ for B

Aerofoil section I (Layers "B", "D" & "E")

Tripwires
0·048" dia.

U_∞

Solid elliptic nose

Suction surface

Flap angle
$\eta \approx 17^0$

Aerofoil section II (Layers "F", "G" & "H")

Fairing added here

Tripwires
0·048" dia.

U_∞

Suction surface

Chord 58"

Flap angle $\eta \approx 12^0$

Aerofoil section III (Layer "J")
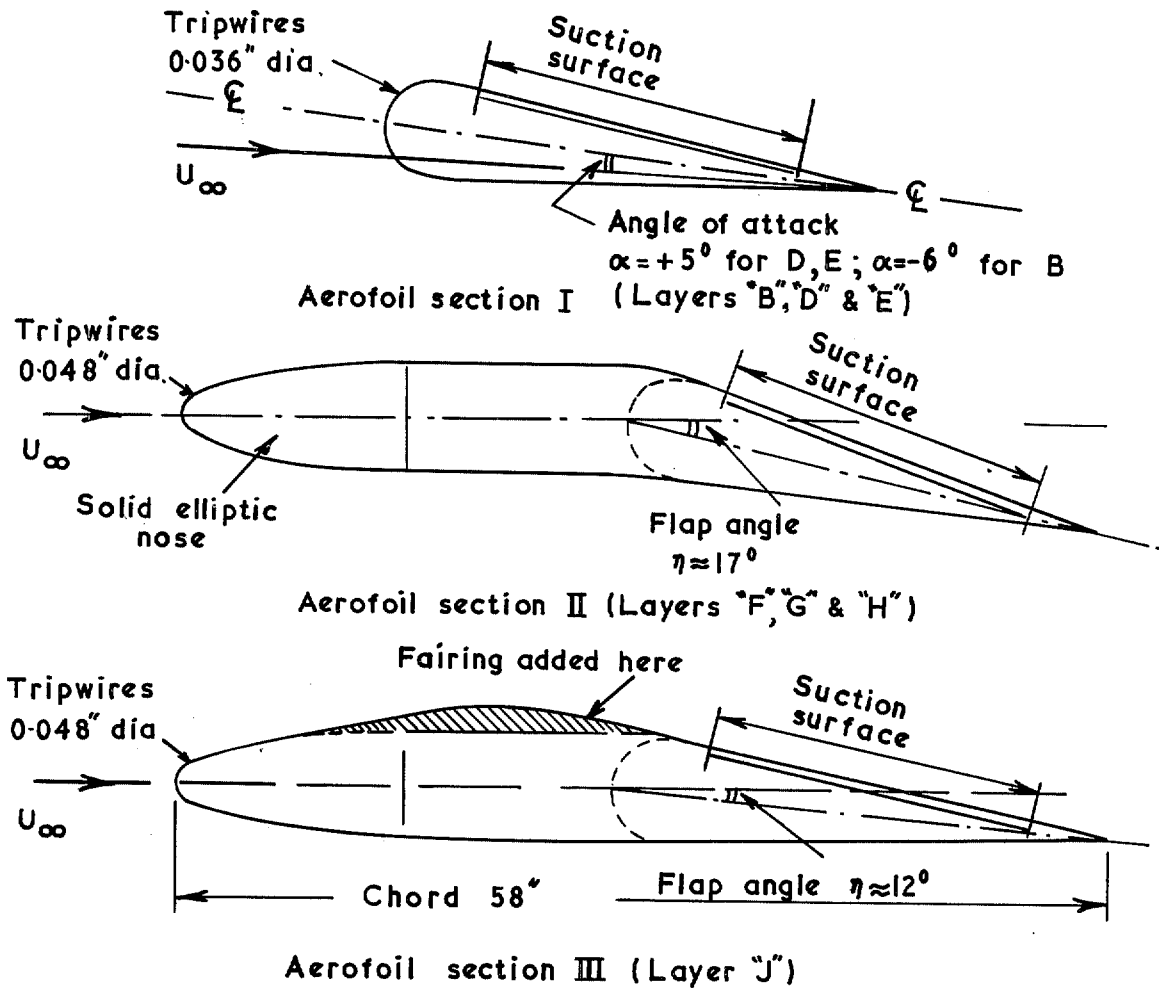
FIG. 12.   Comparison of the three aerofoil sections used in the boundary layer measurements.
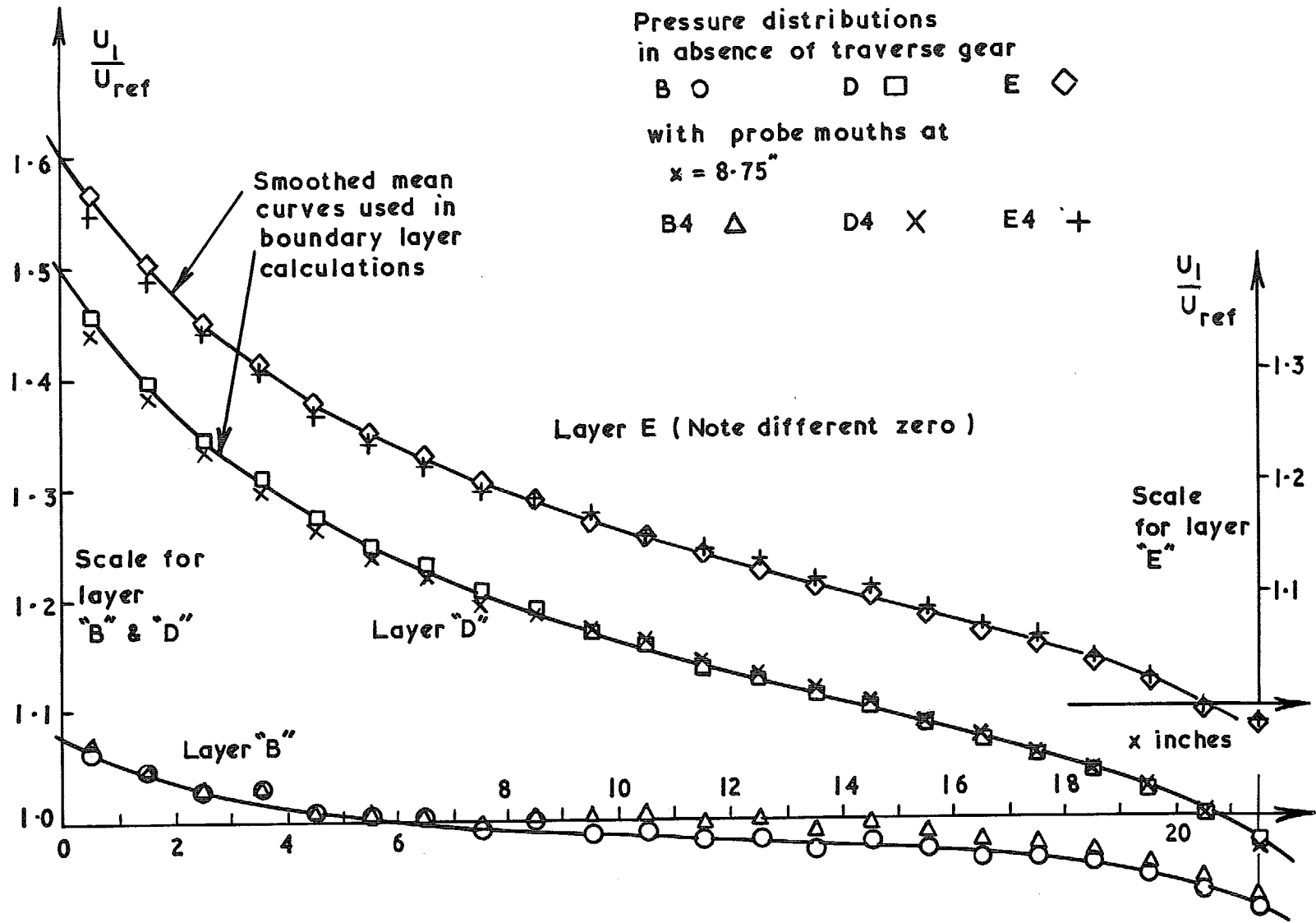
FIG. 13.   Free stream velocity distributions along centre line ($z = 0$).
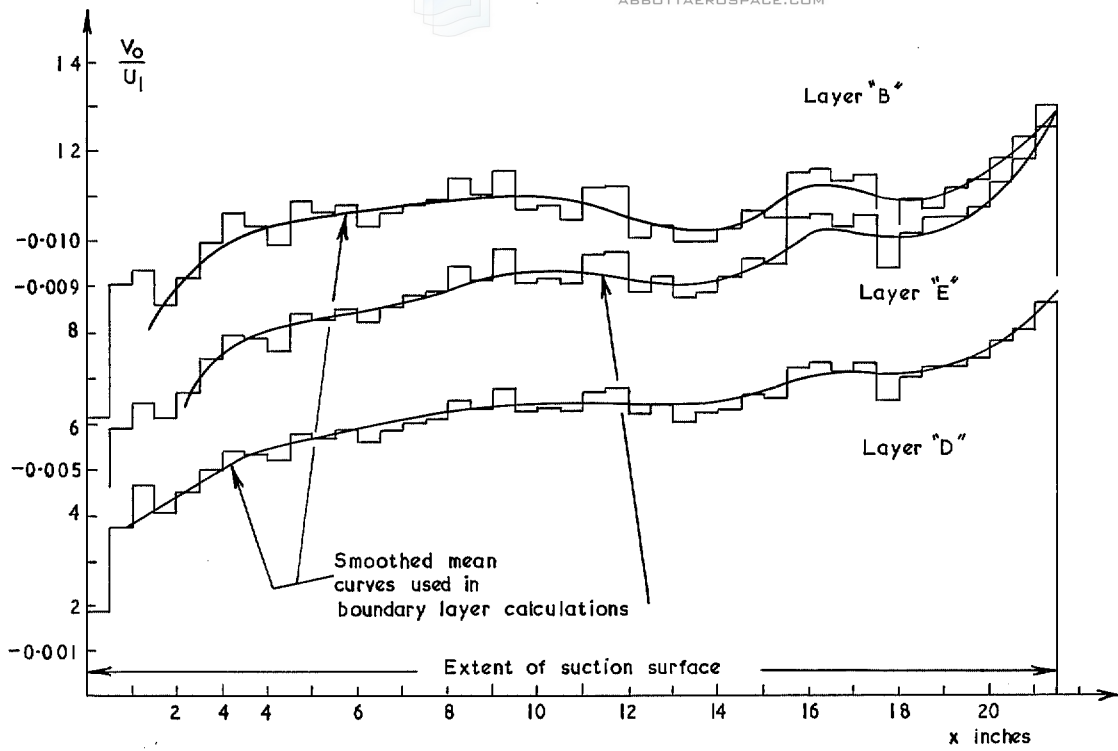
FIG. 14.   Suction velocity distributions.
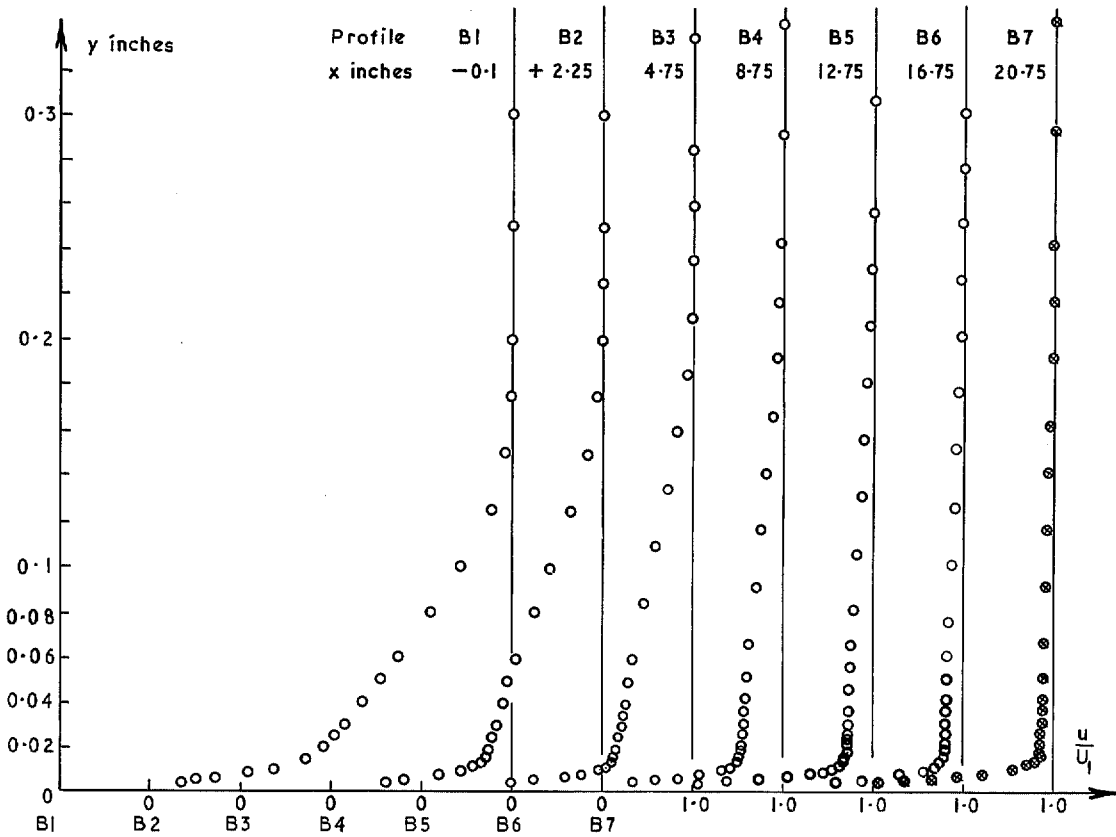
FIG. 15.   Mean velocity profiles. Layer 'B' (along $z = -1 \cdot 0''$).

43
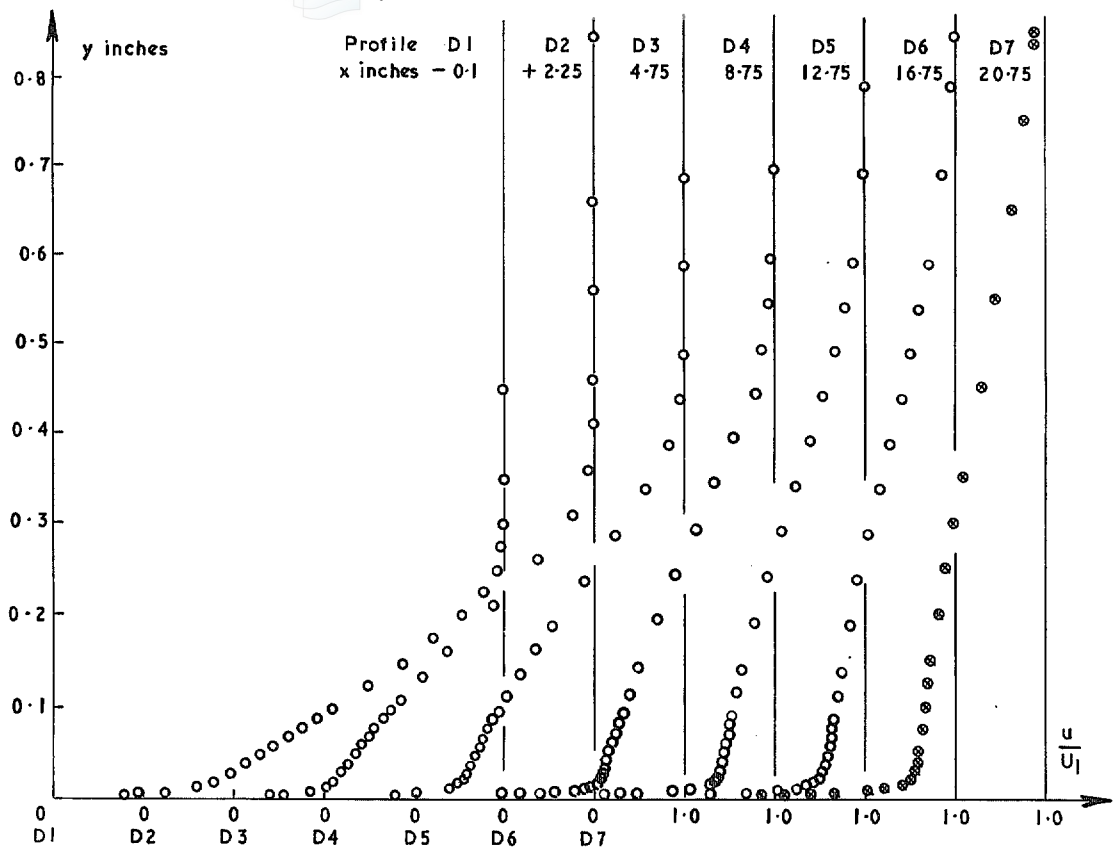
FIG. 16.   Mean velocity profiles. Layer '*D*' (along $z = -1\cdot0''$).
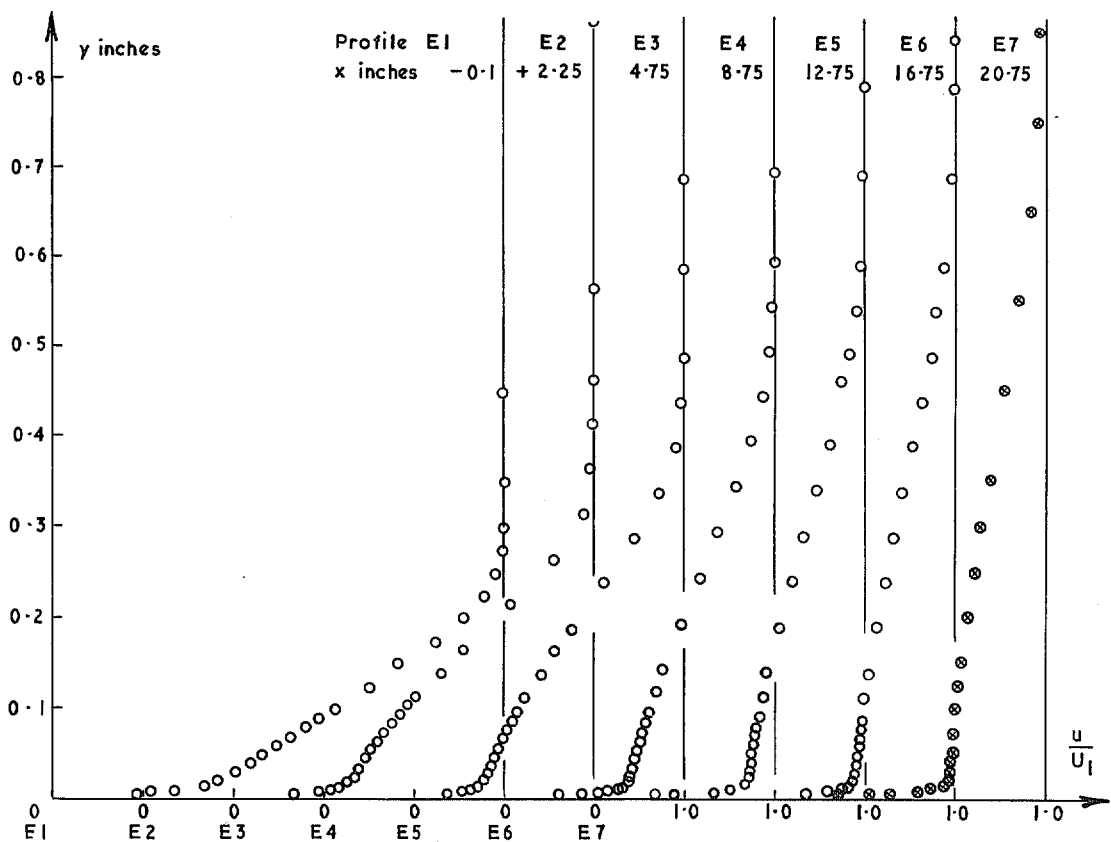
FIG. 17.   Mean velocity profiles. Layer '*E*' (along $z = -1\cdot0''$).
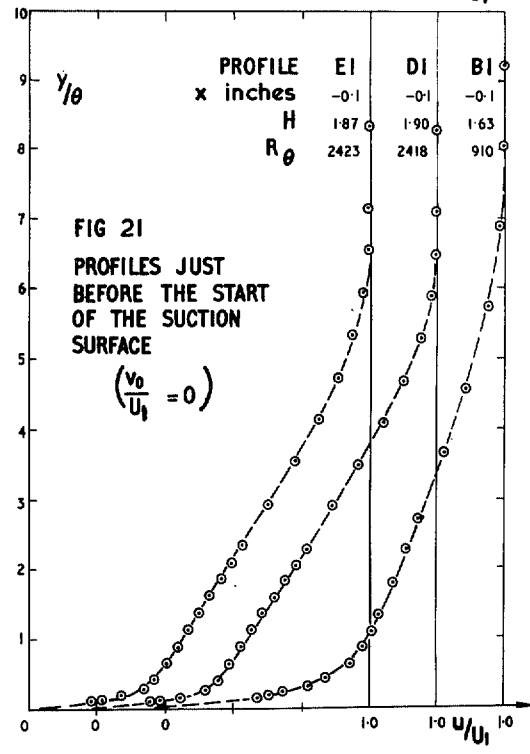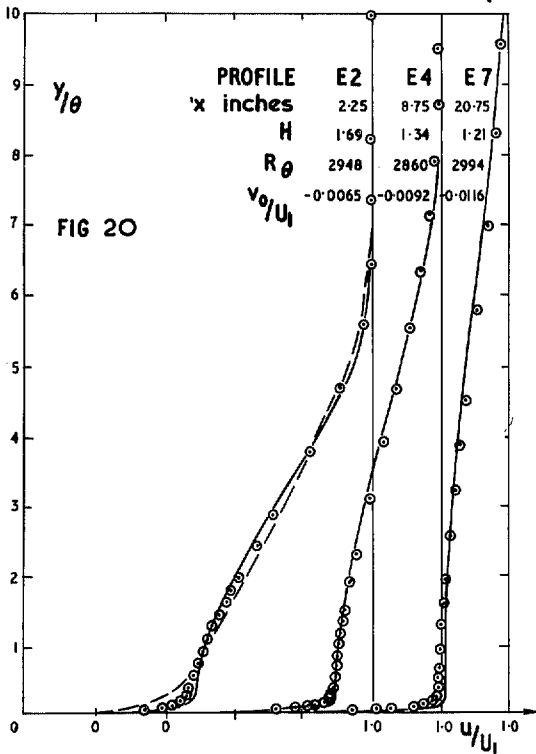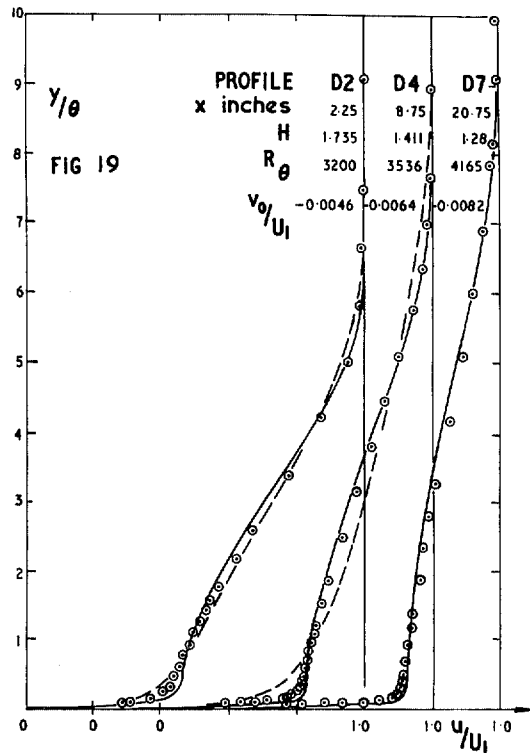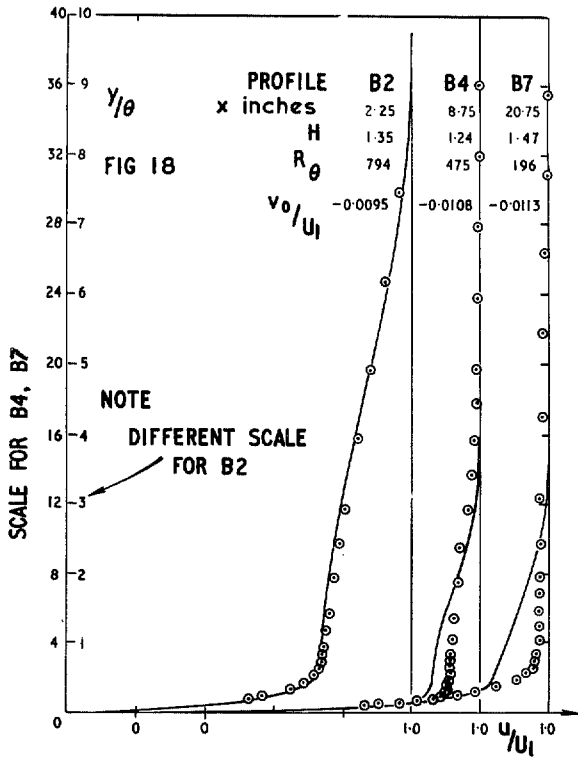
FIGS. 18 to 21. Comparison of profile family with measurements. ————Prediction of complete family (Thompson[15]). — — — — Prediction of solid surface family (Thompson[14])
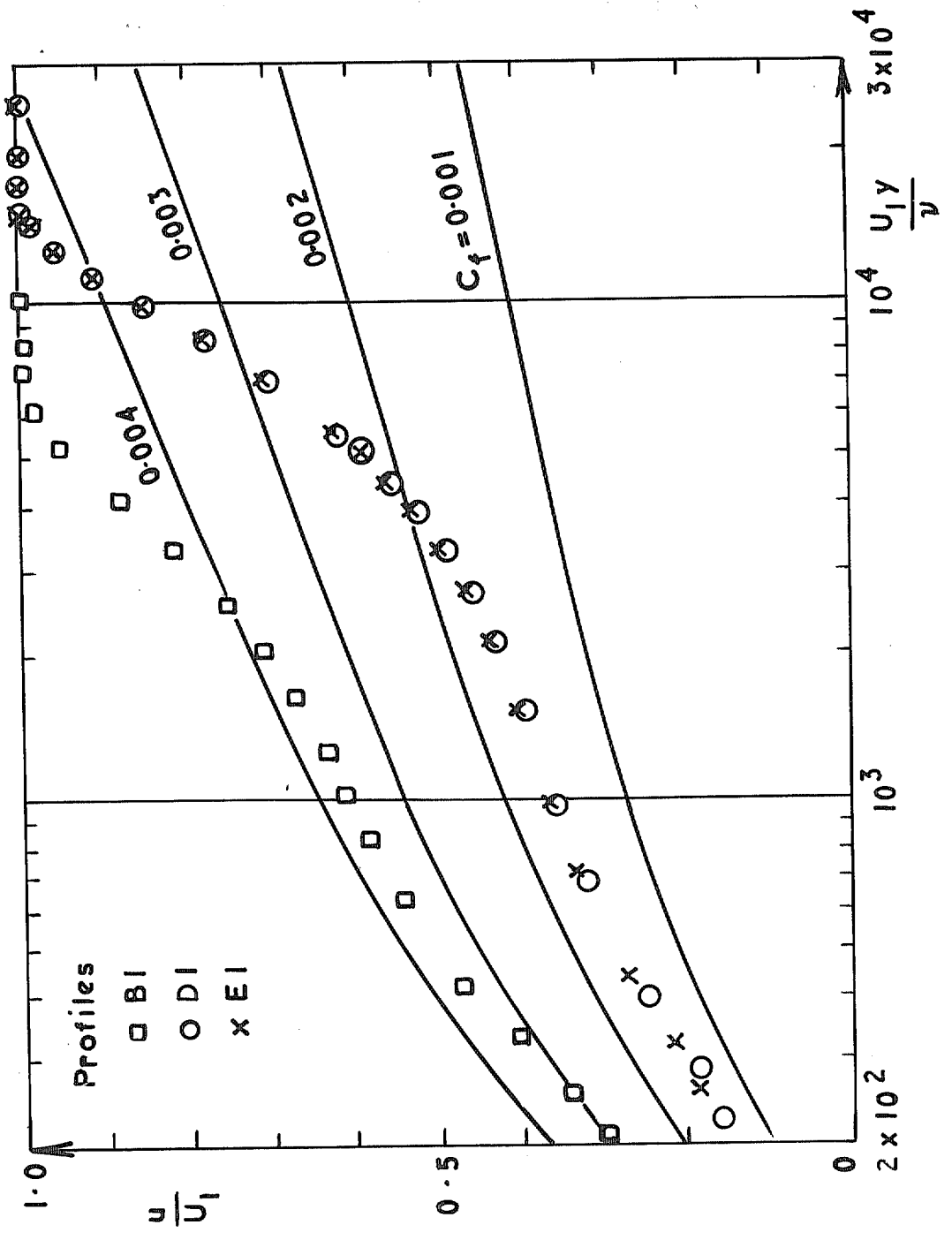
FIG. 22.   Comparison of inner region profiles (before start of suction) with

Clauser plot for $\dfrac{u}{U_\tau} = 5\cdot4 + 5\cdot5 \log_{10} \dfrac{U_\tau y}{v}$.

FIG. 23
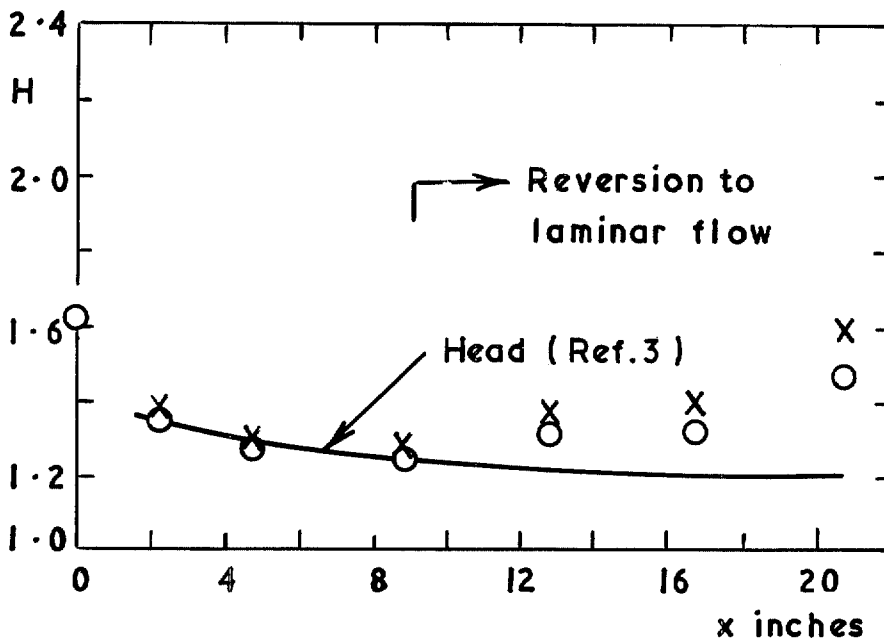
FIG. 24
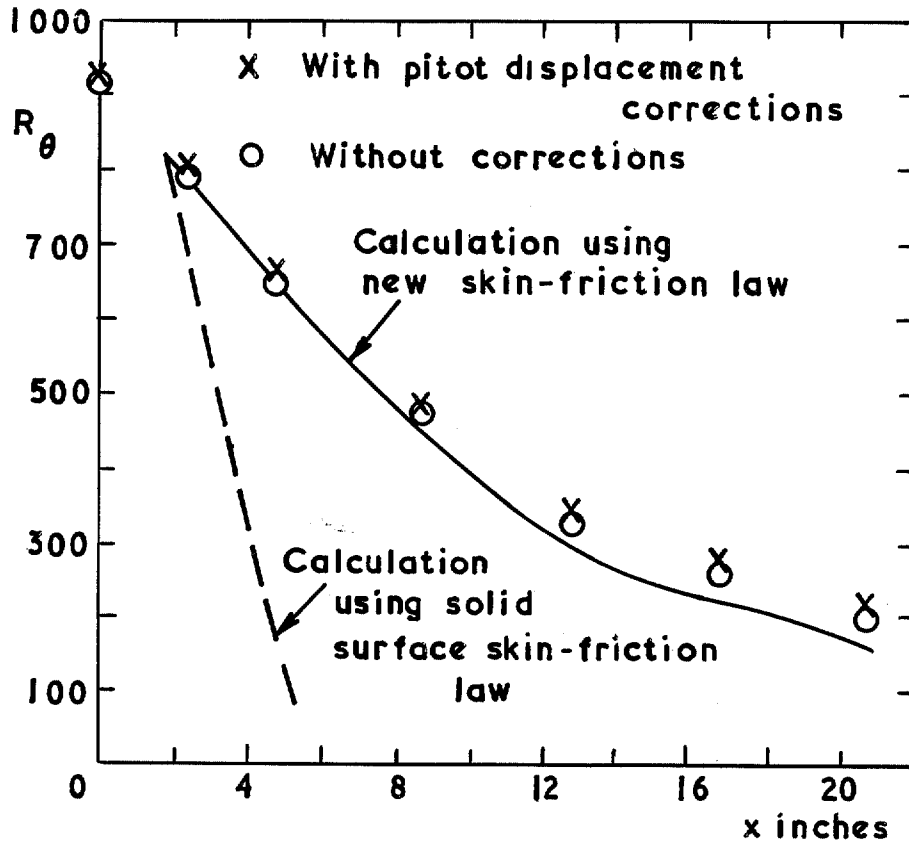
FIGS. 23 & 24.   Comparison between expt. and calculation. Layer '*B*'.

FIG. 25
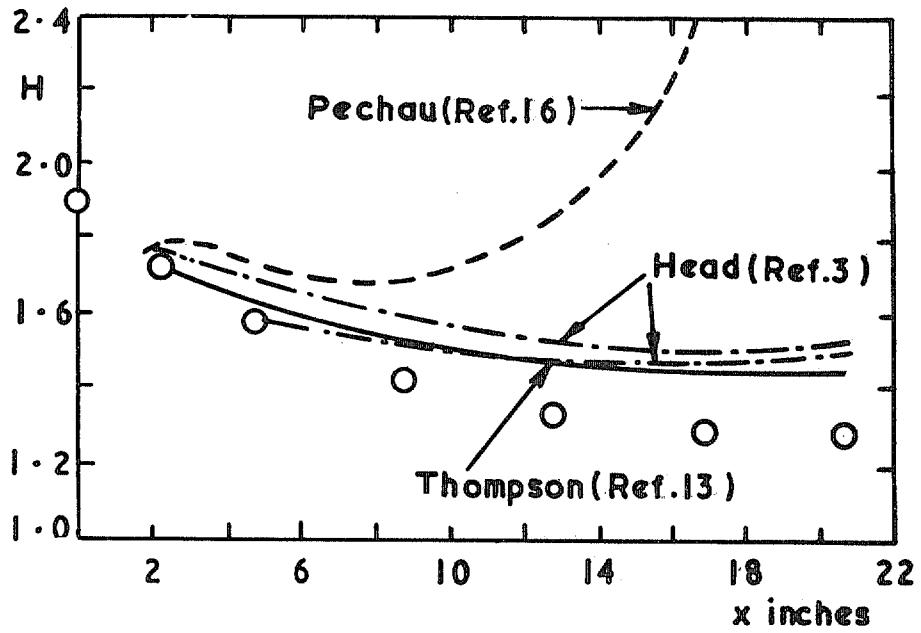
FIG. 26
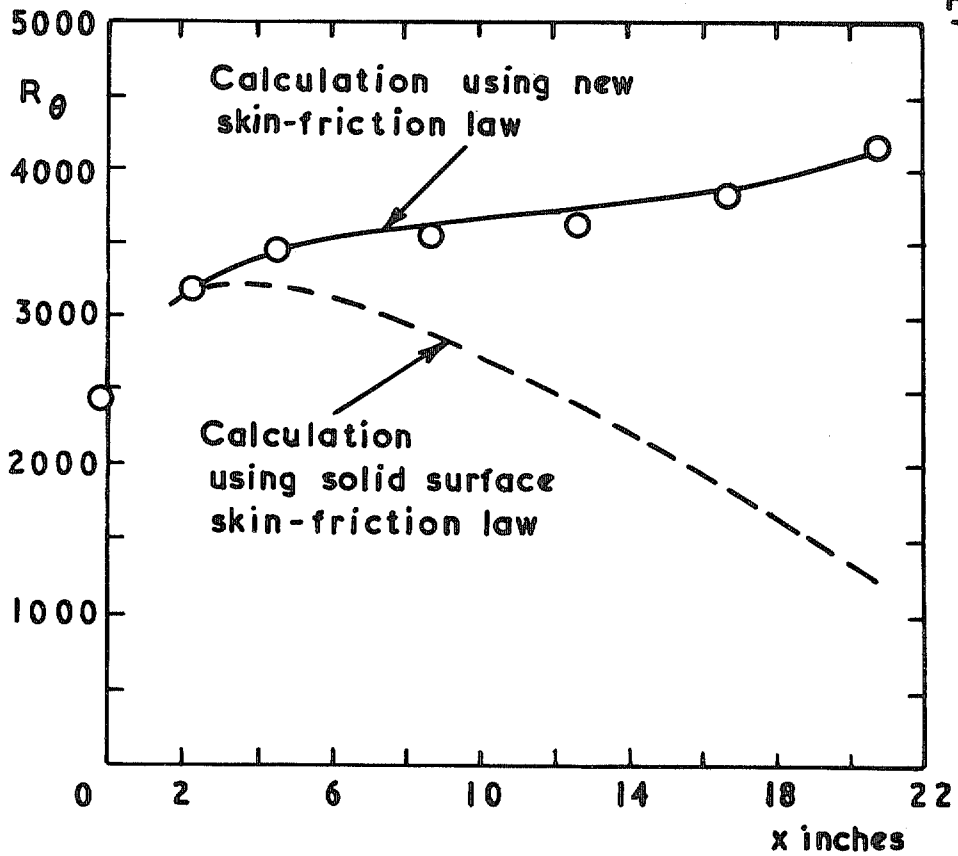
FIGS. 25 & 26.   Comparison between expt. and calculation. Layer 'D'.

FIG.27
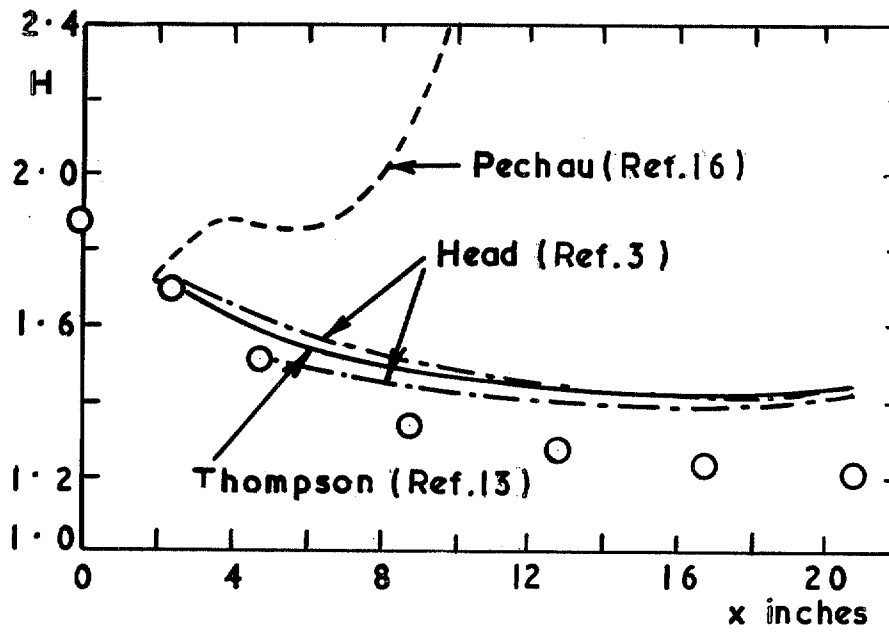
FIG.28
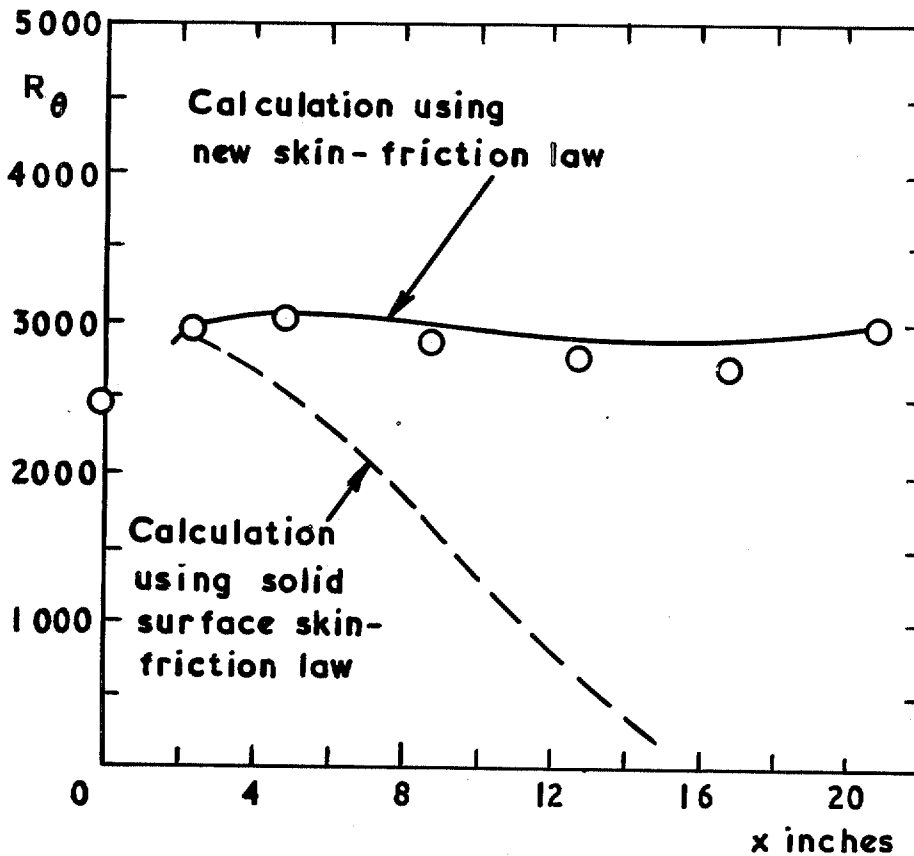
FIGS. 27 & 28.   Comparison between expt. and calculation. Layer '*E*'.

FIG. 29. Variation of inner region with suction. (Layer *B*).

FIG. 30. Sublayer behaviour in Layer *B*.
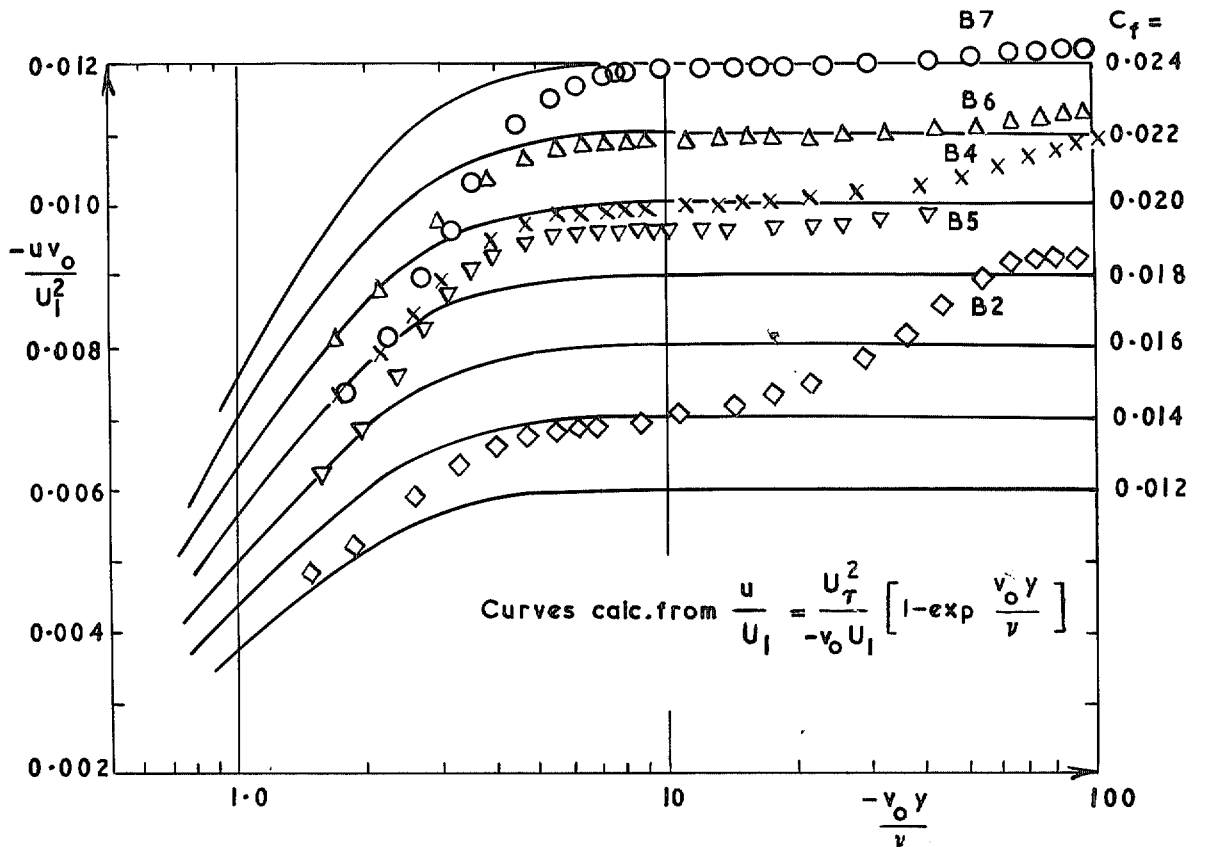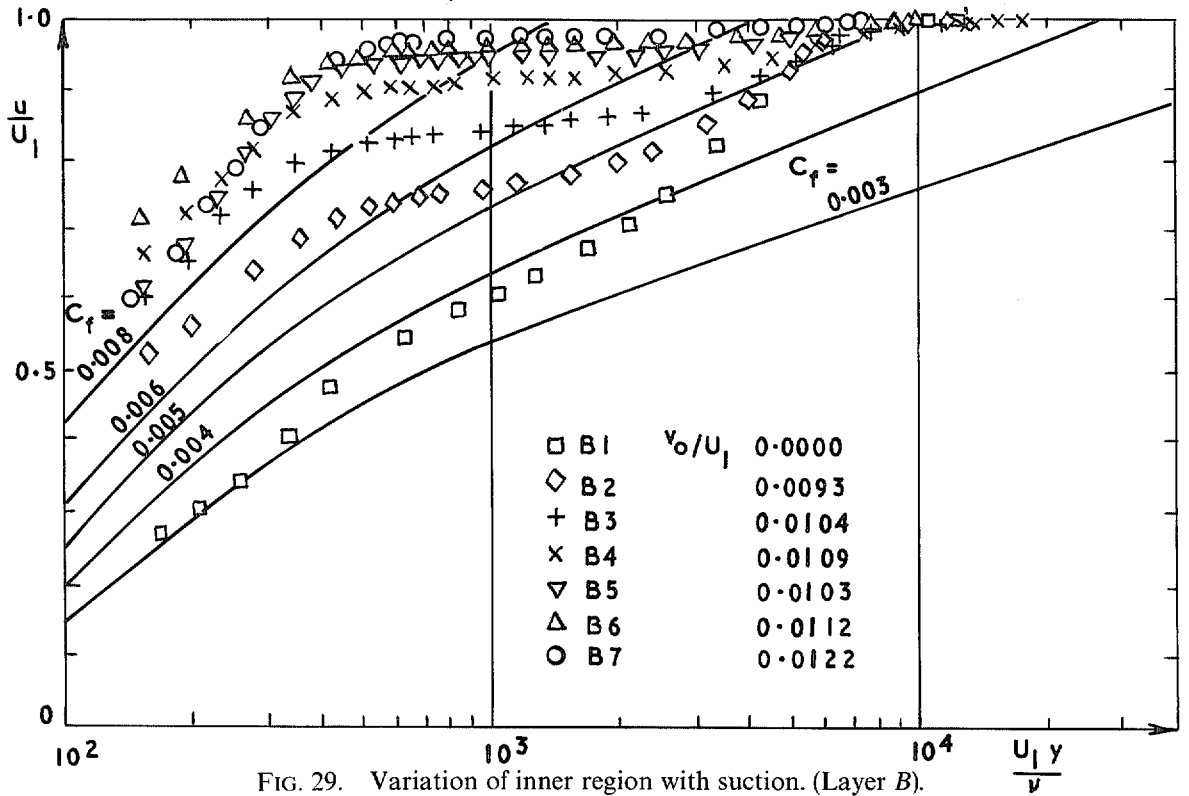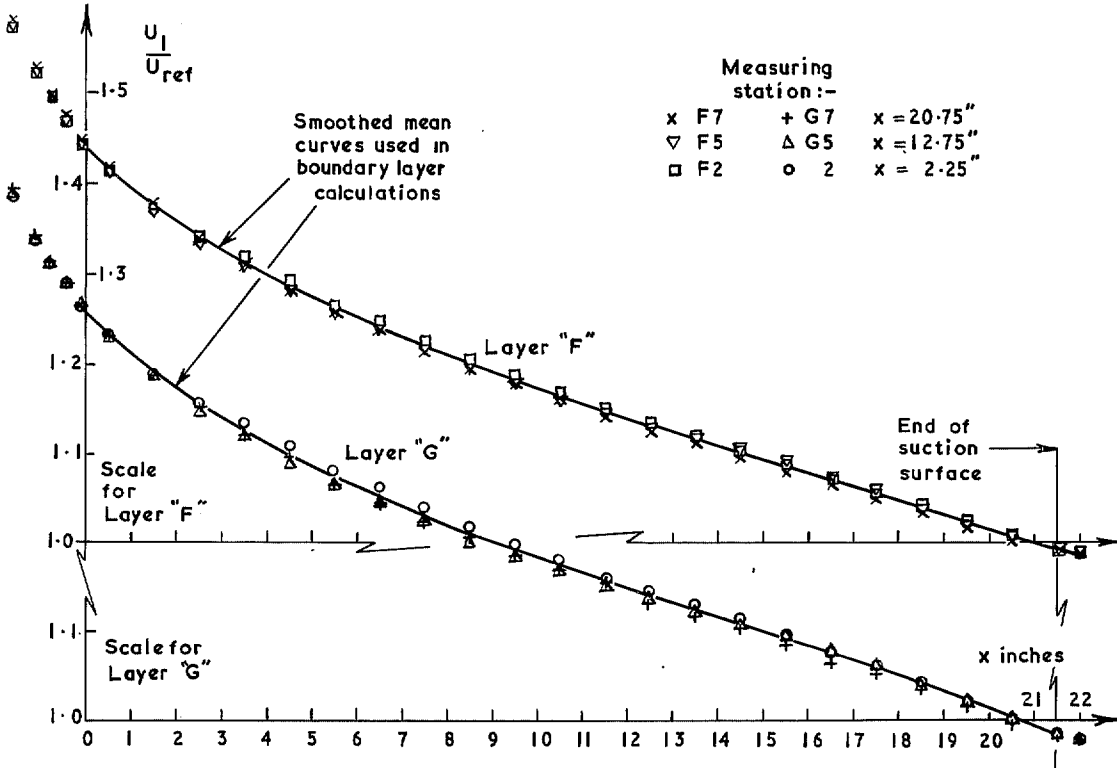
FIG. 31. Free-stream velocity distributions along the centreline ($z = 0$).
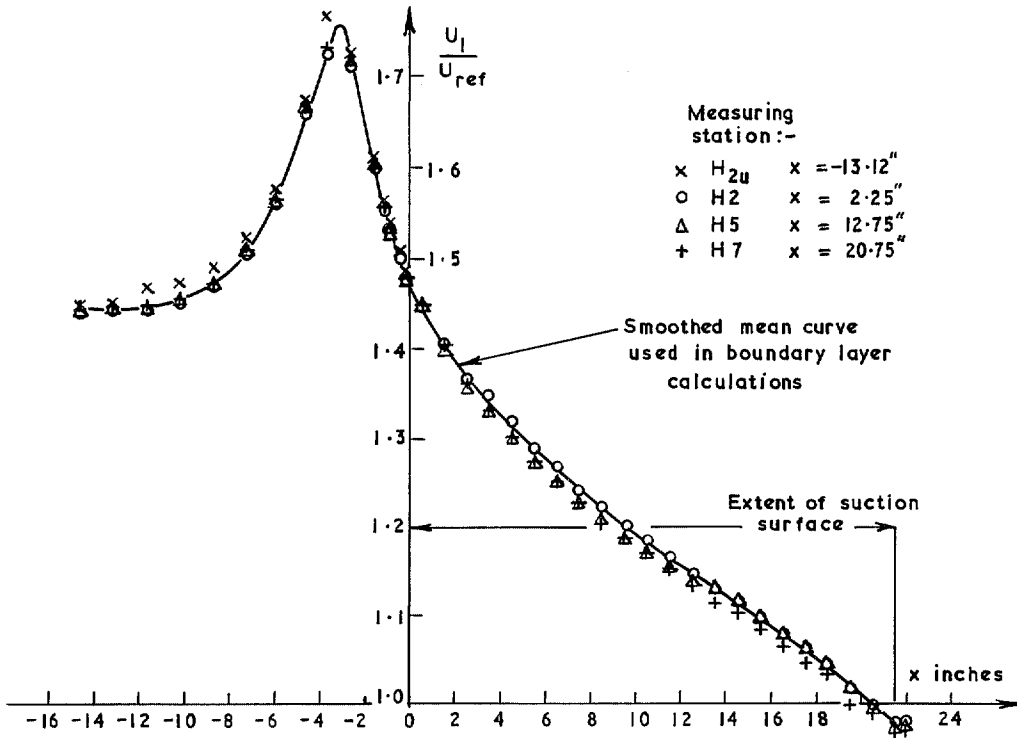
FIG. 32. Free-stream velocity distribution. Layer 'H'.
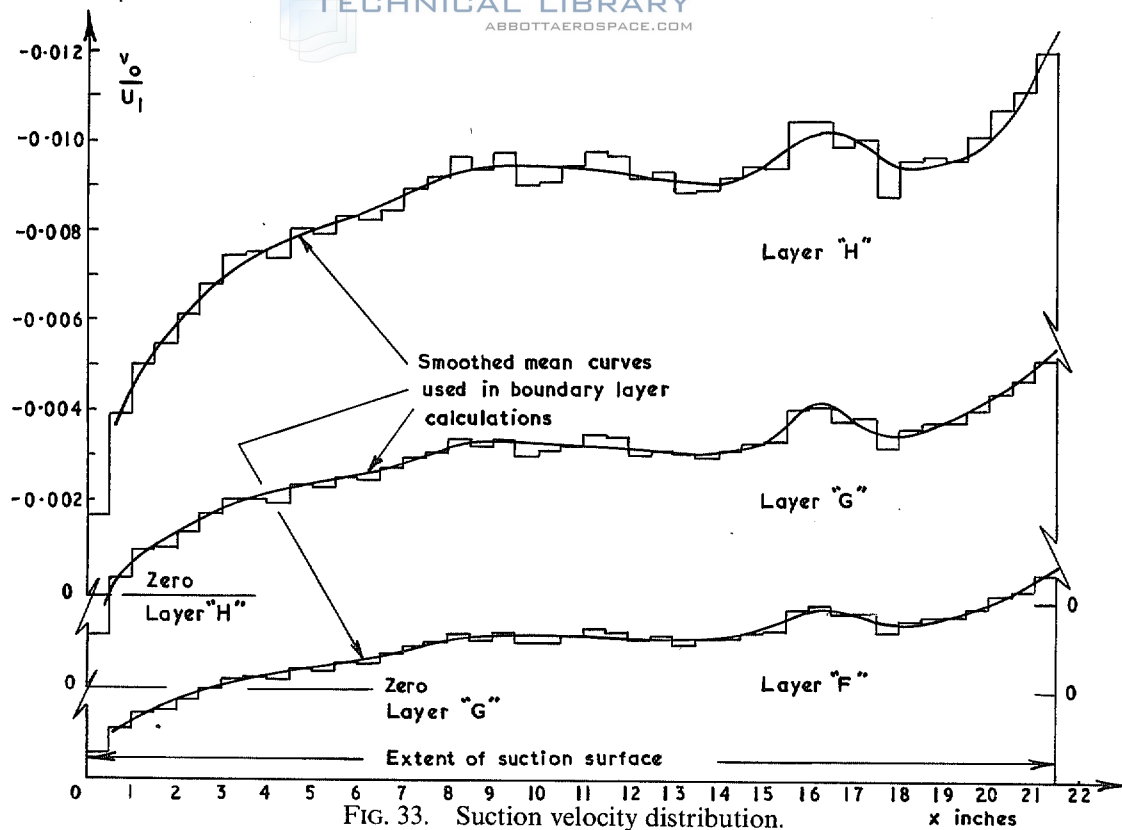
FIG. 33.   Suction velocity distribution.
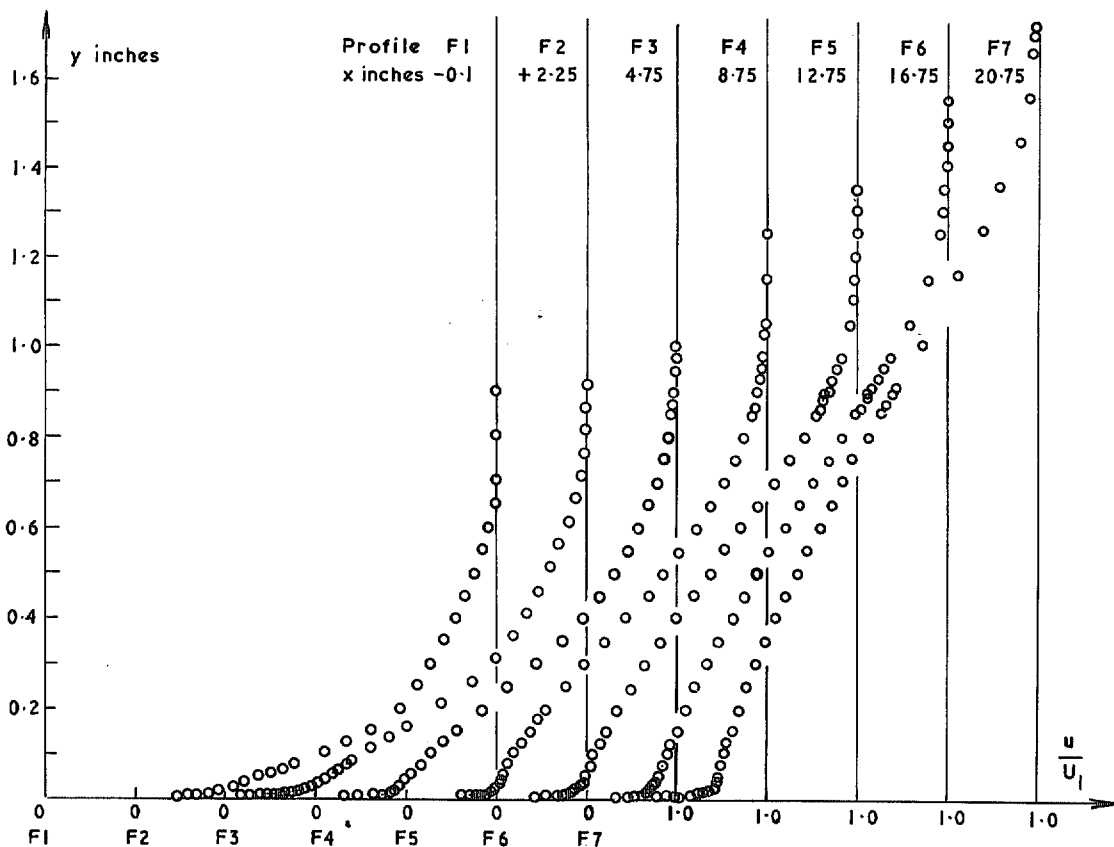
FIG. 34.   Mean velocity profiles. Layer F (along $z = -1 \cdot 0$).
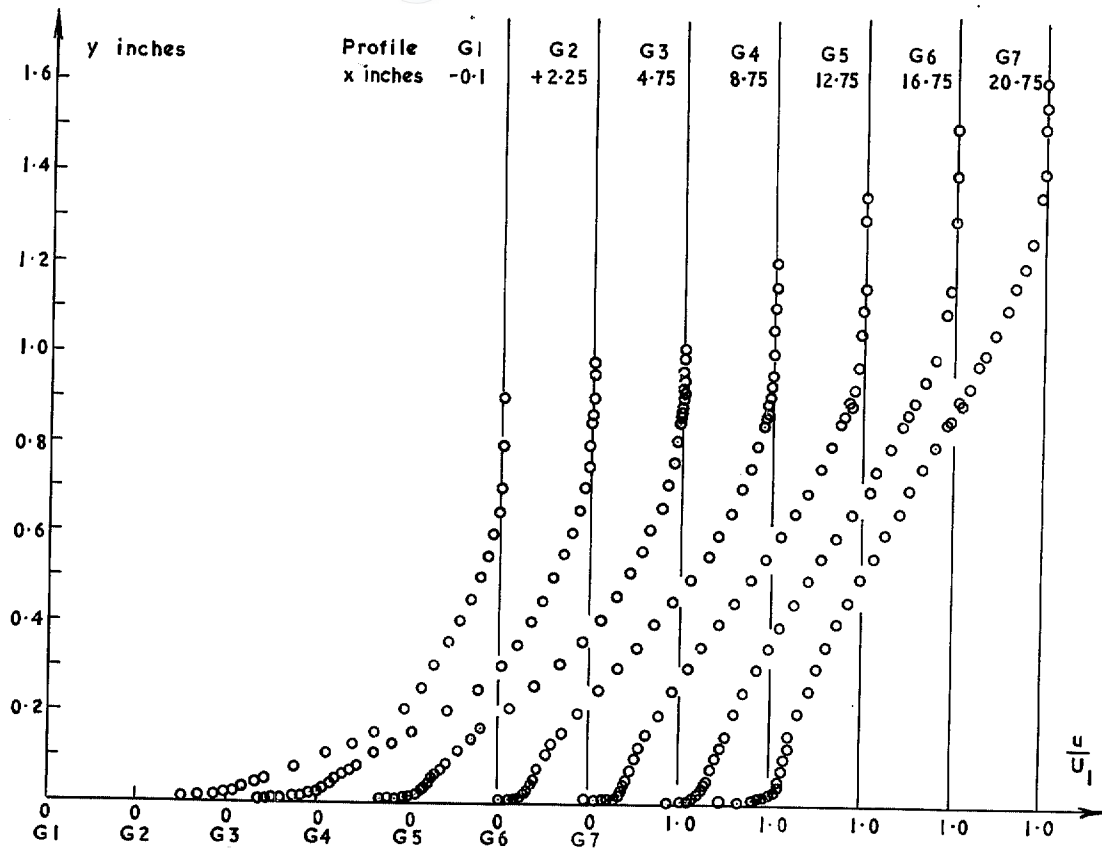
FIG. 35. Mean velocity profiles. Layer G (along $z = -1 \cdot 0$).
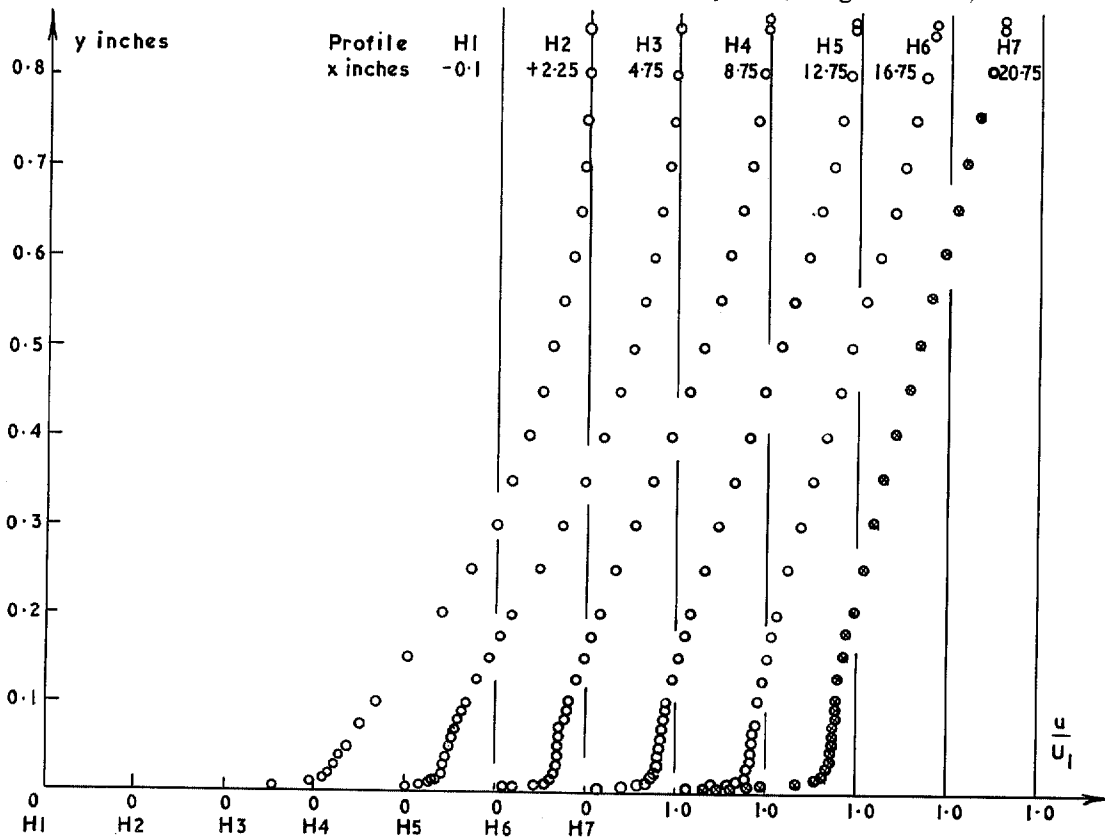

FIG. 36. Mean velocity profiles. Layer H (along $z = -1 \cdot 0$).
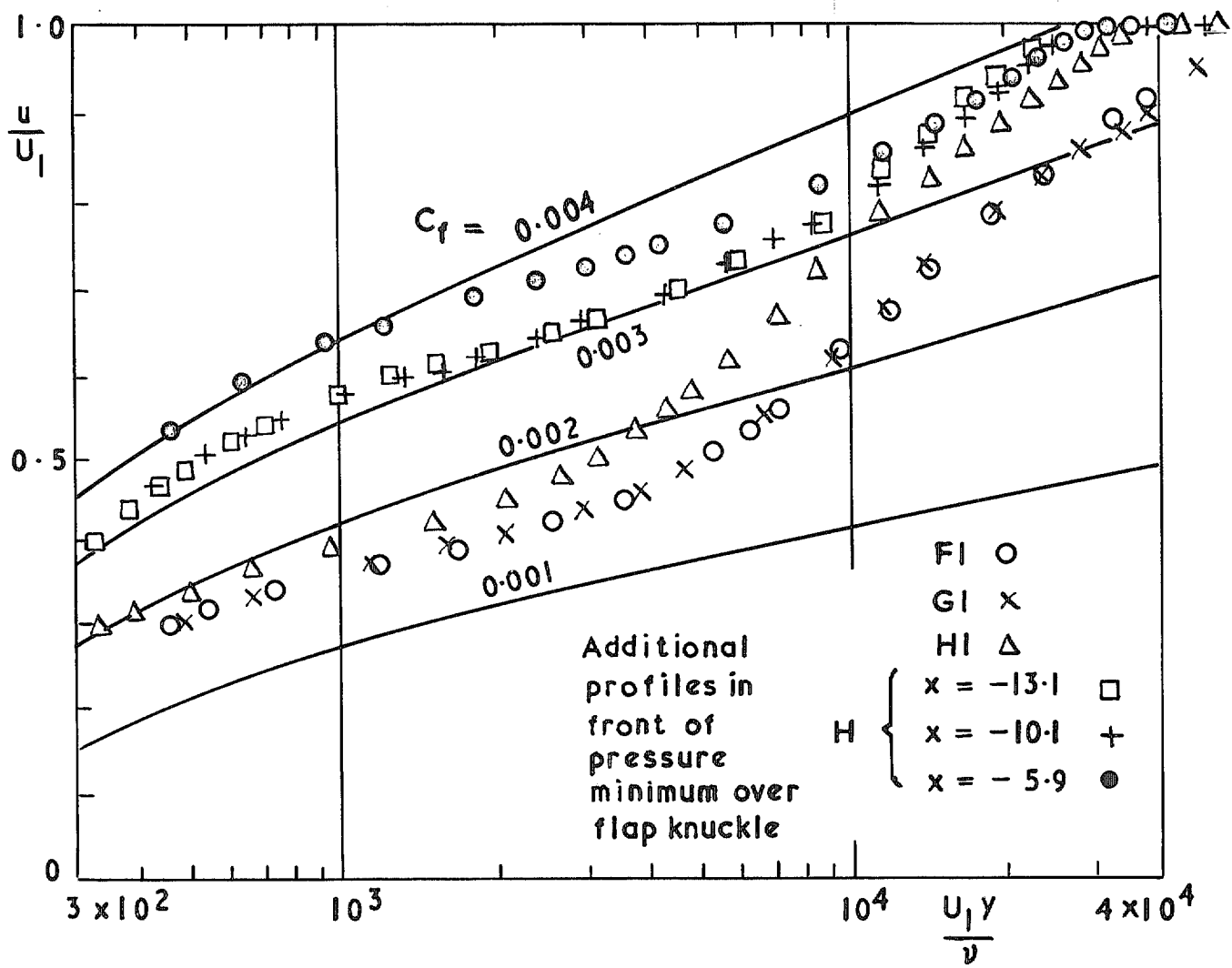
FIG. 37. Comparison of inner region profiles before start of suction

with Clauser plot for $\dfrac{u}{U_\tau} = 5\cdot4 + 5\cdot5 \log_{10} \dfrac{U_\tau y}{v}$.
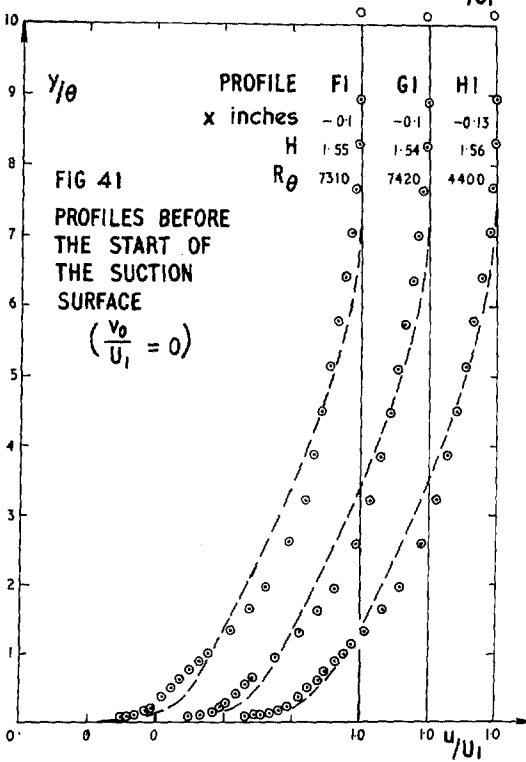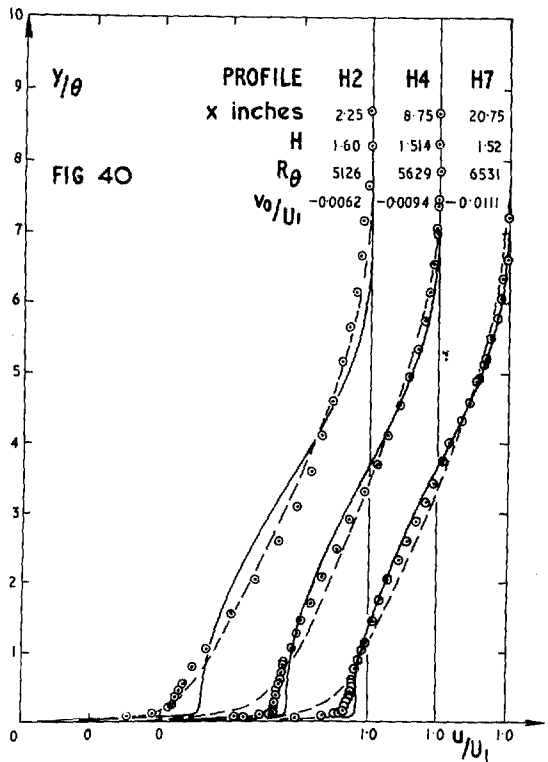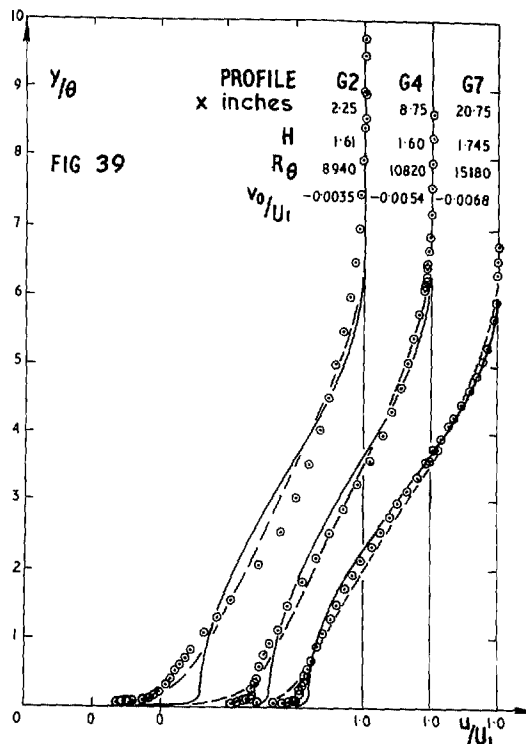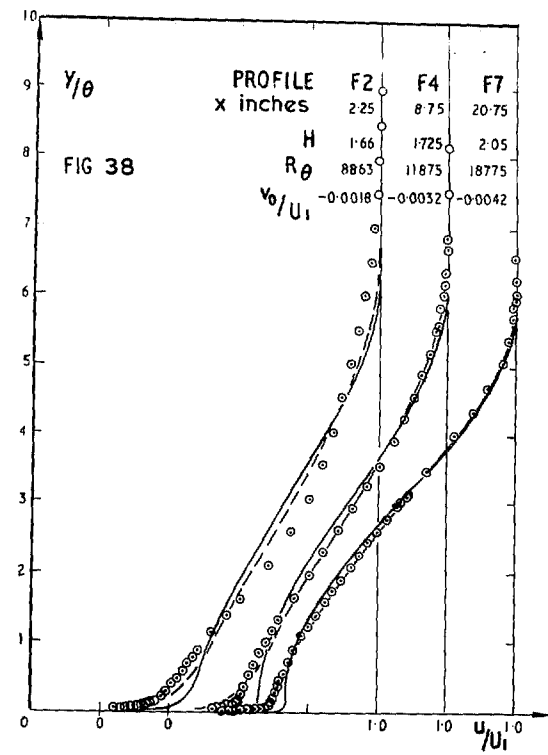
FIG. 38–41. Comparison of profile family with measurements. ——— Prediction from complete family (Thompson[14]). — — — Prediction from solid surface family (Thompson[15]).
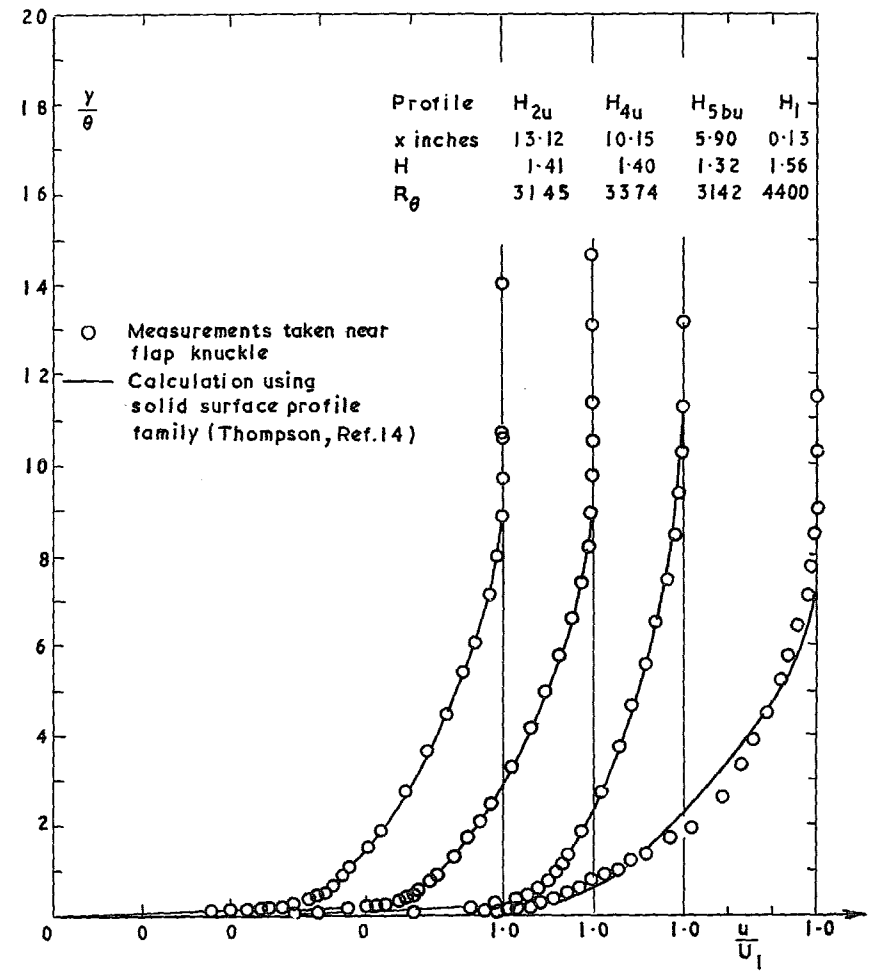
FIG. 42. Profile comparisons. Layer *H* before suction.
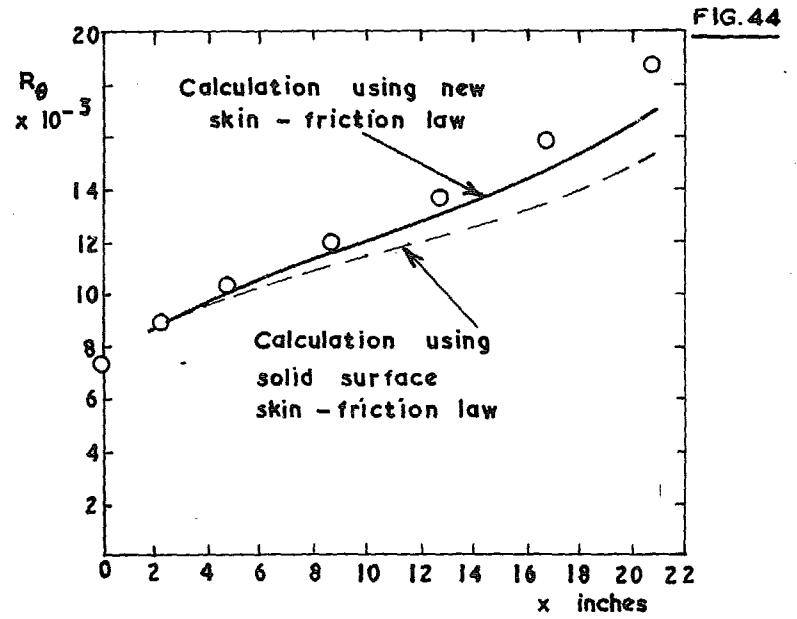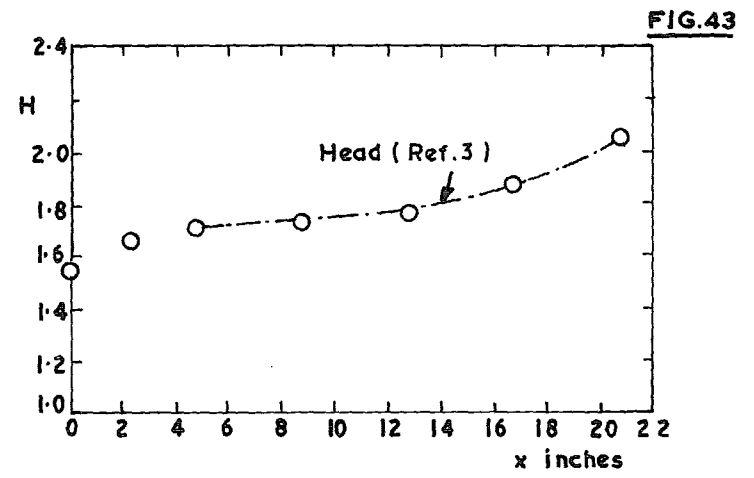
FIG. 43 & 44. Comparison between experiment and calculation. Layer *F*.

FIG. 45

Head (Ref.3)

FIG. 47

Head (Ref.3)

FIG. 46

$R_\theta \times 10^{-3}$

Calculation using new
skin – friction law

Calculation using
solid surface
skin – friction law

FIG. 48

$R_\theta \times 10^{-3}$

Calculation using new skin – friction law,
Thompson (Ref.15)

Calculation using
solid surface
skin – friction law

57
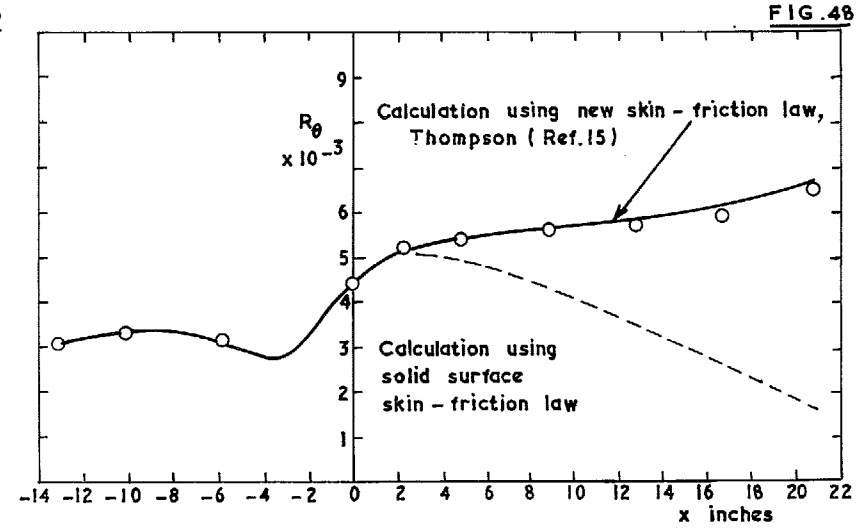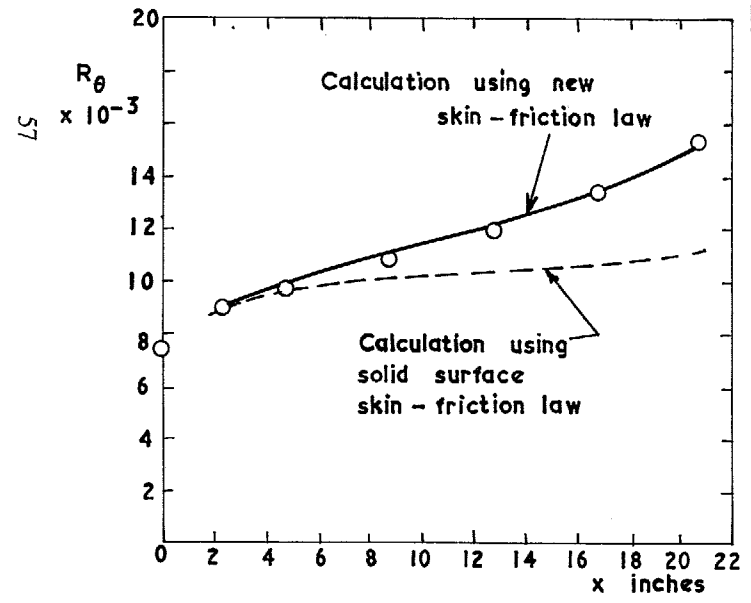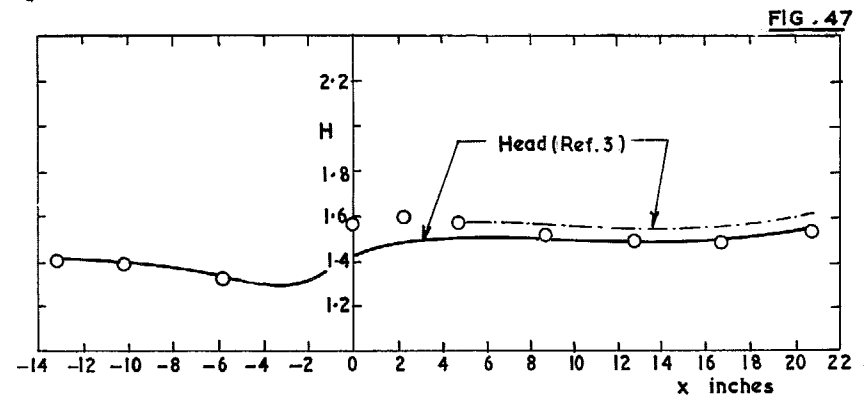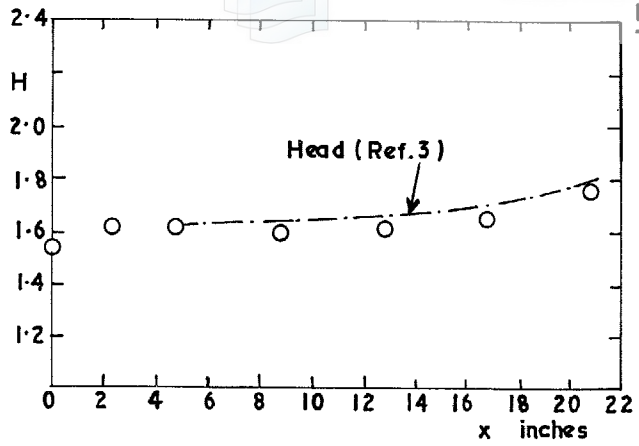
FIG. 45 & 46.   Comparison between experiment
and calculation. Layer *G*.

FIGS. 47 & 48.   Comparison between experiment
and calculation. Layer *H*.

FIG. 49. Suction aerofoil II. Looking upstream towards the wind tunnel contraction—the two l.e. cylinders (arrowed) and the traverse arrangement for the spanwise pitot traverses can be seen. The lower pulley and the flexible drive for the chordwise traverses are also shown. The aerofoil is set up as for boundary layer H.
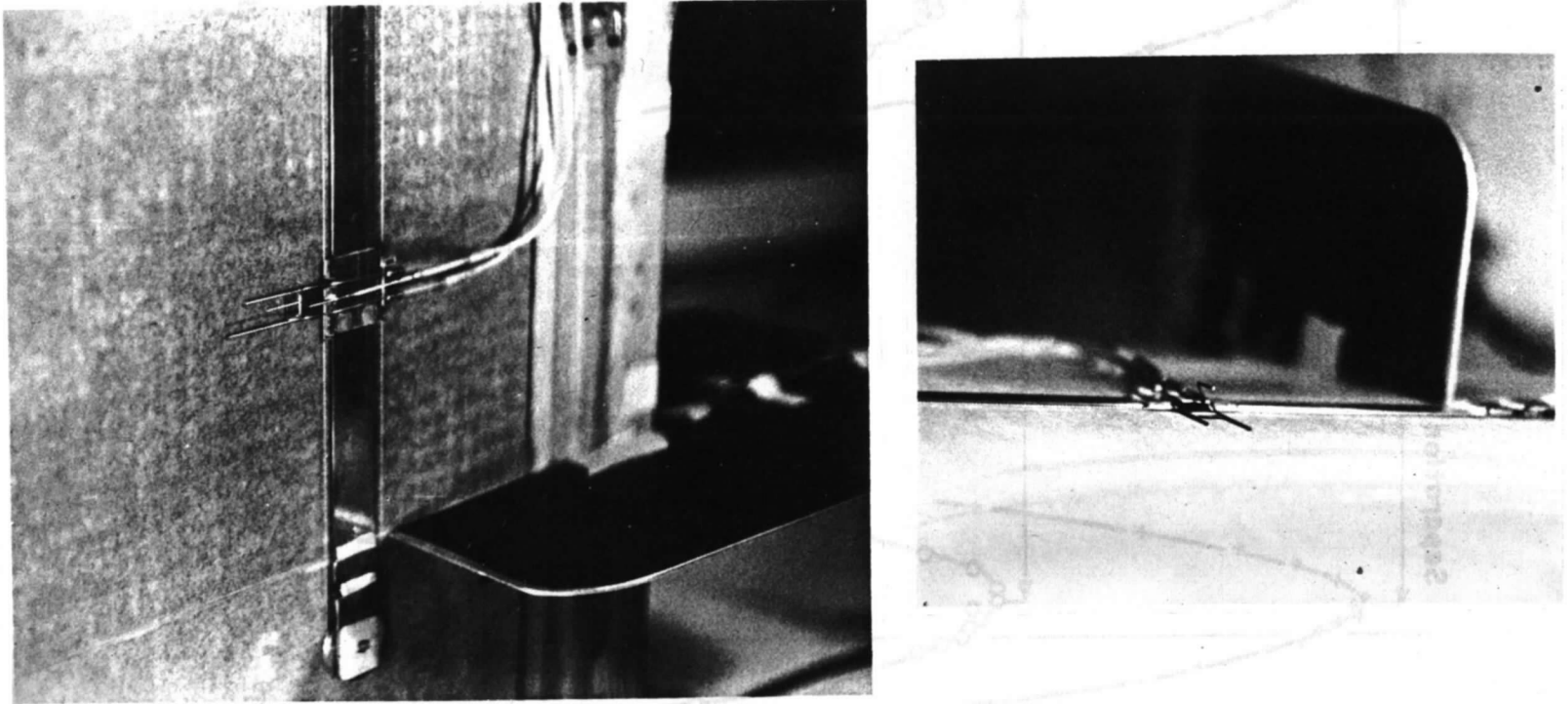
FIG. 50.   Spanwise traversing arrangement set up for layer H.
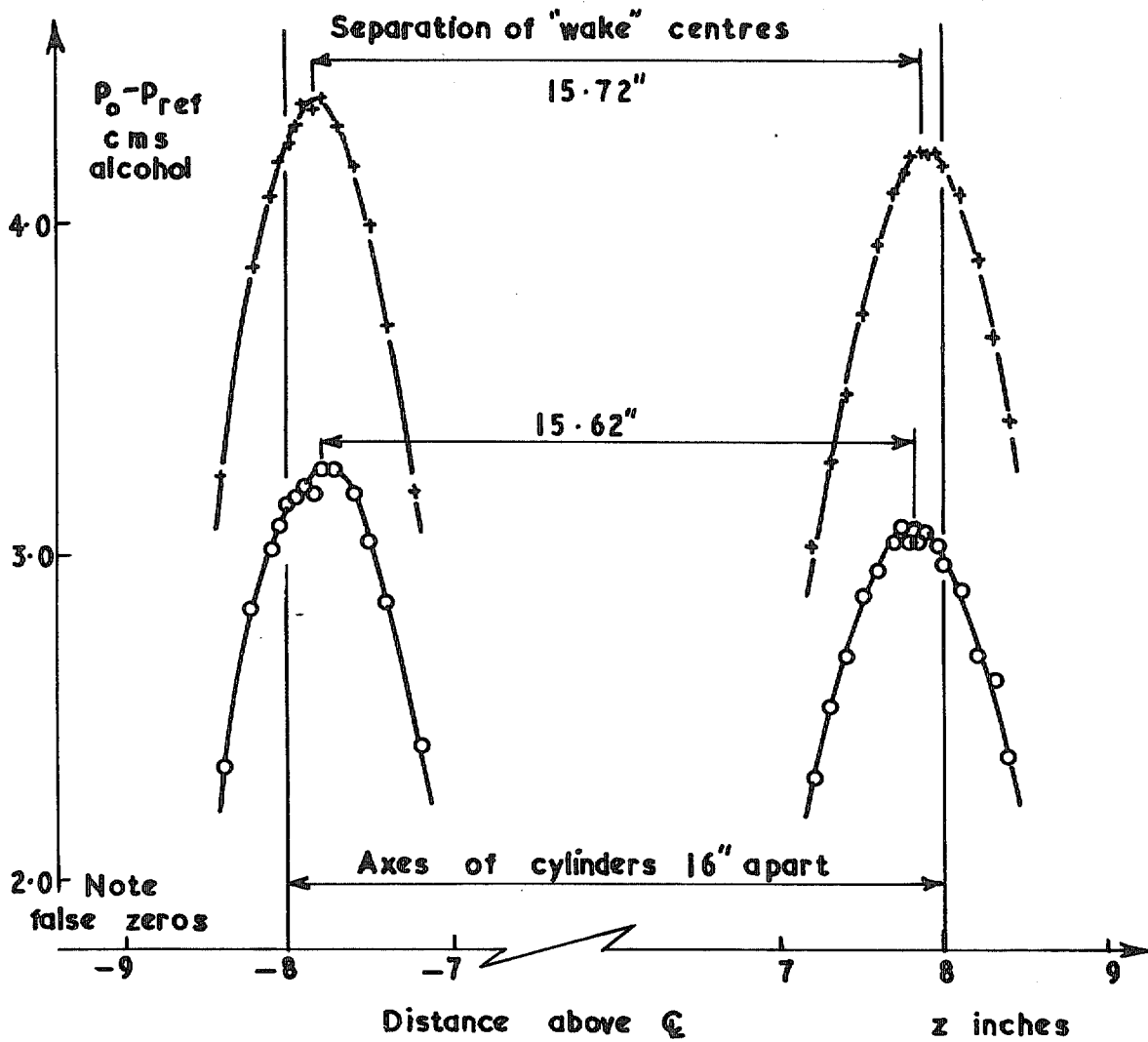
FIG. 51. Spanwise variation of total pressure in layer *H*.

60
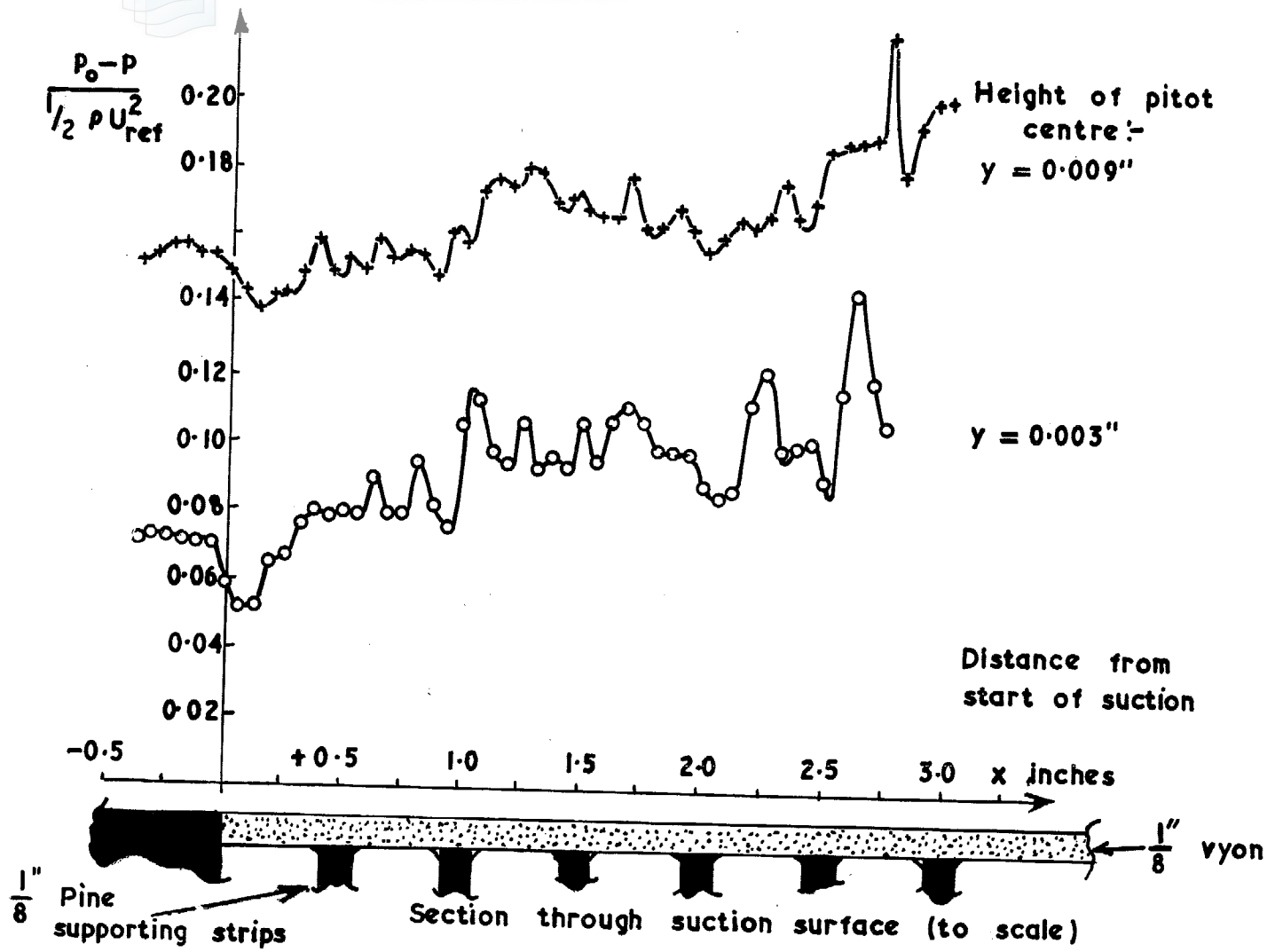
FIG. 52. Chordwise variations of dynamic pressure in boundary layer H.
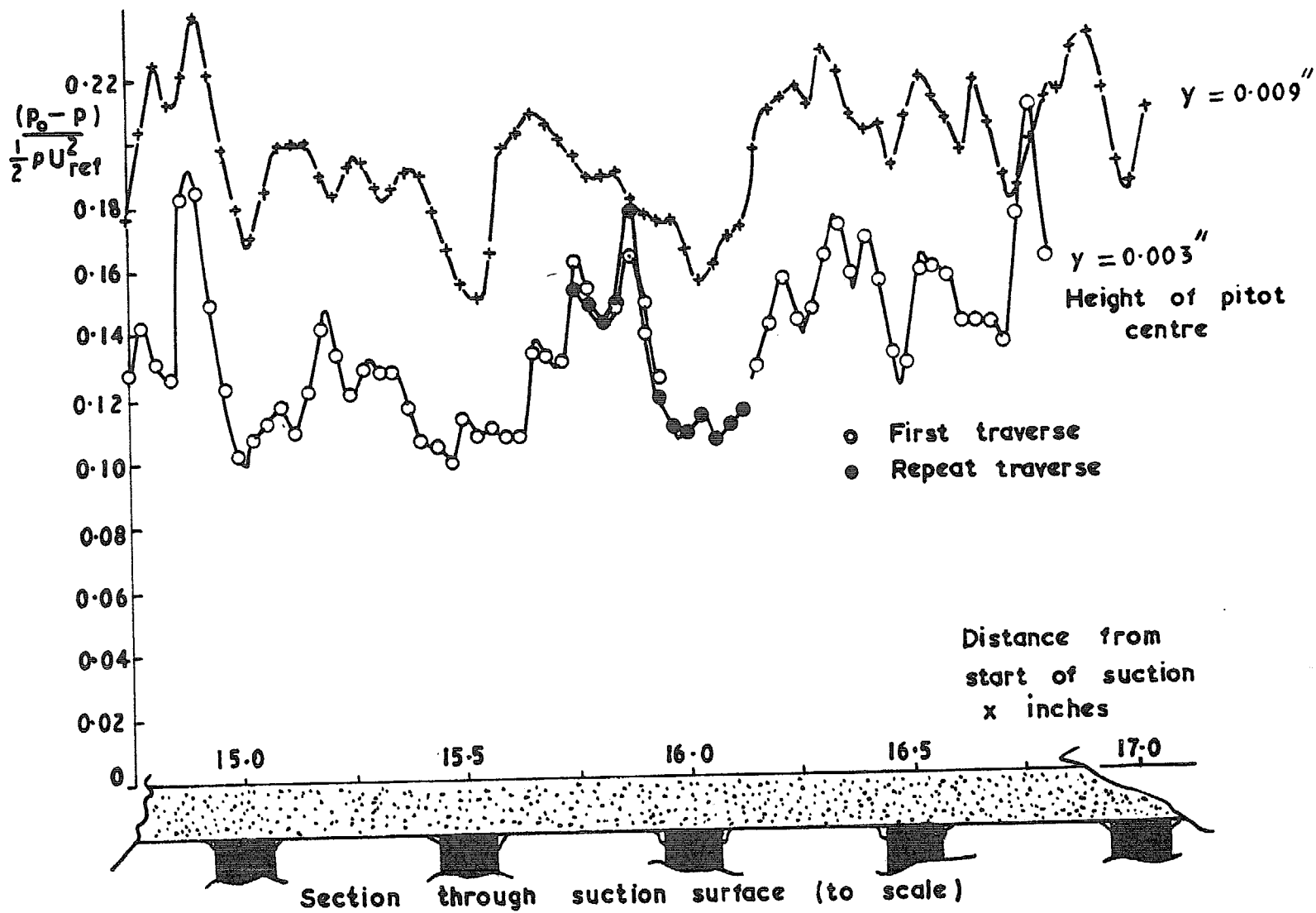
FIG. 53. Chordwise variation of dynamic pressure in boundary layer *H*.
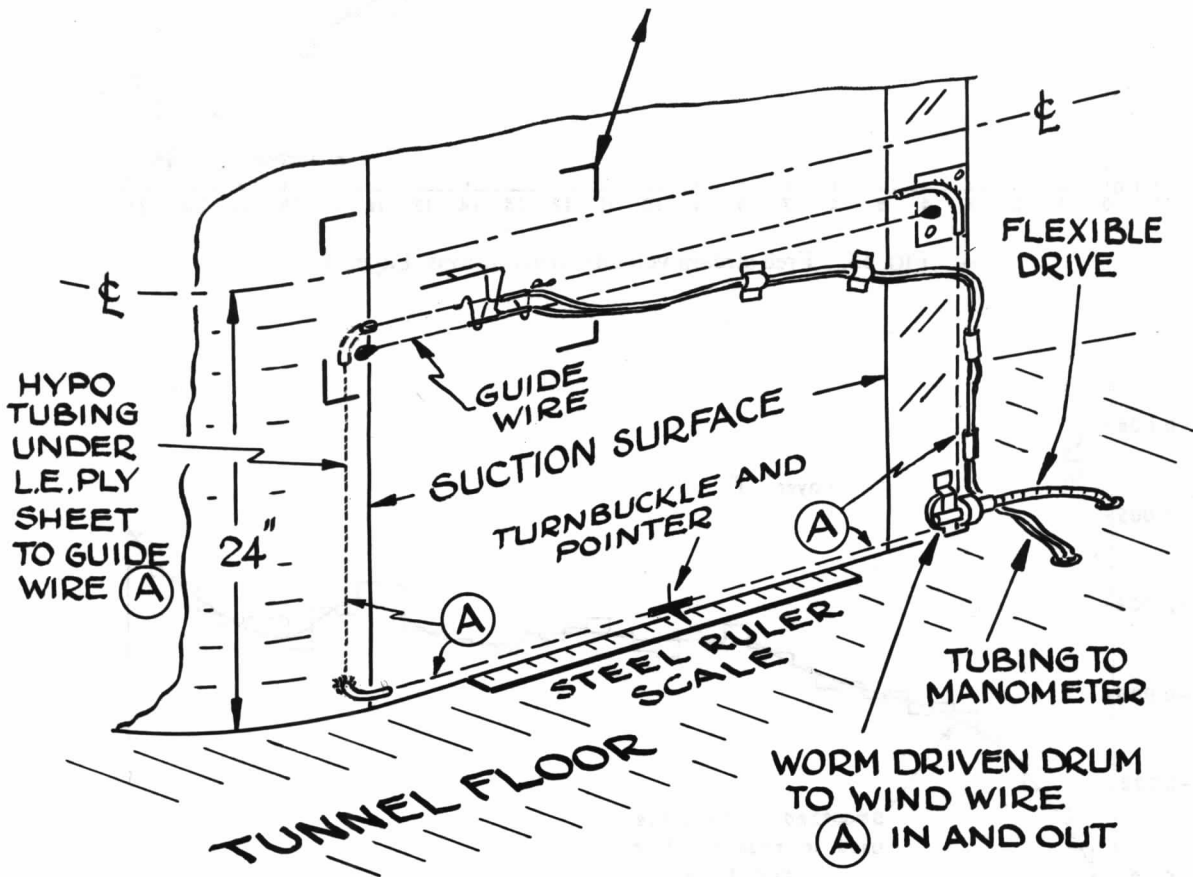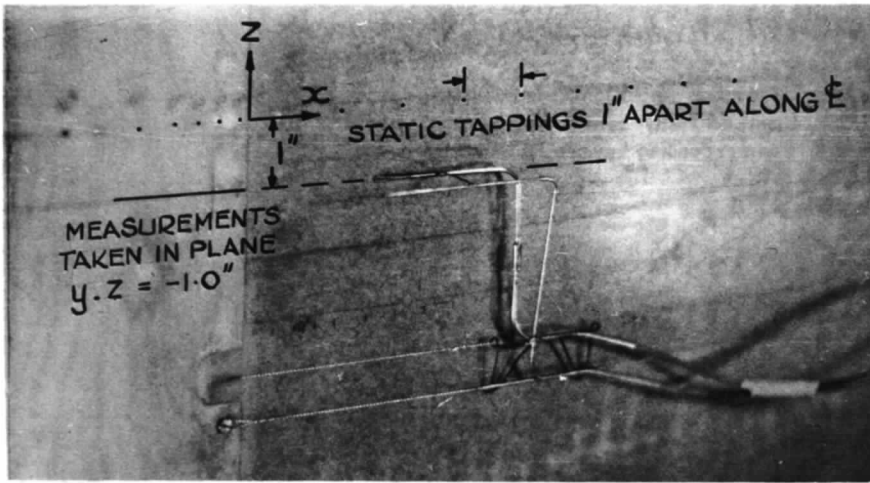
FIG. 54. Chordwise traverse gear arrangement.
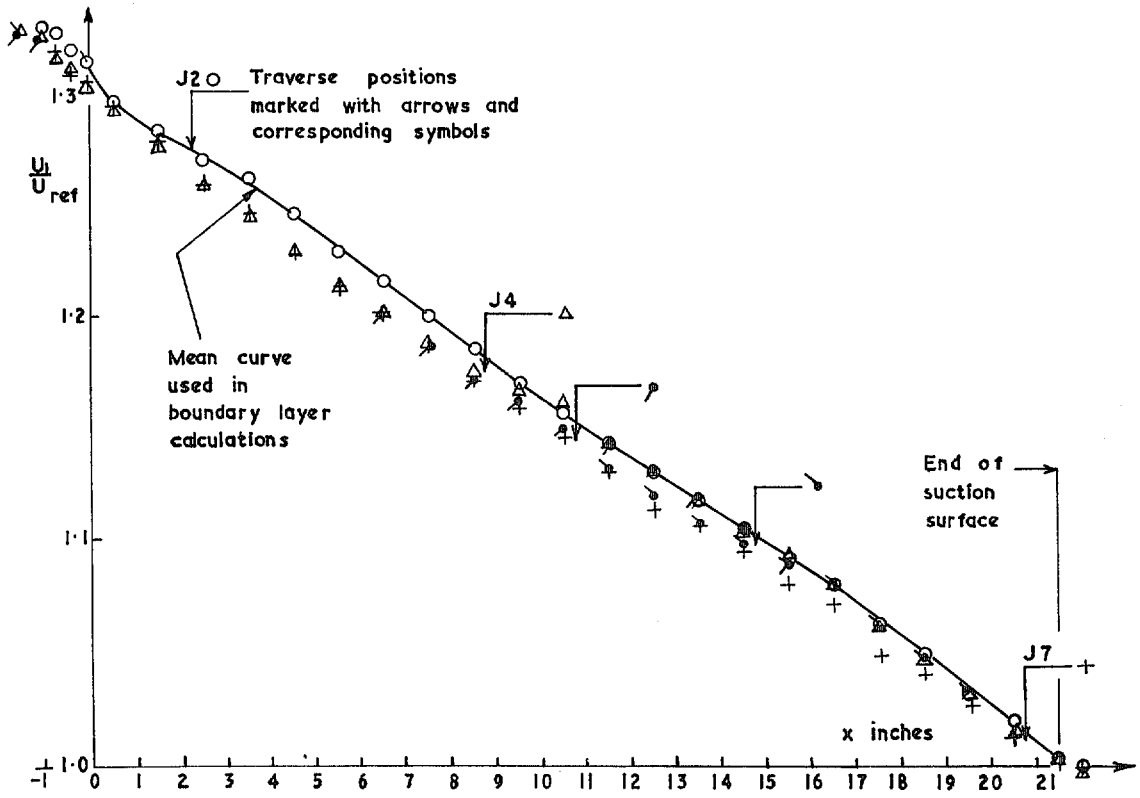
FIG. 55. Free stream velocity distributions. Layer J.
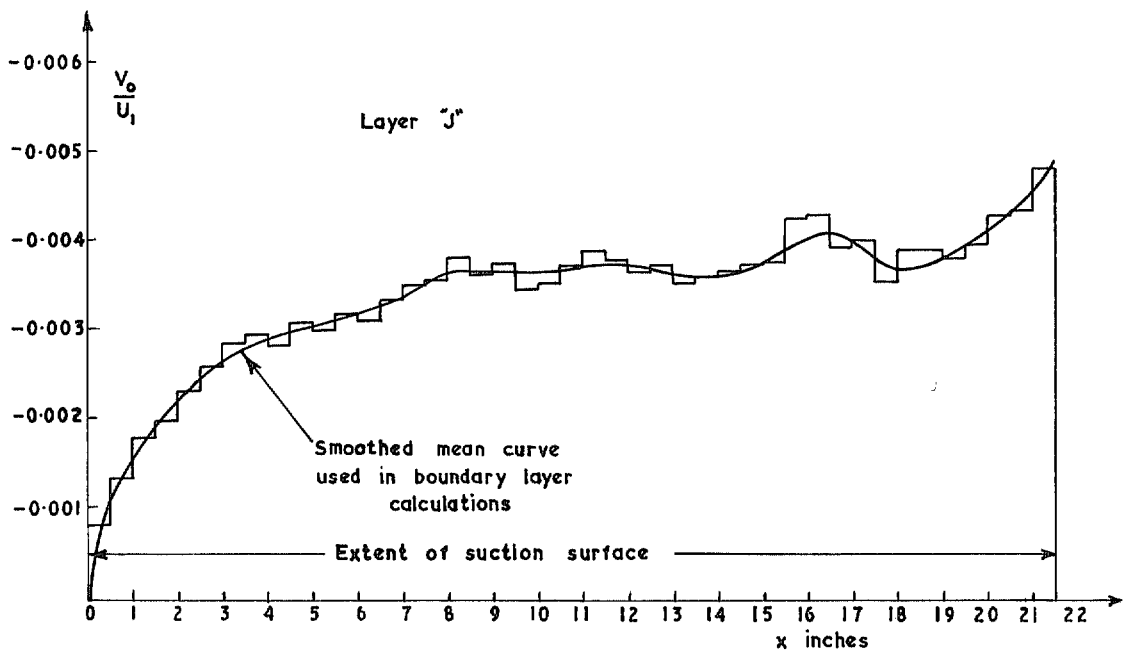
FIG. 56. Suction velocity distribution.

64
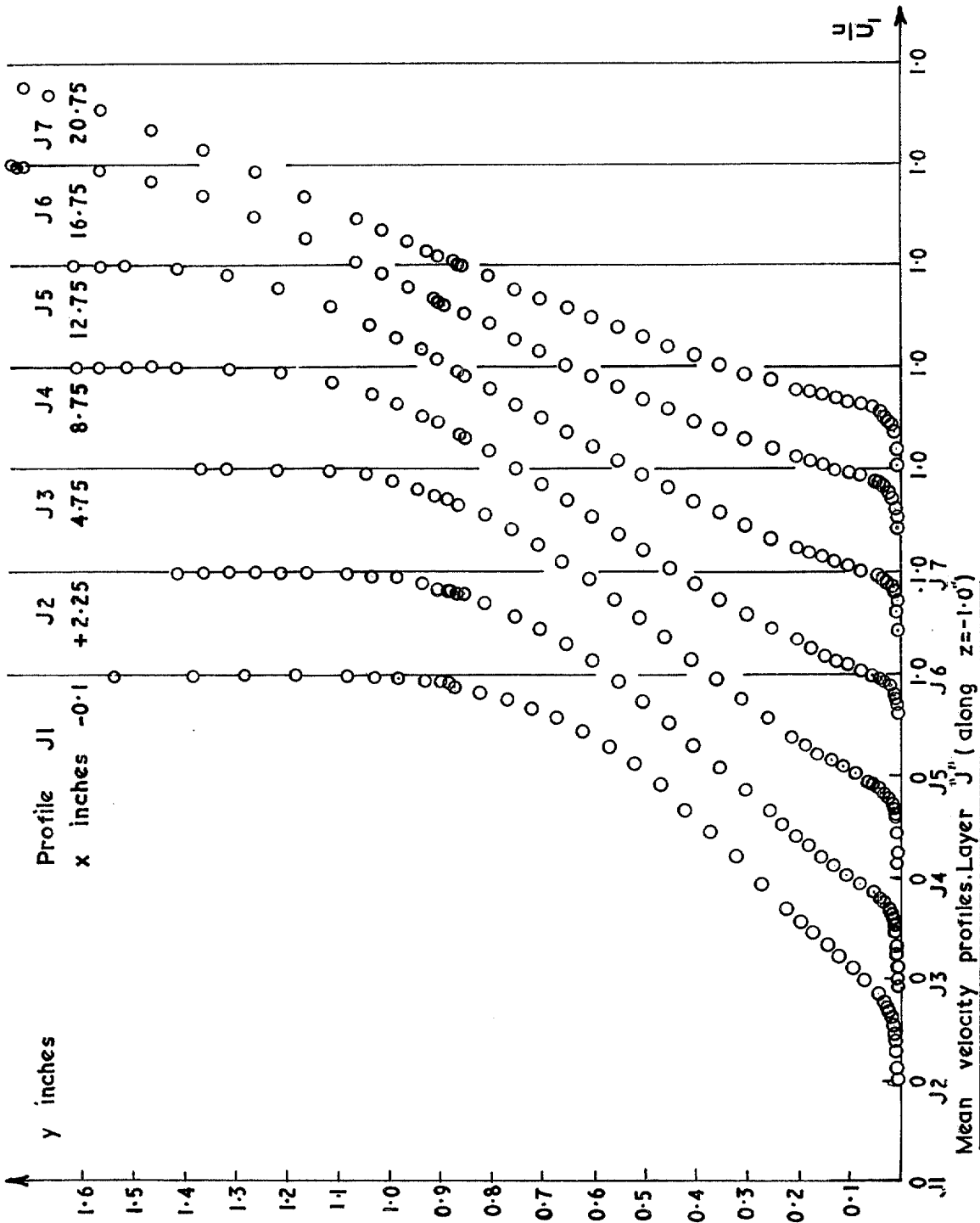
FIG. 57.   Mean velocity profiles. Layer J (along $z = -1 \cdot 0''$).
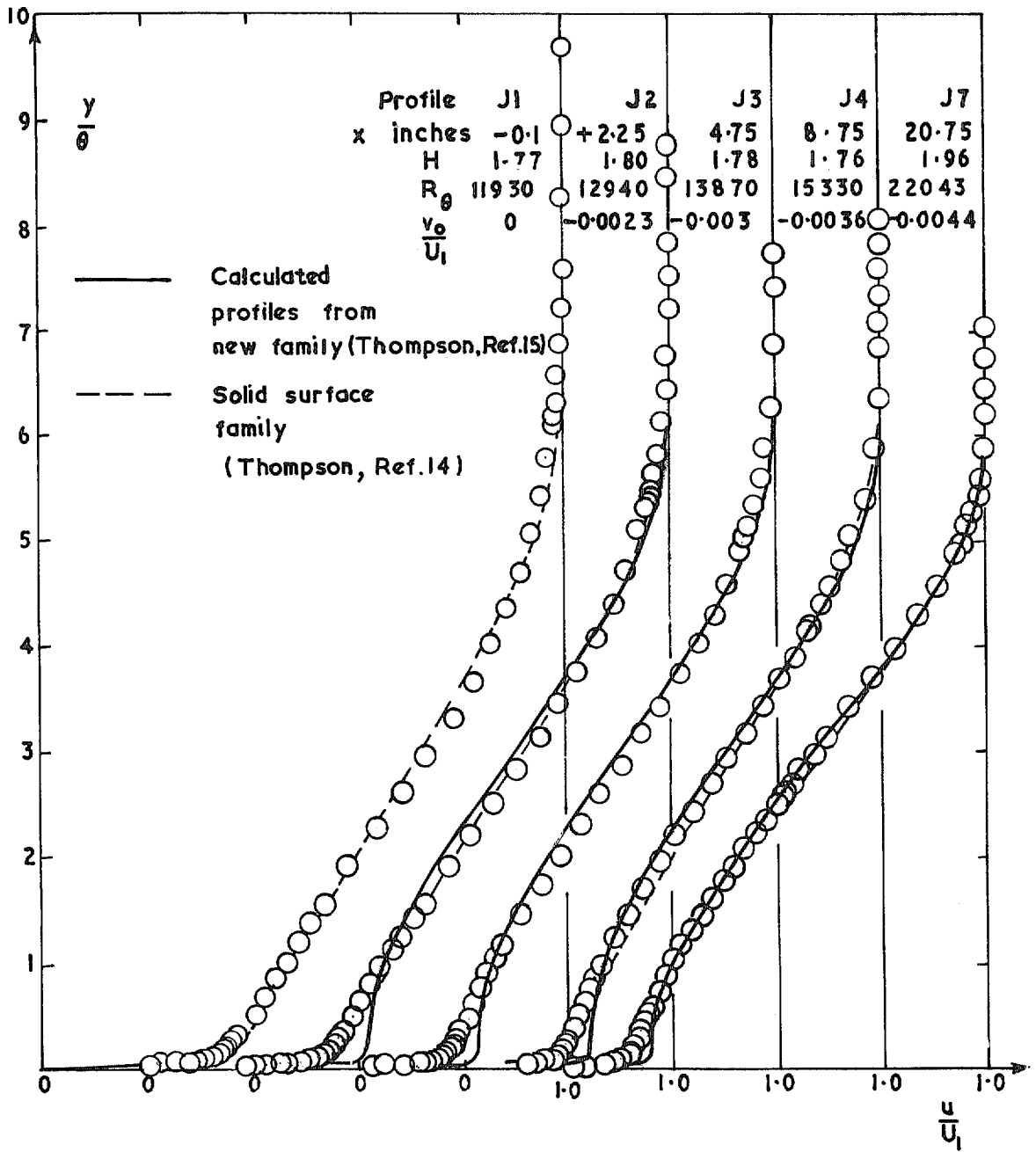
FIG. 58.   Profile comparisons. Layer J.

FIG. 59

FIG. 60
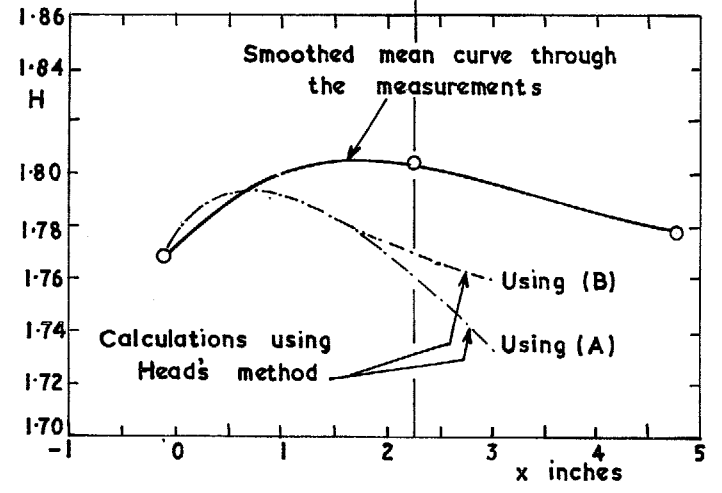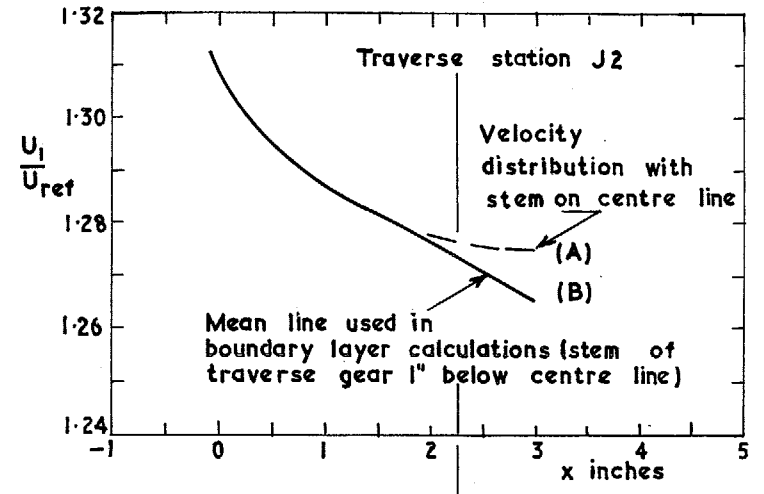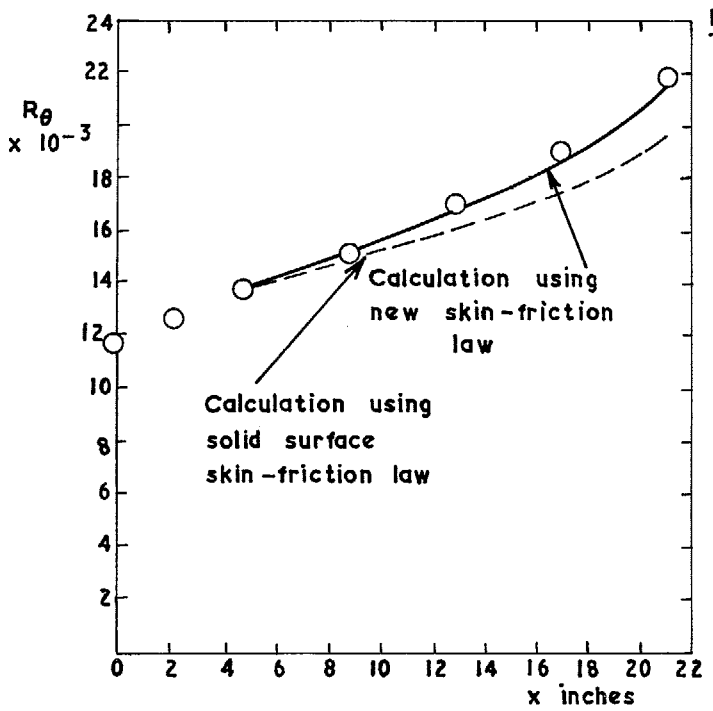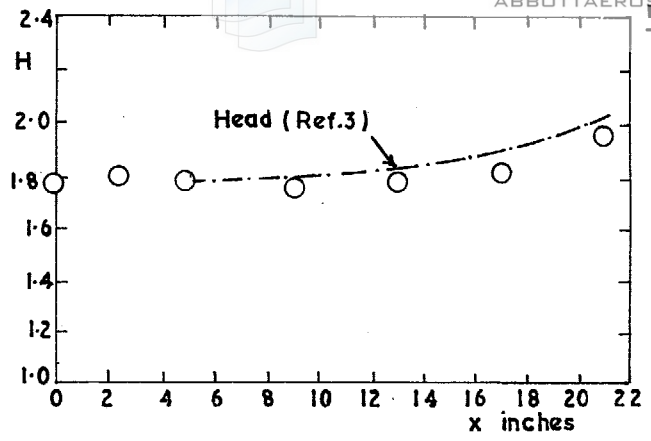
FIGS. 59 & 60.   Comparison between experiment and calculation. Layer *J*.

FIG. 61.   Traverse gear interference.

67
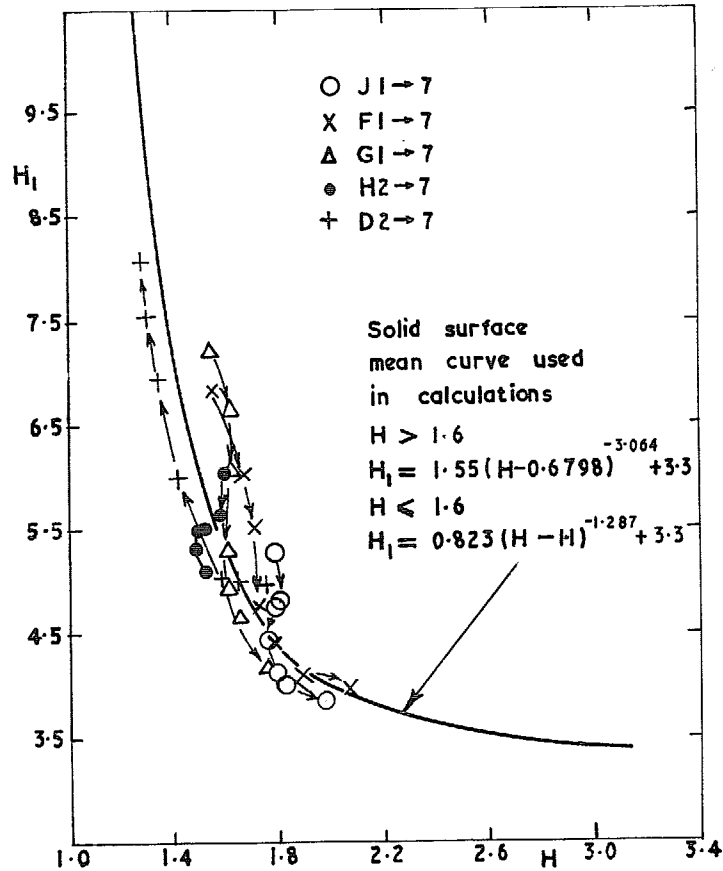
FIG. 62. Comparison of new measurements with Head's shape factor relationship for solid surfaces.

FIG. 63

FIG. 64

Shape factor calculations
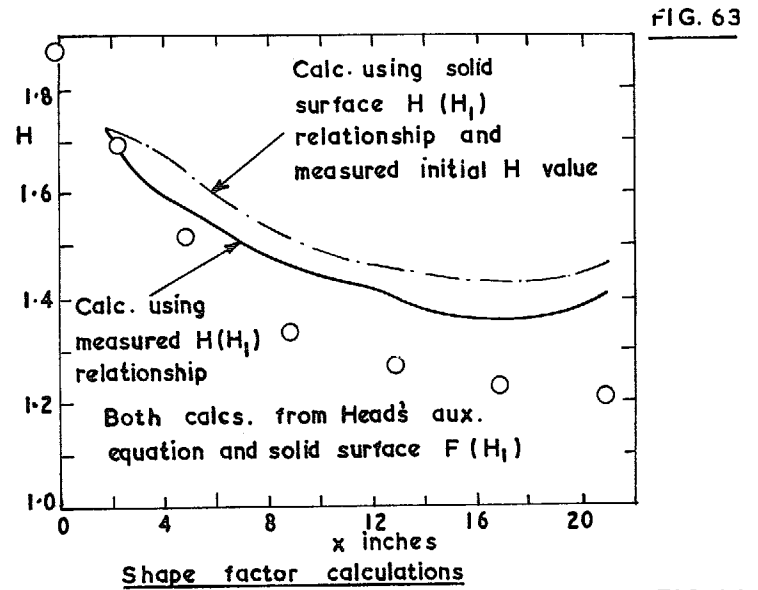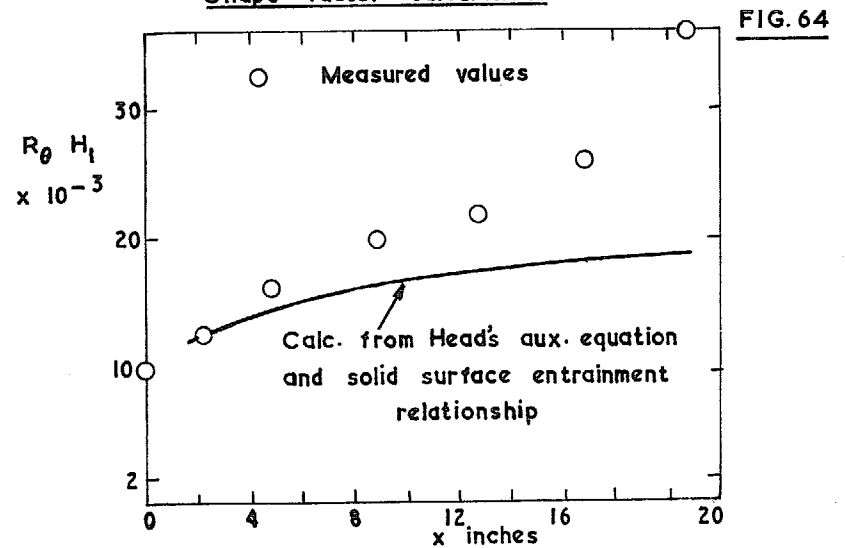
FIGS. 63 & 64. Flux calculation. Layer *E*.

89

FIG. 65

Shape factor calculations

FIG. 66
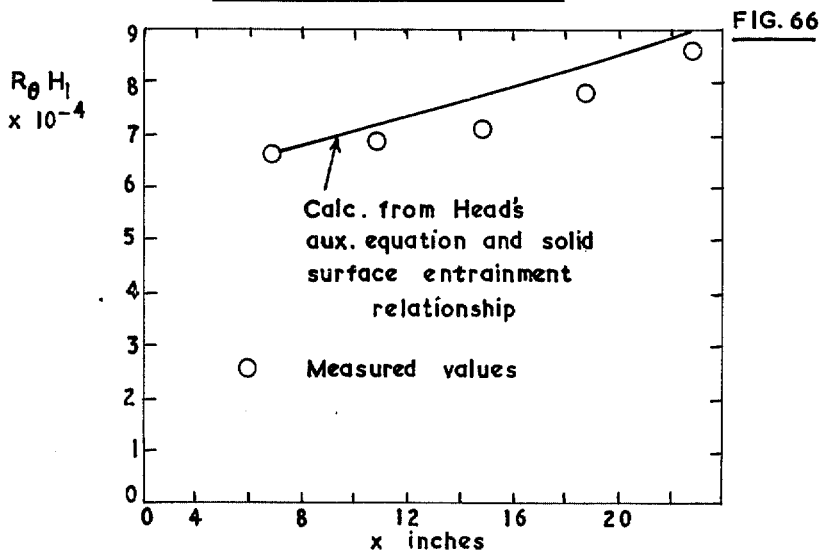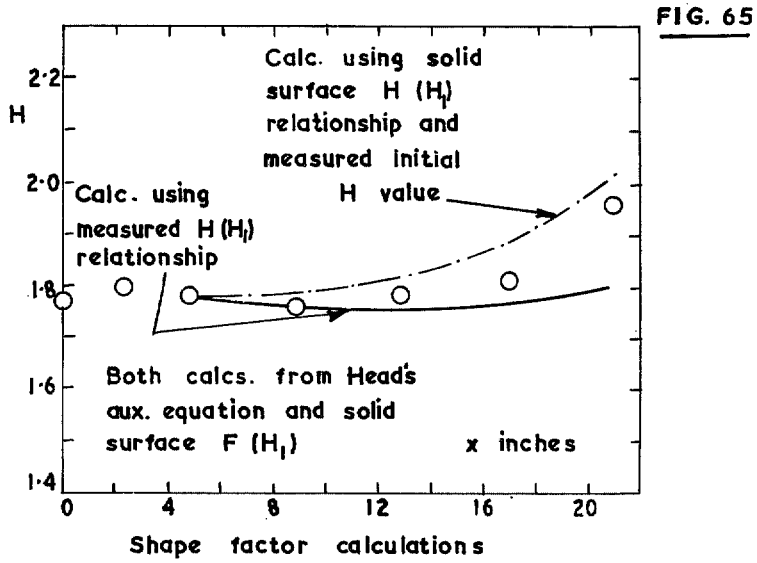
FIG. 65 & 66.   Flux calculation. Layer *J*.